University of L'Aquila

DEPARTMENT OF BIOTECHNOLOGICAL AND APPLIED CLINICAL SCIENCES

Doctoral School in EXPERIMENTAL MEDICINE
Curricula Biotechnology and Biochemical Sciences

XXXVI cycle

Natural compounds as potential inhibitors of viral 3-chymotrypsin-like protease (3CL^{pro})

SSD: BIO/12

Lorenza Fagnani

Programme coordinator

Prof.ssa Mariagrazia Perilli

Tutor

Prof. Giuseppe Celenza

Co-Tutor

Dott. Pierangelo Bellio

Academic Year 2022/2023

Table of contents

Abstract 1

Introduction 3

Chapter I 5

Coronaviruses (CoVs): an in-dept overview 5

1.1 The emergence of a third, novel coronavirus: SARS-CoV-2 8

1.1.1 SARS-CoV-2 genome and structure 10

1.1.1.1 Non-structural proteins and their functions 12

1.1.1.2 Structural proteins 14

1.1.1.3 Accessory proteins 16

1.1.2 Coronaviruses replication cycle 17

1.1.3 Insights into the structure and function of SARS-CoV-2 main protease 18

1.1.3.1 Structure comparison of $3CL^{pro}$s from SARS-CoV, MERS-CoV and SARS-CoV-2 19

1.1.3.2 $3CL^{pro}$ as a promising antiviral target 20

1.1.3.2.1 Targeting the substrate-binding pocket 21

1.1.3.2.2 Targeting the dimerization 22

Chapter II 24

Natural compounds 24

2.1 Lichen secondary metabolites 25

2.1.1 Exploring the multifaceted biological activities of lichens 29

2.2 Curcuminoids 35

2.2.1 Pharmacological effects 37

2.2.2 Bioavailability 40

2.2.3 Formulation and challenges 42

2.2.4 Curcumin and derivatives 42

2.3 Phenylpropanoid compounds 44

2.3.1 Vanillin 45

2.3.2 Vanillic acid 46

2.3.3 Ferulic acid 47

2.3.4 Caffeic acid 47

2.3.5 Chicoric acid 48

2.3.6 Rosmarinic acid 49

2.3.7 Salvianolic acid 50

Chapter III 52

Materials and methods 52
3.1 Reagents 52
3.2 Spectrofluorimetric assay 52
3.3 Determination of kinetic parameters 54
3.3.1 Theoretical basis for approximation to a Michaelis-Menten model 54
3.3.1.1 Equation derivation 56
3.4 Inhibition assay 59
3.5 Determination of the mechanism of inhibition 62
3.6 Molecular docking 63
3.6.1 Molecular docking: salazinic and protocetraric acids 63
3.6.1.1 Docking protocol validation 64
3.6.1.2 Extra Precision (XP) and Covalent Docking (CovDOCK) 64
3.6.2 Molecular docking: perlatolinic acid 65
3.6.3 Molecular docking: fumarprotocetraric acid 66
3.7 Cell culture and viability assay 66
3.8 Statistics and data analysis 67
Capitolo IV 68
Results 68
4.1 Determination of the kinetic parameters 68
4.2 Screening of natural compounds 69
4.3 Detailed results from in-dept investigations 73
4.3.1 Lichen secondary metabolites 74
4.3.1.1 Salazinic and protocetraric acids 74
4.3.1.2 Perlatolinic acid 82
4.3.1.3 Fumarprotocetraric acid 89
4.3.1.4 Alpha-collatolic acid 91
4.3.1.5 Norstictic acid 92
4.3.1.6 Ephiphorellic acid 94
4.3.1.7 Gyrophoric acid, tumidulin and rhizocarpic acid 95
4.3.1.8 Lichesterinic acid 95
4.3.2 Curcuminoids 96
Capitolo V 98
Discussion 98
5.1 Lichen secondary metabolites 99
5.2 Curcuminoids 108
5.3 Phenylpropanoid compounds 112

5.4 Final remarks 115
Conclusion 115
References 118

Abstract

Despite the recent advances to control the ongoing SARS-CoV-2 pandemic, the rapid spread of the virus is still challenging to face. Although the scientific community has turned to the development of effective vaccines, the repurposing of approved drugs and natural compounds has emerged as a particularly promising strategy for combating the virus infection. The strategic repurposing of such agents, especially those targeting the SARS-CoV-2 3CL main protease, a critical enzyme in viral replication, holds considerable potential for therapeutic intervention.

Within the vast spectrum of natural compounds, lichen secondary metabolites, curcuminoids, and various phenylpropanoid compounds have been identified as potential candidates due to their broad spectrum of biological activities. However, their therapeutic potential has yet to be fully exploited.

An initial screening of natural compounds was conducted to identify their inhibitory potential on $3CL^{pro}$, focusing subsequently on those demonstrating the most promise.

The investigation into their inhibitory activity involved kinetic parameter assessment through fluorescence intensity measurements using a microtiter plate-reading fluorimeter and a fluorogenic substrate designed specifically for this purpose. Additionally, the cytotoxicity of some compounds was evaluated on murine Sertoli TM4 cells to ensure their safety for potential therapeutic use, along with computational studies to elucidate the interaction dynamics between the selected compounds and the enzyme.

Our findings reveal that some compounds exhibit no inhibitory effects on $3CL^{pro}$, while lichen secondary metabolites and most of the curcuminoids demonstrate significant inhibitory activity, acting as slow-binding inhibitors of the enzyme. Analysis of the mechanism of inhibition reveals the presence of both competitive and noncompetitive inhibitors among the compounds, highlighting a dual approach to inhibit the protease that involves targeting the substrate-binding site and the enzyme's dimerization interface, respectively. None of the tested compounds exhibit cytotoxic effects on murine epithelial cells, corroborating their safety profile and potential for therapeutic application. Computational studies, providing insights into the interaction dynamics between the natural compounds and the protease, reinforce the biochemical data.

The findings contribute significantly to the existing knowledge of the biological activities of natural compounds. Based on the outcomes of kinetic analyses, computational studies, and cytotoxicity studies, we can conclude that some

examined natural compounds can be considered suitable scaffolds for developing effective inhibitors of the cysteine enzyme of SARS-CoV-2.

Introduction

Epidemics and pandemics, irrespective of their origin, represent formidable challenges to global health and well-being, necessitating multifaceted strategies for their containment and mitigation. The inherent complexity of managing such crises stems from their unpredictable nature and capacity for mutation, the rapid global spread facilitated by modern connectivity, and the critical need for robust international and national coordination. In an era marked by unprecedented globalization and the swift movement of people and goods across borders, the ability to rapidly respond to and manage such health emergencies is more critical than ever.

One of the primary challenges in addressing these health crises is the dissemination of timely, comprehensible, and accurate information to healthcare professionals and the broader public. Achieving a delicate balance between raising awareness of potential or confirmed cases and avoiding unnecessary panic is paramount. This task is further exacerbated by the pervasive spread of misinformation, necessitating the refutation of false claims by trusted sources to prevent additional personal, social, and economic damages. The repercussions of misinformation can lead to severe consequences, including anxiety, psychosis, and unjustified discrimination against specific ethnic groups, adversely affecting key economic sectors such as tourism, commerce, and hospitality.

Moreover, the phenomenon of "unnecessary prevention" can burden health services, leading to inflated healthcare costs through the procurement of protective measures, unwarranted diagnostic tests, and needless medical consultations. Such actions divert essential resources from critical health services and interventions. Conversely, the promotion of non-medical, cost-effective, or cost-free behaviours that contribute to disease prevention and mitigation, alongside fostering social and psychological support, is imperative. These practices are invaluable, particularly in times of crisis, playing a pivotal role in strengthening community resilience and cohesion. This aspect is especially relevant in individualistic societies prevalent in Western countries, where community solidarity, though not inherently strong, is crucial for collective well-being.

In light of these considerations, this introduction aims to underscore the multifaceted challenges posed by pandemics and epidemics. It highlights the critical importance of accurate information dissemination, international cooperation, and the promotion of healthy behaviours to combat not only the current COVID-19 pandemic but also future health crises. The pursuit of scientific research into natural compounds as potential inhibitors of the 3-chymotrypsin-like protease ($3CL^{pro}$) of SARS-CoV-2 is a testament to the innovative approaches being

undertaken to find effective treatments. This research not only contributes to the ongoing fight against COVID-19 but also underscores the indispensable role of science in addressing global health emergencies.

Chapter I

Coronaviruses (CoVs): an in-dept overview

Since the onset of the 21st century, the global community has grappled with several viral outbreaks, notably respiratory syndromes caused by coronaviruses.

Coronaviruses (CoVs) are a type of virus belonging to the subfamily *Orthocoronavirinae* of the family *Coronaviridae*, which is part of the suborder *Cornidovirineae* and order *Nidovirales*. By a phylogenetic grouping, they are further classified into four genera: alphacoronavirus, betacoronavirus, gammacoronavirus, and deltacoronavirus (Cui J. et al., 2019) (Goyal B. and Goyal D., 2020). The literature indicates that these coronaviruses probably diverged around 2400-3000 BC, infecting different animal groups (Singh D. and Yi SV., 2021). While alphacoronaviruses and betacoronaviruses primarily infect mammals like bats, gammacoronaviruses and deltacoronaviruses exhibit a broader host range encompassing avian species (V'kovski P. et al., 2021; Goyal B. and Goyal D., 2020; Singh D. and Yi SV., 2021; Wertheim JO. et al., 2013; Banerjee A. et al., 2019; Paules CI. et al., 2020).

Coronaviruses manifest as large spherical entities with diameters ranging from 80 to 160 nm (Cui J. et al., 2019). Under the electron microscope, the main structural feature of coronaviruses is the presence of club-shaped projections on the virion surface, attributed to the Spike proteins, creating an image reminiscent of a royal crown or a solar corona, thus their name (Yang H. et al., 2006; Fehr AR. et al., 2015). Coronaviruses constitute a highly diverse family of enveloped positive-sense single-stranded RNA viruses. Notable for their extensive RNA sequence, ranging in length from 26 to 32 kb, these viruses are significantly larger than many others, like Human Immunodeficiency Virus (HIV) which is approximately 9 kb long (Denison MR. et al., 2011).

Coronaviruses are infectious agents prevalent in a wide range of vertebrates, including animals, such as camels, bats, domestic animals, livestock, and poultry, but in some cases, albeit rarely, they can adapt and infect humans before spreading within the population.

Since the initial discovery of coronavirus in the 1930s and identification of the first human coronaviruses in the 1960s (V'kovski P. et al., 2021; Tyrrell DA. et al., 1966), a total of seven human CoVs have been isolated (Bradburne AF. et al., 1967; Fung TS. et al., 2019). These viruses are distinguished by their capacity to cause a range

of diseases in humans, particularly affecting the upper respiratory and gastrointestinal tracts. Human coronaviruses, including human coronaviruses such as HCoV-229E (α-CoV), HCoV-OC43 (β-CoV), HCoV-NL63 (α-CoV), and HCoV-HKU1 (β-CoV), commonly cause seasonal mild respiratory tract infections associated with “common cold”-like symptoms (Zhang SF. et al., 2018; Corman VM. et al., 2018). However, recent coronaviruses such as the Severe Acute Respiratory Syndrome Coronavirus (SARS-CoV), the Middle East Respiratory Syndrome Coronavirus (MERS-CoV), and the ongoing SARS-CoV-2, which emerged in the past two decades, have demonstrated heightened pathogenicity (Zumla A. et al., 2016; de Groot RJ. et al., 2013). Infections by these latter viruses can lead to severe, life-threatening respiratory pathologies and lung injuries for which specific prophylactic or treatments are yet to be approved. Classified under the *Betacoronavirus* genus, specifically within group 2 (Harrison AG. et al., 2020), SARS-CoV, MERS-CoV, and SARS-CoV-2 are known to affect the lower respiratory tract, leading to viral pneumonia (Su S. et al., 2016; Song Z. et al., 2019). Before 2002, coronaviruses were considered exclusively as veterinary pathogens and causal agents of the common cold in humans. However, this perception shifted dramatically during the SARS epidemic of 2002-2003, when the significant impact of coronaviruses on human health became evident (Coleman CM. et al., 2014; Fehr AR. and Perlman S., 2015).

Phylogenetic studies have revealed that coronaviruses, to transition into the human population, typically require an intermediate host that has substantial contact with humans. Bats serve as the intermediary for coronaviruses 229E and NL63, whereas OC43 and HKU1 are thought to have originated from rodents. Notably, SARS-CoV and MERS-CoV, which are responsible for zoonotic diseases, made their cross-species leap to humans through recognized intermediate hosts: civets for SARS-CoV and dromedaries for MERS-CoV (Forni D. et al., 2017; Cui J. et al., 2019; Ye ZW. et al., 2020; Luk HKH. et al., 2019; Zhou P. et al., 2020), both highly pathogenic agents that have led to epidemics in the last two decades (Fehr AR. and Perlman S., 2015). SARS-CoV-2 has been proposed to originate from the bat virus Bat-CoV RaTG13, sharing 96% identity. However, the species acting as an intermediary for SARS-CoV-2 to jump from bats to humans remains undefined (Santos-López G. et al., 2021). Pangolins are also believed to be one of the intermediate hosts for viral species transfer to humans, while other intermediate hosts remain currently undefined (Lam TT. et al., 2020).

The coronaviruses NL63 and HKU1, which are associated with milder respiratory infections, were identified during the period of 2004 to 2005. In contrast, the severe acute respiratory syndrome virus, a more virulent strain, was first transmitted to humans in Foshan, Guangdong province, China, in November 2002, with subsequent cases emerging in Guangzhou, Guangdong province, in February

2003. The SARS epidemic represented a significant global health crisis, culminating in over 8,000 confirmed cases across 29 countries and resulting in 774 fatalities, which corresponds to an estimated fatality rate of approximately 10% between November 2002 and July 2003 (World Health Organization, 2015). Following aggressive containment measures, the SARS-CoV virus was successfully controlled, with no new cases reported post-2004. Despite this success, uncertainties remain regarding the epidemiology and ecological dynamics of the infection. Research has pinpointed bats as the natural reservoir of the virus, although zoonotic transmission to humans is facilitated through an intermediary host, specifically the civet, a species consumed as a delicacy in certain regions of China. The pathogenesis of SARS is characterized by acute respiratory distress syndrome (ARDS), initiated by the viral surface protein's interaction with the ACE2 receptor on the epithelium of the lower respiratory tract. This interaction triggers severe pulmonary inflammation, leading to the deposition of fibrin on the alveolar surfaces, which severely impedes gas exchange. Such pathological changes necessitate advanced medical interventions, including Extracorporeal Membrane Oxygenation (ECMO), for patient management. As of the latest updates, there have been no effective antiviral drugs or vaccines developed specifically for SARS-CoV (World Health Organization; European Center for Disease Control).

MERS-CoV was first identified in Jeddah, Saudi Arabia, in 2012 (Zaki AM. et al., 2012). The virus has since spread to other countries within the Middle East and, at the epidemic's zenith, was reported in 27 countries globally, including regions in Europe. Distinct from SARS-CoV, MERS-CoV continues to pose a significant public health threat, with ongoing transmissions from camels to humans and human-to-human transmission primarily occurring among healthcare workers providing patient care. As of January 2020, sporadic cases were still being reported, notably in the United Arab Emirates. The World Health Organization has reported a cumulative total of approximately 2,500 confirmed MERS cases, with 861 resultant deaths, translating to an estimated mortality rate of 34.4% (World Health Organization, 2019). The prevailing scientific consensus suggests bats as the original reservoir for MERS-CoV, with dromedaries serving as the intermediary host facilitating transmission to humans. However, both the precise mechanism of species jump and subsequent human infection remain to be fully elucidated. Clinically, MERS-CoV infection manifests with severe respiratory symptoms, significant gastrointestinal complications, and in some cases, acute renal impairment. This broader clinical spectrum is attributed to the virus's utilization of a distinct viral entry receptor. Unlike SARS-CoV and SARS-CoV-2, which enter host cells via the angiotensin-converting enzyme 2 (ACE2) receptor, binding to the receptor-binding domain (RBD) of its spike (S) protein, MERS-CoV also owes its entry to the dipeptidyl peptidase 4 (DPP4 or CD26). DPP4 is expressed across a variety of tissues, including the epithelia of the lower respiratory tract, intestines,

and kidneys, facilitating the virus's diverse pathogenic effects. Like SARS, no specific antiviral treatments or vaccines have been developed for MERS, underscoring the critical need for robust containment and prevention strategies (World Health Organization; European Center for Disease Control).

1.1 The emergence of a third, novel coronavirus: SARS-CoV-2

Over the past two decades, coronaviruses have been at the forefront of three significant health crises: the severe acute respiratory syndrome (SARS) outbreak in 2003, the Middle East respiratory syndrome (MERS) in 2012, and the ongoing Coronavirus Disease 2019 (COVID-19) pandemic (Harrison AG. et al., 2020; Dudas G. et al., 2018). These events underscore the evolving nature and impact of coronaviruses on global public health.

SARS-CoV-2, the causative agent of COVID-19, belongs to the *Coronaviridae* family, similar to SARS-CoV and MERS-CoV (Dong E. et al, 2020). The novel virus exhibits a spectrum of symptoms, from mild respiratory syndromes to severe conditions including multi-organ failure and shock, especially in patients with critical and fatal conditions (Stein S.R. et al., 2022).

Despite insights gained from previous coronavirus epidemics, the world is currently unprepared to effectively control the emergent coronavirus, resulting in a significant global health crisis. Unlike its predecessors, SARS-CoV and MERS-CoV, the global community was largely unprepared for the swift emergence and spread of SARS-CoV-2. Contrary to its predecessors, which were contained relatively swiftly, SARS-CoV-2 has caused extensive morbidity and mortality, triggering a global pandemic with far-reaching impacts on public health and the global economy.

SARS-CoV-2 and COVID-19 have imposed the most significant burden on global public health in recent years, representing one of the most severe respiratory diseases encountered (Gebru AA. et al., 2021). The virus was initially identified in a cluster of pneumonia cases in Wuhan, a city in eastern China with a population of over 11 million people in the Hubei province (Yang J. et al., 2020), in late December 2019 (Harrison AG. et al., 2020). The World Health Organization (WHO) quickly recognized the severity of the situation, declaring COVID-19 a Public Health Emergency of International Concern in January 2020 (World Health Organization, 2020) and a pandemic by March 2020 (World Health Organization, 2021).

At the national level, in Italy, the first COVID-19 case was detected on February 21, 2020, in a 38-year-old man from Lombardy. The epidemic swiftly expanded, with Italy experiencing a tragic milestone in March 2020 as it surpassed China in the number of deaths from COVID-19 (Nioi M. et al., 2021). By May 2020, the pandemic had caused over 3.5 million cases and 245,150 deaths globally. As of December 2022, there have been more than 641 million cases and over 6.6 million deaths, underscoring the unprecedented scale and impact of the COVID-19 pandemic (Carabelli A.M. et al., 2023). The COVID-19 pandemic continued to rise significantly in the following months, with widespread and devastating effects of SARS-CoV-2, thus making it one of the most notorious pandemics in recorded human history. In addition, it continues to pose a severe challenge to public health systems worldwide.

SARS-CoV-2 exhibits both similarities and differences compared to previous coronaviruses. It is distinguished by its high transmissibility (World Health Organization, 2021), although its lethality is lower compared to SARS-CoV and MERS-CoV (Holmes EC. et al., 2021). The emergent CoV, the ninth documented human coronavirus, shares phylogenetic roots with its predecessors, underscoring the recurring theme of zoonotic origins in coronavirus evolution. This link is particularly evident in the context of the virus's emergence in Wuhan, where associations with animal markets parallel zoonotic patterns observed in other coronaviruses.

Focused epidemiological investigations have identified the Huanan seafood market in Wuhan as a potential epicenter for the virus’s initial spread. However, the comprehensive dynamics of transmission and the evolutionary trajectory of SARS-CoV-2 remain contentious and are the subject of intense study and debate. Initial epidemiological data indicated a significant correlation between the outbreak’s inception and these marketplaces. Indeed, a meticulous analysis ascertained that approximately 55% of the COVID-19 cases in December 2019 had connections to the Huanan market or other Wuhan markets, predominantly in the early part of the month (World Health Organisation, 2021). The identification of the virus in 2019 was initially nebulous, with its impact and transmissibility not fully comprehended. Following investigations into this probable zoonotic spillover, researchers confirmed the pathogen as a novel *Betacoronavirus*, closely related to the SARS-CoV strain (Harrison AG. et al., 2020).

Genetically, SARS-CoV-2 is the singular member of the *Sarbecovirus* subgenus predominantly found in horseshoe bats, thus suggesting a zoonotic origin (Gorbalenya, AE. et al., 2020). The exact mechanism of transmission to humans, possibly involving an intermediate host, remains a subject of investigation. However, like its predecessors, the zoonotic origin of SARS-CoV-2 is a shared trait among the majority of human-affecting viruses (Holmes EC. et al., 2021). This is

corroborated by its close genetic relationship to a bat coronavirus, with which it shares over 96% of its genome (Zhou P. et al., 2020). In particular, the species of origin (reservoir) for SARS-CoV-2, while not definitively identified, is widely presumed to be bats of the *Rhinolophus affinis* species. This presumption is based on the potential for either direct transmission to humans or transmission through other, yet-to-be-identified intermediate hosts. The natural behaviour of bats, including their close interactions with both other wildlife and humans, might have facilitated the necessary mutations for the virus to jump species. This mechanism is consistent with the emergence of other respiratory illnesses caused by *Betacoronaviruses*. However, the hypothesis of zoonotic transmission directly from the Wuhan seafood market has not been universally confirmed across all cases (Zhou P. et al., 2020; Lu R. et al., 2020). Despite this, there is a significant epidemiological link establishing the Wuhan seafood wholesale market as the epicenter of the outbreak (Paules C. et al., 2020; Li Q. et al., 2020).

The global response to the COVID-19 pandemic has been marked by the rapid development and distribution of vaccines, highlighting the importance of international collaboration in addressing public health emergencies. Despite challenges in achieving equitable vaccine distribution, the World Health Organization's declaration of the end of the global emergency status for COVID-19 in May 2023 signifies a transition towards long-term management of the virus (Giovanetti M. et al., 2023; World Health Organization).

1.1.1 SARS-CoV-2 genome and structure

SARS-CoV-2, classified within the *β*-coronavirus group, exhibits the intricate genomic and structural organization characteristics of the *Coronaviridae* family.

As previously mentioned, it is characterized by an enveloped structure and a single-stranded, positive-sense RNA genome, approximately 30 kb in length, making it one of the largest among RNA viruses. The nucleotide sequence of SARS-CoV-2 displays about 80% sequence identity with SARS-CoV and approximately 50% with MERS-CoV (Harrison AG. et al., 2020). Moreover, it shares a close genetic relationship with the bat-origin coronaviruses (bat-SL-CoVZC45), exhibiting a nucleotide sequence identity of about 90-96% (Ren LL. et al., 2020). The RNA genome of coronaviruses, being among the most expansive, is susceptible to recurrent recombination processes, yielding new strains with varying virulence (Sobhia ME. et al., 2021). The genome features large open reading frames (ORFs) that encode structural and non-structural proteins, including a variety of accessory proteins that contribute to modulating host responses to infection and viral pathogenicity (V'kovski, P. et al., 2021; Singh D. and Yi SV., 2021). In detail, the

SARS-CoV-2 genome consists of a 5’-capped structure and a 3’-polyadenylated tail, enhancing stability and translational efficiency, thereby enabling it to function as messenger RNA within the cellular environment. This strategic configuration facilitates the virus's use of host cellular machinery for protein synthesis, a hallmark of its high infectivity and rapid propagation. Central to the genomic architecture of SARS-CoV-2 are two overlapping open reading frames, designated ORF1a and ORF1b, which collectively occupy approximately two-thirds of the genome proximal to the 5’-end. The translation of these ORFs into polypeptides results in the formation of two large precursor polyproteins, pp1a and pp1ab. These polyproteins are subsequently processed through proteolytic cleavage by viral-encoded proteases, yielding a total of 16 non-structural proteins (nsps), numbered nsps 1 to 16. The ensemble of these nsps forms the replication-transcription complex (RTC), a critical component necessary for the replication of the viral genome and transcription of its mRNA. Specifically, the polyprotein pp1a undergoes proteolytic cleavage, resulting in 11 functional nsps, while pp1ab is cleaved into 15 nsps (Wu CR. et al., 2022) (Figure 1). This process is crucial for the production of proteins that perform various roles, ranging from specific to multifunctional, within the viral life cycle. Furthermore, the remaining one-third of the genome, located at the 3’-end, encodes several ORFs, responsible for producing nine accessory proteins and four structural proteins essential for the virus: spike (S), envelope (E), membrane (M), and nucleocapsid (N). The S, E, and M are integral components of the virion membrane, while the N protein is involved in the binding and packing of the RNA genome (Wu CR. et al., 2022; Santos-López G. et al., 2021).

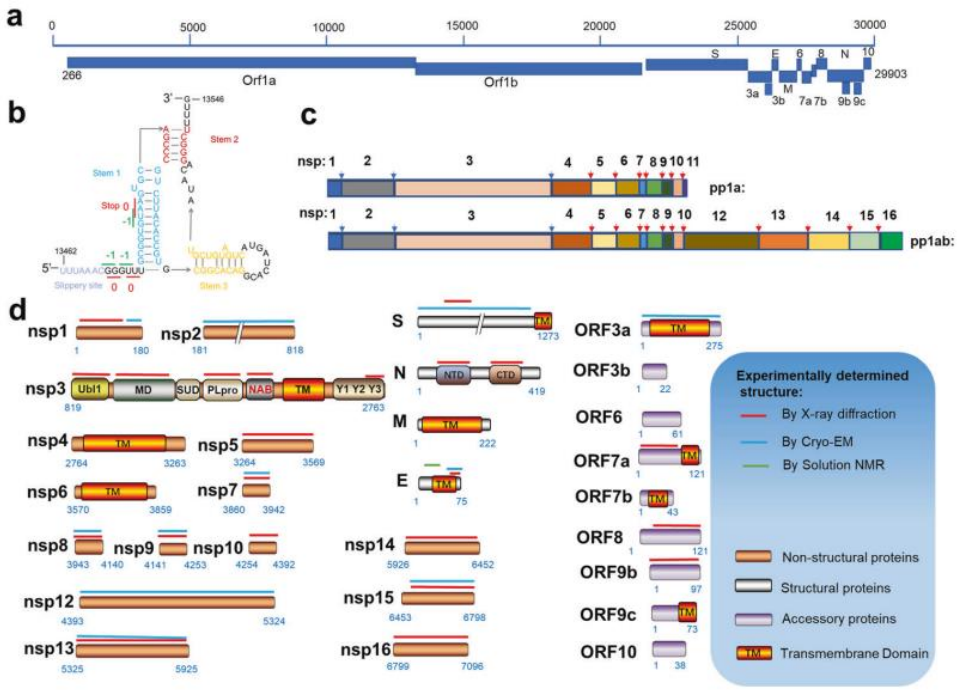


Figure 1. The genome of SARS-CoV-2 and its proteins. **a)** The organization of the SARS-CoV-2 genome. **b)** illustration of the secondary structure of the frameshift stimulation element −1 programmed ribosomal frameshifting, with different functional regions labeled and colored accordingly. **c)** The rectangle represents the non-structural proteins that are produced from the processing of the pp1a and pp1ab polyproteins, with each protein being clearly labeled. The cleavage site for the papain-like protease (PL^{pro}) is indicated by a blue arrow, while the cleavage site for the main protease (M^{pro}) is marked with a red arrow. **d)** The domain architectures of proteins coded by the SARS-CoV-2 genome are outlined along with a summary of the structural characterization of individual proteins (Wu CR. et al., 2022).

1.1.1.1 Non-structural proteins and their functions

In the SARS-CoV-2 genome, the production of non-structural proteins is a sophisticated process initiated by the proteolytic cleavage of the polyproteins encoded by open reading frames ORF1a and ORF1b. This cleavage is catalyzed by viral proteases and results in the generation of a series of nsps, each possessing unique or multiple functions pivotal to the viral replication cycle. Specifically, nsps numbered 1 through 11 derive from the cleavage of the ORF1a polyprotein. In contrast, nsps 12 through 16 are the products of ORF1b polyprotein processing. The orchestration of these proteins' functions underscores the complexity of the viral replication cycle and highlights the potential targets for antiviral drug development. By inhibiting the activity of specific nsps, it may be possible to disrupt the replication cycle of SARS-CoV-2, offering avenues for therapeutic intervention.

Nsp1: known as the leader protein, nsp1 plays a critical role in inhibiting host gene expression, thereby subverting the host's innate immune response. It interacts with the host's 40S ribosomal subunit, resulting in the arrest of host mRNA translation, thus inhibiting the synthesis of host proteins (Wu CR. et al., 2022).

Nsp2: although its exact function remains to be fully elucidated, it is involved in synchronizing viral transcription with translation by simultaneously interacting with both ribosomes and replication-transcription complexes (RTC) (Gupta M. et al., 2021).

Nsp3: as the largest nsp, it possesses the papain-like protease (PL^{pro}) activity, crucial for cleaving the viral polypeptide into mature and functional nsps 1-3. Beyond its role in viral maturation, nsp3's PL^{pro} activity modulates host immune responses (Anand K. et al., 2003; Yang H. et al., 2005), a testament to its multifunctional nature. It also contains several domains, including the ubiquitin-like domain, the macrodomain (also known as the 'X domain'), a nucleic acid-binding domain (NAB), a unique SARS coronavirus domain, a transmembrane domain, and the Y1-3 domain. The transmembrane domain suggests a potential role in viral-host membrane interactions, which could be integral to the virus's lifecycle and pathogenicity (Lei J. et al., 2017).

Nsp4 and *nsp6*: both are involved in the formation of double-membrane vesicles (DMVs), which serve as protective niches for viral RNA synthesis, shielding viral RNA from detection by host cellular sensors (Oostra M. et al., 2008).

Nsp5 (also named as Main Protease, M^{pro}, or $3CL^{pro}$): this protein undertakes a critical function in the viral replication cycle by cleaving polyproteins pp1a and pp1ab at 11 distinct sites. This process is essential for the release and functionalization of mature nsps 4–16, highlighting its centrality in viral maturation (Fehr AR. and Perlman S., 2015).

Nsp7 and *nsp8*: acting as essential cofactors for the RNA-dependent RNA polymerase (RdRp, Nsp12), nsp7 and nsp8 significantly enhance the enzymatic activity of RdRp, underlining their importance in the viral RNA synthesis process (Wu CR. et al., 2022).

Nsp9: recognized for its RNA-binding capability, nsp9 is believed to play a role in viral RNA replication and may regulate replication and transcription processes by inhibiting the nucleotidyltransferase activity of nsp12 (Yan L. et al., 2020).

Nsp10: it is a cofactor for several other nsps, including nsp14 and nsp16 (Jiang Y. et al., 2020), enhancing their activities in mRNA capping and proofreading, which are vital for maintaining the integrity of the viral genome.

Nsp11: it is essentially considered a part of nsp12 in the context of SARS-CoV-2, as the cleavage product of pp1ab. It is often not distinguished as a separate functional protein due to its overlap and continuity with nsp12 in polyprotein processing.

Nsp12: also known as the central component of the viral replication-transcription complex, RdRp, it is responsible for the synthesis of viral RNA. Its function as an RNA-dependent RNA polymerase and nucleotidyltransferase is crucial for the replication of the viral genome (Yin W. et al., 2021).

Nsp13: it acts as a helicase that unwinds RNA, an essential process during viral replication and transcription of the viral RNA (Wu CR. et al., 2022).

Nsp14: it contains an exoribonuclease (ExoN) domain for proofreading, which is unique among RNA viruses, and an N7-methyltransferase domain for mRNA capping, critical for viral mRNA stability and immune evasion (Lin S. et al., 2021).

Nsp15: a uridine-specific endoribonuclease, nsp15 assists the virus in evading the host's immune response by processing viral RNA to limit its recognition by the host's immune sensors (Kim Y. et al., 2020).

Nsp16: this protein works in conjunction with nsp10 to methylate the 5' cap of the viral mRNA, mimicking host mRNA structure to evade immune detection. This modification is crucial for the successful replication and spread of the virus within the host (Rosas-Lemus M. et al., 2020).

In conclusion, the critical roles played by nsps, particularly the main protease (M^{pro}) and papain-like protease (PL^{pro}), in the maturation and functionality of the viral replication machinery have positioned them as significant targets for COVID-19 therapeutic intervention. This focus underscores the potential for developing antiviral drugs aimed at inhibiting these key viral enzymes (Wu CR. et al., 2022).

1.1.1.2 Structural proteins

Structural proteins are pivotal in constituting the viral particle of SARS-CoV-2 (Kang S. et al., 2020; Lu R. et al., 2020). Among these proteins, the spike protein is particularly notable for its highly antigenic nature and its position on the exterior of the virus, which significantly contributes to the crown-shaped appearance of the virion. It plays an essential role in mediating the binding to host receptors and promoting membrane fusion, essential for viral entry (Moreira RA. et al., 2020). The nucleocapsid protein provides genomic protection and participates actively in the synthesis of viral RNA, while the membrane protein imparts structural integrity and stability to the virion. The envelope protein, functioning as an ion channel, is crucial during the virion assembly and release from the host cell (Lim YX. et al.,

2016). Specifically, the four structural proteins and their functions are analyzed in detail, highlighting their significance in the virus's life cycle.

Spike Protein (S): the S protein, a trimeric glycoprotein (Li F., 2016) that protrudes from the viral surface, is instrumental in giving the virus its distinctive crown-like appearance. Genetic analysis reveals that the S gene of SARS-CoV-2 exhibits considerable variability when compared to its SARS-CoV counterpart, with less than 75% nucleotide identity (Harrison AG. et al., 2020). This protein plays a critical role in mediating the virus's entry into host cells (Thomas S., 2021), primarily through its binding to the angiotensin-converting enzyme 2 (ACE2) receptor. Structurally, the S protein is divided into two subunits: S1, which houses the receptor-binding domain (RBD) that directly engages with ACE2, and S2, responsible for the fusion of the viral and cellular membranes. A notable feature of the S protein is its S1/S2 polybasic cleavage site, which undergoes proteolytic cleavage by cellular enzymes such as cellular cathepsin L and transmembrane protease serine 2 (TMPRSS2). This cleavage is a crucial step, enhancing the virus's ability to enter host cells (Harrison AG. et al., 2020; Moreira RA. et al., 2020; Huang Y. et al., 2020).

Envelope Protein (E): the E protein is a small integral membrane protein involved in virus assembly and release, contributing to the virus's pathogenesis through its ion channel activity (Nieto-Torres JL. et al., 2014; Schoeman D. and Fielding BC., 2019).

Membrane Protein (M): being the most abundant structural protein in the virion, the M protein plays a fundamental role in shaping the virus and facilitating the nucleocapsid encapsulation, thus playing a pivotal role in virus assembly, associated with N protein and other viral structural proteins, budding, and envelope formation (Fu YZ. et al., 2021; Siu YL. Get al., 2008).

Nucleocapsid Protein (N): the N protein protects the genome from host cells and is involved in viral RNA synthesis. In detail, it packages the RNA genome into a helical ribonucleocapsid (RNP) and contributes to viral replication, cell cycle modulation, and host cell response, thereby promoting virion assembly (Sheikh A. et al., 2020; Zeng W. et al., 2020; Wu CR. et al., 2022).

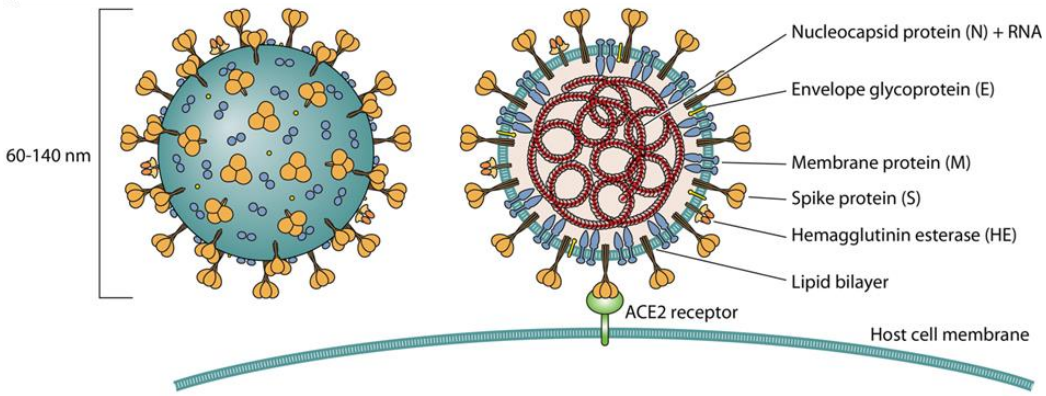


Figure 2. Structure of SARS-CoV-2: diagram of the virion (Safiabadi Tali SH. et al., 2021).

1.1.1.3 Accessory proteins

Besides the structural proteins, the SARS-CoV-2 genome encodes several accessory proteins. These proteins, though not essential for replication, significantly influence the host's immune response and contribute to the virus's virulence and adaptability.

The coding regions for accessory proteins, located in the 3' region, are named ORF3a, ORF6, ORF7a, ORF7b, ORF8, ORF9b, and ORF10.

ORF3a: it encodes the accessory protein 3a, which is involved in virus replication and has been implicated in modulating the host's immune response. It is known to form an ion channel in the host cell membrane and plays a role in virus release from host cells (Wu CR. et al., 2022; Kern DM. et al., 2021).

ORF6: the protein has a role in immune evasion by interfering with the host's interferon signaling, a key aspect of the immune system's strategy to combat viral infections.

ORF7a: as a type I transmembrane protein, ORF7a encodes the accessory protein 7a, which is believed to be involved in apoptosis. It is also an immunomodulatory factor for immune cell binding and is involved in dramatic inflammatory responses.

ORF7b: a smaller ORF, partially overlapping with ORF7a, encodes the accessory protein 7b. Its function is not fully understood but is thought to increase the virulence of SARS-CoV-2 (McBride R. and Fielding BC., 2012).

ORF8: it encodes the accessory protein 8, which plays a role in immune evasion by interacting with major histocompatibility complexes I, thus modulating its

degradation in cell cultures, thereby contributing to immune evasion (Zhang Y. et al., 2021).

ORF9b: it encodes the accessory protein 9, which is involved in suppressing the host's interferon response (Gao X. et al., 2021).

ORF10: this ORF encodes the accessory protein 10, which is less understood than other accessory proteins. Its function in the viral life cycle and pathogenesis is currently under investigation (Pancer K. et al., 2020).

To date, only the structures of ORF3b, ORF6, ORF9c, and ORF10 remain unsolved (Wu CR. et al., 2022).

1.1.2 Coronaviruses replication cycle

The replication cycle of SARS-CoV-2 infection within the host cell can be divided into several key steps: *(a)* attachment and cell entry, *(b)* viral replication transcription, *(c)* genomic transcription and replication, *(d)* translation of structural proteins, and *(e)* assembly and release of virions (Hoffmann M. et al., 2020).

The cycle begins with the SARS-CoV-2 Spike protein binding to the ACE2 receptor, abundantly present on cells in the respiratory tract, from the nasal and oral cavities to the pulmonary alveoli (Hoffmann M. et al., 2020; Zhou P. et al., 2020; Zhang W. et al., 2020; V'kovski, P. et al., 2021). This interaction is facilitated by the host protein, called transmembrane serine protease 2 (TMPRSS2), which activates the S protein, enabling viral entry through endocytosis (Hoffmann M. et al., 2020). The entry of the virus induces a conformational change in the S protein, leading to the fusion of viral and endosomal membranes and the subsequent release of the nucleocapsid into the cytoplasm. Here, the genomic RNA is directly translated into the ribosome, resulting in the production of polyprotein pp1a (Santos-López G. et al., 2021; Liu DX. et al., 2014). A ribosomal frameshift at the end of the pp1a coding sequence extends the reading frame to produce the pp1ab polyprotein. These polyproteins are then cleaved by viral proteases PL^{pro} and $3CL^{pro}$ into 16 non-structural proteins with pivotal roles in viral replication and assembly. These nsps induce the rearrangement of cellular membranes to form double-membrane vesicles (DMVs) (Angelini MM. et al., 2013), where the viral replication-transcription complex is assembled. This complex synthesizes new genomic RNA and a set of negative-sense subgenomic RNAs acting as templates for structural and accessory proteins (Wrapp D. et al., 2020). The structural proteins S, E, M, and hemagglutinin-esterase (HE) are synthesized in the endoplasmic reticulum, while nucleocapsid proteins are produced in the cytosol. Virus assembly occurs in the ER-Golgi intermediate compartment (ERGIC), predominantly orchestrated by the

M protein, which facilitates the recruitment of structural components and virion morphogenesis. The envelope protein facilitates the assembly process by interacting with the M protein. Ultimately, newly formed coronavirus particles are then enclosed within vesicles, trafficked through the secretory pathway, and finally new virions are released from the host cell via exocytosis (Santos-López G. et al., 2021; Lim YX. et al., 2016).

The replication cycle of coronavirus within the host cell is depicted in Figure 3.

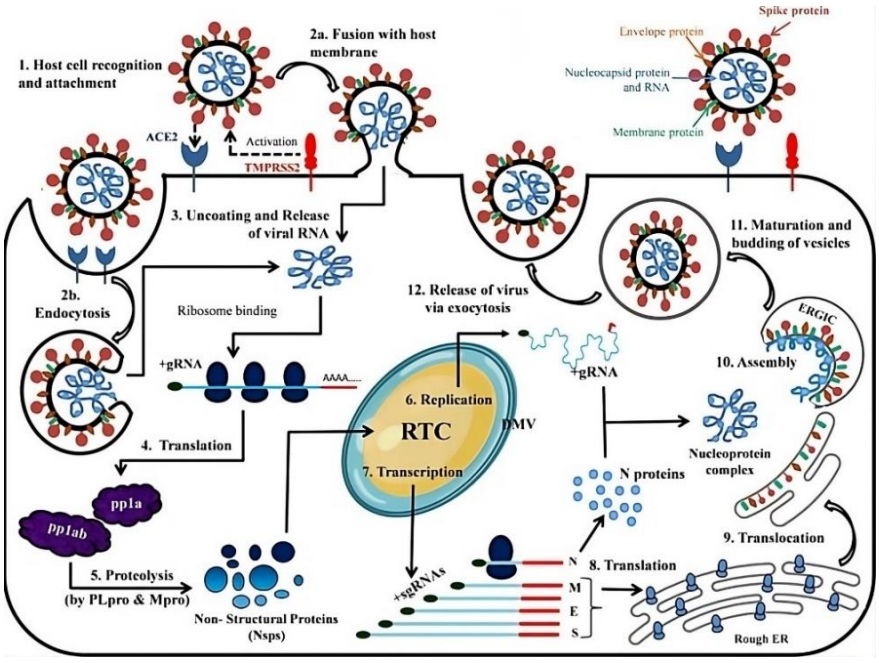


Figure 3. Stages of SARS-CoV-2 replication within the host cell: a step-by-step illustration (Arya R. et al., 2021).

1.1.3 Insights into the structure and function of SARS-CoV-2 main protease

The chymotrypsin-like protease ($3CL^{pro}$), also recognized as the main protease (M^{pro}) or formally C30 endopeptidase (Ahmad B. et al., 2021), is a critical cysteine protease in coronaviruses, essential for viral replication and maturation. It orchestrates the maturation of several proteins by acting on 11 cleavage sites, mainly at the Leu-Gln↓(Ser/Ala/Gly) sequence in the viral genome translation products (Fehr AR. and Perlman S., 2015).

This protease is active as a homodimer but exists in a dynamic monomer-dimer equilibrium in solution (Graziano V. et al., 2006; Chen H. et al., 2006; Shi J. and

Song J., 2006; Needle D. et al., 2015; Shi J. et al, 2008). In fact, it consists of two monomers arranged nearly perpendicular to each other (Zhang L. et al., 2020), creating a substantial dimer interface through their C- and N-termini, more closely held in the dimeric state compared to the monomeric state. Each monomer is organized in three domains: domain I (residues 8–101), domain II (residues 102–184), and domain III (residues 201–303), with the catalytic Cysteine-Histidine dyad (His41 and Cys145) nestled in the active site between domains I and II (Fan K. et al., 2004). Structurally, domains I and II are predominantly β-sheets, while the dimer interface is composed of adjacent helices (domain III) and loops (Dubanevics I. and McLeish TCB., 2021; Pillaiyar T. et al., 2016).In the active site, a hydrogen-bond interaction between Ser1 (the N-terminal residue) of a protomer and residue Glu166 from another protomer is essential for keeping the active pocket in the correct shape and conformation for efficient catalysis. The dimerization of SARS-CoV-2 main protease, crucial for enzymatic activity, hinges on the interaction between the N-finger of each monomer and Glu166 of the other monomer, ensuring the correct orientation of the S1 pocket in the substrate binding site (Goyal B. and Goyal D., 2020).

Biochemical analysis revealed that both the integrity of the catalytic site and dimerization are essential for the protease enzymatic efficacy (Yang H. et al., 2003; Chen CC. et al., 2021), underscoring their indispensable roles in catalytic activity.

1.1.3.1 Structure comparison of 3CL^{pro}s from SARS-CoV, MERS-CoV and SARS-CoV-2

The 3CL^{pro}, pivotal in coronavirus replication, is highly conserved among different species (Sobhia ME. et al., 2021; Yang H. et al., 2005; Chen CC. et al., 2021).

The structural and functional properties of SARS-CoV-2 3CL^{pro} closely align with those of MERS-CoV and SARS-CoV (Chen CC. et al., 2021; Ho BL. et al., 2015; Cheng SC. et al., 2010). Specifically, through the three-dimensional structural configuration, the SARS-CoV-2 main protease exhibits a 96% sequence identity with SARS-CoV M^{pro} (Goyal B. and Goyal D., 2020) and 52% with MERS-CoV M^{pro} (Chen CC. et al., 2021), suggesting a shared catalytic mechanism between them. Out of the total 306 amino acid residues that constitute the SARS-CoV-2 M^{pro}, only 12 differ from those in SARS-CoV. However, it is notable that these variant residues -T35V, A46S, S65N, L86V, R88K, S94A, H134F, K180N, L202V, A267S, T285A, and I286L- do not significantly influence the catalytic activity of SARS-CoV-2 M^{pro}. Consequently, the overall structure of SARS-CoV-2 M^{pro} remains largely unaffected by these mutations, aligning closely with the structure of SARS-CoV M^{pro} (Goyal B. and Goyal D., 2020; Sobhia ME. et al., 2021). This similarity is further corroborated

by homology models, reinforcing the M^{pro} enzymes' structural congruence (Goyal B. and Goyal D., 2020).

1.1.3.2 $3CL^{pro}$ as a promising antiviral target

The structural conservation of main proteases among different coronaviruses, coupled with their critical roles in viral replication, underscores their importance as promising and attractive targets for broad-spectrum antiviral strategies (Yang H. et al., 2005; Sobhia ME. et al., 2021). Considering the extensive research on SARS-CoV during the past few decades, it serves as a model for understanding the structural basis of SARS-CoV-2 $3CL^{pro}$ mechanism (Chen CC. et al., 2021), presenting opportunities for designing a variety of coronavirus 3CL protease inhibitors.

The previously mentioned similarity between SARS-CoV and SARS-CoV-2 suggests that inhibitors originally designed to target SARS-CoV M^{pro} could also effectively inhibit the enzymatic activity of the main protease of SARS-CoV-2. This hypothesis is supported by research showing that inhibitors effective against SARS-CoV M^{pro} have also shown efficacy against MERS-CoV (Li Q. et al., 2020; Sobhia ME. et al., 2021). Moreover, protease inhibitors have drastically reduced mortality rates for HCV/HIV, highlighting their therapeutic potential (Kurt Yilmaz N. et al., 2016).

The main protease inhibitors present a paramount aspect in the realm of antiviral therapeutics, primarily due to their distinct specificity and low probability of inducing toxicity in human cells. This advantage stems from the absence of analogous human proteases with a similar cleavage specificity, notably the Leu-Gln↓(Ser/Ala/Gly) sequence, which is uniquely recognized by the M^{pro}. Targeting this specific cleavage sequence offers a strategic and effective method to impede viral replication, thereby serving as a pivotal pathway in the development of antiviral agents.

The role of the enzyme in coronavirus replication without adverse toxicity, coupled with its high degree of conservation across strains, underscores its potential as a strategic target for drug development.

The ongoing research on M^{pro} inhibitors is a cornerstone in the global effort to develop effective therapies against SARS-CoV-2 and other coronaviruses, in live with the broader objective of curbing the spread and impact of current and future coronavirus pandemics.

Having established the pivotal role of employing the 3CL protease to mitigate the spread of SARS-CoV-2, it is appropriate to delve into potential strategies, especially considering that the development of the main protease inhibitors opens new

avenues for effective drug discovery against a range of coronaviruses, including SARS-CoV, SARS-CoV-2, and MERS-CoV.

Central to the appeal of M^{pro} as a therapeutic target is the dual strategy it presents for inhibitor development: targeting its substrate-binding pocket to impede catalytic activity, and inhibiting the dimerization process, which is essential for the protease's functionality.

The exploration of this dual approach can pave the way for effective drugs against various coronaviruses, including SARS-CoV-2.

1.1.3.2.1 Targeting the substrate-binding pocket

The substrate-binding pocket inhibitors aim to hinder the enzyme's catalytic function, a key step in the viral replication process. A substantial body of research has focused on the substrate binding pocket of SARS-CoV M^{pro}, resulting in the identification of numerous potential inhibitors. Although several inhibitors have been proposed, their translation into clinical applications is still pending. This gap underscores the critical challenge of converting theoretical inhibitor designs into practical, clinically effective treatments.

The cysteine protease has an essential role in processing the polyproteins necessary for the virus lifecycle. Studies, including those by Bacha et al. and Barrila et al. (Bacha U. et al., 2004; Barrila J. et al., 2006), have highlighted the significance of a cluster of serine residues (Ser139, Ser144, Ser147) adjacent to the active site of SARS-CoV M^{pro}. Alteration of these residues significantly affects the enzyme catalytic efficiency, suggesting their potential as broad-spectrum therapeutic targets against coronaviruses. Further investigations by Chou et al. (Chou CY. et al., 2004) have revealed that environmental factors, such as salt concentration and pH levels, impact the dimerization and activity of the main protease, pointing to the critical roles of Arg4 and Glu290 in maintaining its functional dimerization and enzymatic action. In-depth analyses by Chen et al. (Chen S. et al., 2004) have shown that N-terminal truncation of M^{pro} leads to structural and functional alterations, specifically affecting the dimer's spatial arrangement and substrate-binding capability. Additionally, studies employing crystallography and molecular dynamics simulations have elucidated the conformational flexibility of the enzyme. It was demonstrated that the dimensions and conformation of the substrate binding pocket S1 are influenced by the protonation states of His163 and His172, integral components of the pocket. Significantly, the N-terminus of one monomer in the M^{pro} dimer is crucial for the enzyme's catalytic activity. This region ensures the correct conformation of the oxyanion loop and the S1 substrate binding pocket

through hydrogen bond interactions, which are essential for the enzymatic function of the enzyme (Goyal B. and Goyal D., 2020).

1.1.3.2.2 Targeting the dimerization

Exploring an alternative, and potentially promising, therapeutic strategy involves targeting the structural integrity of the main protease to inhibit its dimerization, a crucial aspect of its enzymatic activity. The functionality of SARS-CoV M^{pro} is contingent upon its dimeric structure, with the monomeric forms being inactive. This characteristic has guided the development of inhibitors that specifically target the dimerization process. While research on substrate-binding pocket inhibitors is more established, the exploration of dimerization inhibitors represents a novel approach offering a different pathway to obstruct the enzymes' functionality.

Dimerization inhibitors, having shown efficacy against HIV protease and other viral enzymes (Ye C. et al., 2019; Pietrucci F. et al., 2015; Bannwarth L. et al., 2009; Schramm HJ. et al., 1991), offer a promising avenue, since it could potentially circumvent drug resistance issues that may arise due to viral mutations, thereby broadening the spectrum of effective antiviral agents.

Exploiting previous research on SARS and MERS provides a solid basis for designing new dimerization inhibitors targeting SARS-CoV-2 3CL protease, addressing the urgent need to combat this rapidly evolving virus on an invisible battlefield.

In this regard, recent studies have identified key residues crucial for the dimerization and catalytic activity of SARS-CoV 3CL protease, paving the way for future inhibitor design. Molecular dynamics analysis of the mentioned enzyme serves as a guide for structure-based design, while existing dimerization inhibitors provide a foundation for further modifications to develop potent antiviral agents. Hsu et al. (Hsu WC. et al., 2005) and subsequent studies have underscored the importance of both N-terminal and C-terminal regions in stabilizing the dimeric structure of 3CL protease and its enzymatic efficiency. These studies indicated that modifications in key residues, such as Arg4, profoundly affect the enzyme's catalytic efficiency and dimeric state. Additionally, research by Graziano et al. and Zheng et al. further have reinforced the necessity of dimerization for protease activity, demonstrating that interactions between the monomers are essential for maintaining the correct conformation of the catalytic pocket. This understanding has profound implications for drug development, as it highlights the potential of targeting the substrate-binding pocket or inhibiting the enzyme's dimerization as effective strategies for blocking viral replication. In 2005, Hsu et al. conducted a study suggesting that targeting the dimer interface with inhibitors could

potentially block the maturation process of the protease (Hsu WC. et al., 2005; Goyal B. and Goyal D., 2020). In 2005, Ding et al. embarked on a study (Ding L. et al., 2005; Goyal B. and Goyal D., 2020) to explore the interaction between the SARS-CoV main protease and a dimerization inhibitor, N8 (SGFRKMAF). Their findings highlighted that hydrophobic contacts and electrostatic interactions were key factors in the binding process of the dimerization inhibitor with SARS-CoV M^{pro}. Subsequent investigations with N8 and its mutant forms demonstrated the effectiveness of N8 in inhibiting the dimerization of the protease enzyme, underscoring the significant role of hydrophobic contact and electrostatic interaction in its binding efficiency (Wei P. et al., 2006). In 2006, Chen et al.'s study, using molecular dynamics simulations and mutational analysis, revealed that the SARS-CoV main protease is catalytically active only in its dimeric form (Chen H. et al., 2006; Goyal B. and Goyal D., 2020). Within the dimer, the monomers are asymmetric, with only one monomer being active at a time. This study showed the importance of the dimerization, necessary for the enzyme's catalytic function. Thus, by inhibiting dimerization, the enzymatic activity can be effectively blocked. The 2007 study by Zheng et al. revealed that interactions between the N-termini of the two monomers are key for maintaining the dimer's enzymatic function (Zheng K. et al., 2007). This finding is significant for designing inhibitors targeting the dimer interface, which could lead to the development of effective treatments against SARS-CoV. Chen et al. focused on the dimerization and enzymatic activity of the major protease of SARS-CoV. They found that specific residues, particularly Ser10, Glu14, and Gly11, located in the α-helix A' of domain I, are crucial for the stability and activity of the enzyme's dimer (Chen S. et al., 2008). Alteration of these residues had a significant impact on the function of the enzyme, resulting in weakened dimerization and loss of enzyme activity, while mutation of Gly11 led to complete inactivation and dissociation of the dimer. The results underscore the importance of these residues in the dimerization-activity relationship of the enzyme and provide insights for the design of antiviral compounds targeting the dimer interface of SARS-CoV $3CL^{pro}$. In their 2008 analysis, Lin et al. investigated C-terminal truncated mutants of the SARS-CoV enzyme. While the deletion of the C-terminus had no impact, the removal of Gln299 or Arg298 significantly reduced catalytic activity, indicating their role in dimerization (Lin PY. et al., 2008; Shi J. et al., 2008).

Chapter II

Natural compounds

Natural compounds, encompassing a vast array of bioactive molecules produced by plants, animals, and microorganisms, serve as a cornerstone in the exploration of biochemical diversity and its application across various scientific and industrial fields.

These bioactive molecules possess a unique chemical diversity, honed through evolutionary processes for optimal interactions with biological macromolecules (Rosén J. et al., 2009), thus playing crucial roles in the defense mechanisms, ecological interactions, and survival strategies of organisms. Their vast array of secondary metabolites, evolved over millennia, significantly impacts pharmacology, biotechnology, and sustainable development sectors.

Historically, natural products have been a foundational source for drug discovery, contributing to more than half of all drug approvals since the introduction of modern screening technologies. This is especially notable in oncology and infectious disease research, where over a hundred natural-product-derived compounds are currently undergoing clinical trials, showcasing the ongoing relevance of these substances (Harvey AL., 2008). The integration of molecular biology techniques with traditional approaches has enhanced the accessibility and production of novel compounds, allowing for their synthesis in microorganisms and the application of combinatorial chemistry to create libraries based on natural product frameworks. This approach, alongside advanced screening methods, data mining, and virtual screening, is streamlining the incorporation of natural products into drug discovery campaigns. Approximately 40% of therapeutic drugs approved by the US Food and Drug Administration (FDA) in the past three decades are attributed to natural products, underscoring their significance in modern medicine (Harvey AL. et al., 2015). Despite their proven efficacy, evidenced by the approval of significant drugs and the compliance of many with Lipinski's “Rule of Five” (Lipinski CA. et al., 1997), the pharmaceutical industry's engagement with natural products has waned due to challenges related to supply, complexity, and intellectual property concerns. However, the trend is shifting with a renewed interest in natural compounds, especially those derived from plants and microbes, across various therapeutic areas. This resurgence is bolstered by the FDA's approval of natural products, highlighting a growing appreciation for the therapeutic potential of natural compound mixtures.

Medicinal plants, in particular, are recognized as a valuable and rich source of new antimicrobial agents, playing a vital role in advancing research within microbiology and the pharmaceutical industry. Extracts derived from plants have historically been a cornerstone of the pharmaceutical sector. As much as 40% of present-day medications originate from natural sources, employing either the natural substances themselves or synthesized versions (Gautam R. et al., 2007). Although medicinal plants have been used for centuries as sources of therapeutic agents worldwide, they cannot be classified as pure and efficient antimicrobial agents. However, even though plant-derived antibacterial compounds generally show a low degree of activity, most plants succeed in fighting infections (Hemaiswarya S. et al., 2008). Plants, in fact, employ 'synergy' as a distinctive paradigm to combat pathogenic microorganisms. Multiple studies have demonstrated that specific natural products, previously ineffective as antimicrobials, can significantly enhance the effectiveness of chemotherapeutic agents against Gram-negative bacteria (Gibbons S. and Udo EE., 2000; Greco WR. et al., 1995; Stavri M., 2007; Tegos G. et al., 2002).

The widespread adoption of nutraceuticals, dietary supplements, and functional foods has surged in popularity over recent decades, propelled by a heightened interest in natural products and their potential health benefits. This interest is also supported by a growing body of scientific literature suggesting that natural products are generally less toxic than their synthetic counterparts (Kotha RR. and Luthria DL., 2019).

Natural compounds continue to play a vital role in both traditional and modern medicine, offering promising therapeutic options for a range of diseases including cancer, cardiovascular diseases, diabetes, Alzheimer's disease, and more (Shahrajabian MH. and Sun W., 2023; Kotha RR. and Luthria DL., 2019; Santosh K. et al., 2007). Their continued study and integration into therapeutic strategies hold the potential for groundbreaking advancements in healthcare and disease management.

2.1 Lichen secondary metabolites

A lichen represents a complex microbial community characterized by a fundamental symbiotic association between at least a mycobiont (a fungal component) and a photobiont (a photoautotrophic partner), which is typically a green alga in “chlorolichens” or cyanobacterium in “cyanolichens” (Insarova ID. and Blagoveshchenskaya EY., 2023). This symbiotic alliance forms a stable taxonomic entity with a rich evolutionary history, positioning lichens among the earliest multicellular organisms to transition from aquatic to terrestrial habitats.

Evidence of their ancient existence is found in marine phosphorite in South China, dating back to between 551 and 635 million years ago. This discovery predates both the earliest known fossil land plant, approximately 475 million years old, and the most ancient terrestrial lichen fossil, *Winfrenatia reticulata*, found in Scotland, dating back to around 400 million years ago. The enduring presence of lichens throughout evolution underscores the remarkable efficacy of their symbiotic relationships (Calcott MJ., et al., 2018). In contemporary times, lichens have adapted to exhibit a vast array of forms, each with the mycobiont body (thallus) adapting in distinct ways to showcase the photobiont for efficient light capture (Petrzik K. et al., 2014). As of 2000, the estimated count of lichen species ranged from 13,500 to 30,000. Current estimates could reasonably be higher; in recent years, the identification of species has surged due to expanded exploration into remote regions, more meticulous examination, and the application of novel sequencing methodologies. The nature of the lichen symbiotic association is an evolving narrative, with unexpected depth and complexity unveiled in recent decades through advancements in molecular biology (Petrzik K. et al., 2014; Calcott MJ., et al., 2018).

Lichen compounds inhabit a wide range of terrestrial environments, from tropical to polar regions, showcasing a rich biodiversity estimated at approximately 17,000 species worldwide (Petrzik K. et al., 2014). Recognized as the earliest colonizers of terrestrial habitats, they demonstrate remarkable adaptability, adding vibrant colors to the surroundings due to the accumulation of diverse secondary metabolites. Specifically, they include 16,750 lichenized *Ascomycetes*, 200 *Deuteromycetes*, and 50 *Basidiomycetes*. The majority of phycobionts belong to the *Chlorococcales* (83%), encompassing genera like *Trebouxia*, *Myrmecia, Chlorella*, *Pleurococcus*, and *Coccomyxa*. Others are found among the Ulotrichales (9%) and cyanobacteria (8%), such as Nostoc, Gloeocapsa, Scytonema, and Calothrix (Ahmadjian, 1993). Japanese researchers made significant strides in characterizing the chemical structures of various lichen compounds. Notably, between 1880 and 1975, Yasuhiko Asahina, Shoii Shibata (Shibata S., 2000), and their colleagues studied the biosynthesis of lichen substances and introduced micro-recrystallization as a straightforward method for determining these substances (Shibata S., 1958; 2000). This method relied on certain reagents inducing characteristic crystal forms in lichen substances, allowing for their microscopic identification.



Figure 4. Lichens exhibit significant diversity in both growth forms and colors. The top row showcases crustose lichens: *Caloplaca epithallina*, *Carbonea vitellinaria*, and *Icmadophila ericetorum*. The middle row features foliose lichens: *Lobaria pulmonaria*, *Arctoparmelia centrifuga*, and *Leptogium saturninum*. The bottom row presents fruticose lichens: *Cladonia stellaris*, *Ramalina calicaris*, and *Bryoria nitidula*. (Asplund J. et al., 2017)

Subsequent utilization of thin-layer chromatography (TLC) and high-performance liquid chromatography (HPLC) by lichen experts greatly enhanced our comprehension of the distribution of secondary metabolites within lichens. This advancement profoundly influenced lichen chemotaxonomy and unveiled intriguing evolutionary connections. Some secondary metabolites are widespread across evolutionary lineages, while others exhibit considerable variability even within a single species. C.F. Culberson published data on approximately 430 lichen substances, detailing their distribution among various species, in three influential books (Culberson, 1969; 1970; Culberson et al., 1977). These works contributed significantly to our understanding of lichen chemistry and its implications for taxonomy. The roster of clearly characterized lichen substances has notably expanded since 1977, with over 800 compounds documented in the most recent comprehensive compilations (Huneck S. and Yoshimura Y., 1996). Structures for over 1000 lichen substances have been elucidated, yet a comparable number of lichen substances are awaiting chemical characterization. However, even with the identification of all readily detectable extrolites, a substantial count of additional secondary metabolites, primarily existing in low concentrations, would undoubtedly still necessitate characterization.

Lichens produce an array of secondary compounds primarily stemming from the secondary metabolism of the fungal component, many of which are unique to lichen production. Chemotaxonomic studies indicate that the most distinctive

lichen metabolites belong to chemical classes such as depsides, depsidones, and dibenzofurans. Among the nearly 800 identified lichen secondary metabolites, classification aligns with classic biosynthetic pathways: the polyketidic path (encompassing monocyclic phenols, depsides, depsidones, dibenzofurans, xanthones, naphthoquinones, anthraquinones, macrocyclic lactones, aliphatic acids, etc.), the mevalonic acid path (involving steroids, carotenoids, etc.), and the shikimic acid path (encompassing derivatives of amino acids, cyclopeptides, etc.) (Huneck S., 1999; Calcott MJ. et al., 2018).

The synthesis of a wide array of metabolites in lichens has been attributed to several ecological and physiological mechanisms, each contributing to the survival and adaptability of lichens in various environments:

1. Lichens exhibit slow growth rates, which may necessitate the synthesis of metabolites with antibiotic properties to fend off microbial competitors and predators (Ingolfsdottir K. et al., 1985).
2. Lichen substances enhance the permeability of the phycobiont cell walls, potentially facilitating nutrient exchange and enhancing symbiotic efficiency (Gardner CR. et al., 1981).
3. Aromatic compounds within lichens can strongly absorb UV light, offering protection to the phycobiont components from harmful radiation (Rundel PW., 1978; Lawrey JD., 1986).
4. Specific lichen metabolites (e.g., norstictic, psoromic, usnic, isousnic acids) have been observed to form complexes with metals (e.g., K, Cu, Fe), suggesting a role in mineral uptake from their substrates, which could be vital for their survival in the nutrient-poor environment (Purvis et al., 1987; Jones D., 1988).
5. Lichen substances exhibit toxicity towards various insects, snails, and nematodes (Lawrey JD., 1986; Ahad AM. et al., 1991), indicating a defensive mechanism to deter herbivory and invasion.
6. Lichen substances can act as stress compounds, organic substances produced by plants under extreme conditions (Lange, 1992) to protect the organism, a feature shared with higher plants.
7. Many lichen metabolites are secreted into the lichen's medulla, where their hydrophobic properties prevent water saturation and facilitate the continuous exchange of gases with the environment, crucial for their photosynthetic and respiratory processes (Armaleo D., 1993).

Over the centuries, lichens and their secondary compounds have served various purposes for both humans and animals. Despite advancements in medical

sciences, tribal communities continue to harness these organisms for their nutritive, medicinal, decorative, brewing, distilling, dyeing, cosmetic, and perfumery properties (Verma N. and Behera BC., 2014). Ethnobotanical studies conducted worldwide in the last five decades have unveiled diverse traditional uses of lichens. Examples include the consumption of *Cetraria islandica* in Europe as a drink for convalescents, its use in France as an emollient (Novaretti R. and Lemordant D., 1990), and in Spain for treating catarrh, asthma, and inflammation (Verma N. and Behera BC., 2014). In Alaska, *Cladonia* species are employed as medicine for diarrhea (Silva JA. et al., 2010), and *Lobaria pulmonaria* is used in Canada to address coughing up blood. Additionally, various *Usnea* species find applications in Chinese medicine for expectorant purposes and ulcer treatment, while *U. africana* is used in East Africa to alleviate stomach pain (Hao YM. et al., 2023; Odabasoglu F. et al., 2005) and *U. filipendula* to protect wounds from bacterial infections (Moskalenko SA., 1986). These examples underline the broad spectrum of lichen uses, reflecting their integral role in traditional healthcare systems. In Asia, the cultural and medicinal use of lichens persists, with *Lobaria pulmonaria* being employed for an array of conditions including eczema, respiratory troubles, hemorrhages, and asthma (Cardinale M. et al., 2012). *Heterodermia diademata* is used for wound care, demonstrating lichens' significance in traditional healing practices (Saklani A. and Upreti DK., 1992). Furthermore, in various regions of India, species from the *Parmeliaceae* family are used for their efficacy in treating gastrointestinal and reproductive system disorders, showcasing the diverse applications of lichens in traditional medicine (Verma N. and Behera BC., 2014).

The widespread use of lichens across different cultures and continents underscores their importance not only in traditional medicine but also in contributing to the well-being of communities. This enduring relevance highlights the need for continued research and conservation of these remarkable organisms, ensuring their availability for future generations while respecting their cultural heritage and ecological significance.

2.1.1 Exploring the multifaceted biological activities of lichens

Lichens, embodying the essence of symbiotic resilience, possess a diverse array of biological properties that have captured the interest of scientists across various fields, setting the stage for groundbreaking research into their potential applications.

Exploring the pharmaceutical horizon, lichens present a spectrum of biological activities with promising therapeutic implications:

1. Antibacterial activity.

   Various studies over the years have explored the antibiotic properties of lichens. Burkholder's pioneering study in 1944 marked the beginning of such investigations (Burkholder PR. et al., 1944). Afterward Vatria, in 1973, delved into the antimicrobial activity of several lichen species (Vartia KO., 1973). Subsequent extensive screenings revealed that more than 50% of studied lichen species exhibit antimicrobial activity. Further research highlighted the inhibitory effects of lichens such as *Ramalina farinacea* and 69 other species from New Zealand against a spectrum of bacterial strains, including *Bacillus*, *Pseudomonas*, *Escherichia coli*, *Streptococcus*, *Staphylococcus*, *Enterococcus*, and *Mycobacterium* (Sargsyan R. et al., 2021; Tay T. et al., 2004). Extracts from the lichen *Usnea ghattensis* demonstrated effectiveness against various bacterial strains (Behera BC. et al., 2005), underscoring the broad-spectrum antimicrobial potential of lichens. The isolation and characterization of lichen compounds, such as depsides, depsidones, and dibenzofuranes, have further elucidated their antimicrobial properties. Methanol extracts from five lichen species exhibited potent antibacterial activity, especially against Gram-positive bacteria (Mitrovic T. et al., 2011). Recent reports from Turkey identified potent antibacterial activity in extracts from specific lichen species. Other lichen metabolites like polyporic acid, atromentin, and alectosarmentin also display antimicrobial activities (Dayan FE. et al., 2002). Verma et al. reported the bactericidal activity in lichens *Cladonia ochrochlora*, *Parmotrema nilgherrense*, and *Parmotrema sancti-angelii*, along with their secondary compounds. These compounds exhibited low MIC values against various bacterial and yeast strains, emphasizing the potential pharmaceutical significance of lichens in combating microbial infections (Verma N. et al., 2011). Usnic acid, widely acknowledged in Europe for its antibacterial properties, has been successfully incorporated into antibacterial creams marketed under the names of "Usno®" and "Evosin®" (Dayan FE. et al., 2002). This compound has been used in products ranging from facial acne control creams to toothpaste (Higuchi M. et al., 1993), demonstrating efficacy in preventing dental cavities and inhibiting the growth of Gram-positive bacteria, notably *Streptococcus mutans*, a primary agent in dental caries (Ferrari G. et al., 1988; Dayan FE. et al., 2002). Moreover, lichen secondary metabolites are demonstrated to be good candidates in combination with “old” antimicrobials, increasing the efficacy of antimicrobials against Multi-Drug Resistance (MDR) methicillin-resistant *Staphylococcus aureus* (Bellio P. et al., 2015; Celenza G. et al., 2012; Segatore B. et al., 2012).

2. Antioxidant activity.

   Lichens have garnered attention for their significant antioxidant activities, positioning them as valuable natural sources of antioxidants. These antioxidants play a crucial role in combating oxidative stress caused by reactive oxygen species (ROS), offering protective mechanisms against cellular damage, aging, and various diseases. Kranner et al. (2005) highlighted the role of antioxidants in photoprotection and desiccation tolerance in *Cladonia valcani* lichen and its isolated symbionts (Kranner I. et al., 2005). Subsequent research has expanded the understanding of lichens' antioxidant properties, with numerous studies highlighting the activities of depsides and depsidones isolated from various lichen species (Hidalgo ME. et al., 1994; Lopes TIB. Et al., 2008; Paudel B. et al., 2008; Lohézic-Le Dévéhat F. et al., 2007). These compounds exhibit potent antioxidant activities, showcasing the chemical diversity and bioactive potential of lichens. Many research findings reveal the antioxidant capacities of several lichen compounds (Behera BC. et al., 2002; Verma N. et al., 2011). Remarkably, lichens from Antarctica demonstrated significant antioxidant properties (Bhattarai HD. et al., 2008), emphasizing the adaptability and resilience of lichens in extreme environments. Comparative analyses of lichen extracts have also shed light on their varying free radical scavenging abilities, underscoring the importance of chemical composition in their antioxidative efficacy (Mitrovic T. et al., 2011). Furthermore, lichen metabolites such as usnic acid, sekikaic acid, and salazinic acid of the *Ramalina* species showed radical scavenging and glucosidase activities (Verma N. et al., 2012). Altogether, all these results highlight the diverse and potent antioxidant activities of lichens and their potential therapeutic applications. Additional antioxidant activities linked to lichen depsides, depsidones, and anthraquinones have been documented (Hidalgo ME. et al., 1994). In particular, the antioxidative properties of specific lichen compounds have been shown to mitigate lipid peroxidation (Ichinose T. et al., 1994).

3. Antifungal activity.

   Lichen species exhibit noteworthy antifungal activity. Manojlovic et al. (2005) identified the anthraquinone parietin, isolated from *Caloplaca cerina*, as demonstrating notable antifungal properties. Schmeda-Hirschmann et al. (2008) showcased the antifungal potential of Andean lichens *Protousnea poeppigii* and *Usnea rigida*, containing divaricatinic acid, isodivaricatinic acid, usnic acid, and 5-resorcinol (Schmeda-Hirschmann G. et al., 2008). Mitrovic et al. reported a robust antifungal effect in *Evernia prunastri* and *Hypogymnia physodes* (Mitrovic T. et al.,

2011), whereas Mahadik et al. demonstrated the antifungal activity of *Usnea complanata* against various fungal strains (White PA. et al., 2014), with usnic and psoromic acid being the primary active components responsible for this activity.

4. Antiviral activity.

   Regarding the antiviral properties of lichen secondary metabolites, Yamamoto et al. (1995) discovered that lichesterinic acid and usnic acid, extracted from the lichen *Dolichousnea longissima* (*Usnea longissima*), effectively inhibited the Epstein–Barr virus activation (Yamamoto Y. et al., 1995). Usnic acid has been shown to exhibit antiviral activity against herpes simplex type 1 and polio type 1 viruses. Further studies have highlighted the antiviral capabilities of lichen compounds against a range of viruses, including the tobacco mosaic virus, HIV, and herpes simplex virus type 1 (Stubler D. et al., 1996; Schinazi RF. Et al., 1990; Cohen PA. et al., 1996). Notably, depsides and depsidones have been found to inhibit the HIV-1 integrase (Neamati N. et al., 1997), suggesting their potential as therapeutic agents for AIDS. Additionally, parietin, extracted from *Teloschistes chrysophthalmus*, demonstrated effectiveness against Junin and Tacaribe arenaviruses (Fazio AT. et al., 2007).

5. Antineoplastic activity.

   The pharmaceutical industry holds great interest in the antineoplastic properties of lichen metabolites. Usnic acid, a dibenzofurane compound abundantly present in various lichen species, has been thoroughly investigated for its antitumor activity since its initial isolation in 1844 (Mitrovic T. et al., 2011; Cardarelli M. et al., 1997; Ingólfsdóttir K. et al., 2022). Other compounds, including pannarin from *Psoroma pholidotoides*, *P. pulchrum*, and *P. pallidum*, have been shown to inhibit cell growth and induce apoptosis in human melanoma cells and prostate carcinoma cells (Russo A. et al., 2008). Protolichesterinic acid, derived from *Cetraria islandica*, has been found to inhibit the growth of breast cancer cell lines (Ogmundsdóttir HM. et al., 1998), while the depside gyrophoric acid, isolated from *Umbilicaria* sp., exhibits cytotoxic and antineoplastic activity (Burlando B. et al., 2009). Furthermore, the anthraquinone emodin has been noted to hinder the mutagenicity and the occurrence of DNA adducts, improving the nucleotide excision repair of IN- and cisplatin-induced DNA damage in human cells (Dayan FE. et al., 2002). In addition, emodin, acting as a tyrosine kinase inhibitor, also suppresses the growth of HER-2/neu-overexpressing breast cancer cells in mice. Moreover, gyrophoric and diffractaic acids show inhibitory properties against the proliferation of

human keratinocyte cells (Dayan FE. et al., 2002). Ursolic acid, a triterpene, has been reported to down-regulate MMP-9 gene expression in HT1080 human fibrosarcoma cells by facilitating the nuclear translocation of a glucocorticoid receptor (Cha HJ. et al., 1998). It also inhibits the growth of human epidermoid carcinoma cells by affecting tyrosine kinase activity (Hollósy F. et al., 2000) and acts as an anticancer agent to suppress metastasis.

Protolichesterinic acid is notable for enhancing doxorubicin-induced apoptosis, suggesting its utility as a coadjuvant in cancer therapy (Brisdelli F. et al., 2016).

6. Anti-inflammatory, analgesic, and antipyretic activities.

   Recent studies have underscored the significance of lichen compounds as a valuable source of pharmacological agents with antipyretic, analgesic, and anti-inflammatory properties. Notably, diffractaic, usnic, and decarboxy stenosporic acid, extracted from *Dolichousnea diffracta* (*Usnea diffracta*), have demonstrated promising results in this regard (Otsuka H. et al., 1972; Okuyama E. et al., 1995). Additionally, both orcinol, isolated from *Umbilicaria esculenta*, and longissiminone A from *Dolichousnea longissima* (*Usnea longissima*), have been identified as potent anti-inflammatory compounds (Choudhary MI. et al., 2005).

   A broad spectrum of lichen compounds exhibits anti-inflammatory effects by targeting key inflammatory mediators such as leukotrienes and prostaglandins (Marx J., 2001). For instance, the depsidone lobaric acid and the para-depsides atranorin, diffractaic, gyrophoric, and obtusatic acids, as well as the meta-depsides boninic, sekikaic, and thamnolic acid, have shown to act as non-redox inhibitors of leukotriene biosynthesis and to inhibit the HaCaT cell growth (Kumar SKC. and Miller K., 2000). Moreover, compounds like emodin and sandostatin have been reported to influence the metabolism of eicosanoids in acute necrotizing pancreatitis (Wu JX. Et al., 2000; Dayan FE. et al., 2022).

7. Insecticidal and herbicidal activities.

   Lichen secondary metabolites offer novel possibilities for the development of insecticidal and herbicidal agents, offering environmentally friendly alternatives to conventional chemicals. For instance, vulpinic acid and usnic acids have been identified as potent repellents against the insect *Spodoptera littoralis* (Dayan FE. et al., 2002), demonstrating their potential in pest management strategies. Furthermore, compounds such as barbatic, gyrophoric, haemathamnolic, and lecanoric acids, have been shown to inhibit photosystem II (Lawrey JD., 1995), suggesting their efficacy as novel

herbicidal agents. Additionally, evernic acid and protolichesterinic acid, extracted from *Dolichousnea longissima* (*Usnea longissima*), have been observed to act as plant growth and photosystem II inhibitors (Nishitoba Y. et al., 1987). Emodin and its analogues have exhibited significant effects on grasses, causing malformation and bleaching in early seedling stages. Usnic acid, in particular, has been noted for its ability to hinder carotenoid biosynthesis (Dayan FE. et al., 2001), further underscoring its herbicidal potency.

8. Utilization in the cosmetic and dye sectors.

   Lichen compounds find application in the perfume sector (Schulz H. and Albroscheit G., 1989), especially extracts from species such as *Evernia prunastri* and *Pseudevernia furfuracea*. These extracts, comprising essential oils and depside derivatives, are employed to extend the duration of fragrance release in perfumes (Dayan FE. et al., 2001). Such natural compounds also play an important role in the treatment of acne thanks to preparations enriched with e.g. usnic acid, although their limited adoption is attributed to potential allergenic reactions in sensitive individuals.

   Historically, lichens have served as a source of dyes since ancient Greece, with *Roccella montagnei* being utilized to produce red or purple dyes. This tradition persists, as seen in Scotland's use of various lichen dyes to produce Harris tweeds, achieving different shades of brown, beige, and orange (Dayan FE. et al., 2001).

   In recent times, researchers have explored the application of lichen metabolites in the development of hair dye (Bachmann H. and Portmann P., 1981). Modified calycins, for instance, have been tested for their ability to bind to hair fibers and skin surfaces. Beyond hair care, lichen-derived sterols, while not exclusive to lichens, have been identified as stimulants for skin cell proliferation and have been patented as innovative active ingredients in cosmetics and dermatology (Ingólfsdóttir K., 2002). Usnic acid, in particular, has gained widespread use in cosmetic products due to its diverse beneficial properties (Ingólfsdóttir K., 2002).

9. Utilization in the pharmaceutical sector.

   Despite their promising and diverse biological activities, the exploitation of lichen-derived compounds within the pharmaceutical industry has historically been hampered by the organisms' slow growth rates and the difficulties associated with their cultivation (Behera BC. et al., 2004; Crittenden PD. and Porter N., 1991). The challenge of harvesting lichens on an industrial scale further complicates their use, prompting researchers to explore in vitro cultures as a sustainable alternative approach for mitigating

the decline in lichen species in protected areas and producing the compounds in high quantity (Yamamoto Y. et al., 1995).

Looking forward, the integration of metabolic engineering and biotechnological strategies offers substantial promise for the production of lichen secondary metabolites. By employing genetic modification techniques and optimizing growth conditions, it is feasible to significantly enhance the yield of target compounds. Such advancements will make lichen-derived products more readily available for pharmaceutical applications, overcoming the natural constraints associated with their growth and extraction. This biotechnological paradigm shift is poised to revolutionize the drug discovery and development process, enabling the broader utilization of lichens in the pharmaceutical industry.

2.2 Curcuminoids

Turmeric (Figure 5A), a spice derived from the plant *Curcuma longa* (Figure 5B), has been recognized to be an excellent example for its myriad of medicinal properties (Hewlings SJ. and Kalman DS., 2017).

Its chemical composition comprises carbohydrates (70%), moisture (13%), protein (6%), essential oils (6%), fat (5%), minerals (3%), curcuminoids (3–5%), and vitamins (Goel A. et al., 2008; Prasad S. et al., 2014; Priyadarsini KI., 2014; Kotha RR. and Luthria DL., 2019; Monton C. et al., 2016), underscoring its complex nutritional profile.

Indigenous to India and now cultivated worldwide, particularly in Southeast Asia, China, and Latin America, turmeric belongs to the ginger family, *Zingiberaceae*. It is celebrated in Asian culinary traditions for its distinctive flavor and color, with India being the leading producer and exporter (Kotha RR. and Luthria DL., 2019; Monton C. et al., 2016).

A



B



Figure 5. A) Turmeric root; Thailand, 24 March 2008, Badagnani. **B)** *Zingiberaceae*, *Curcuma Longa*; Hong Kong, Joseph Wong.

The active components of turmeric, namely curcumin, demethoxycurcumin, and bisdemethoxycurcumin (collectively known as curcuminoids), are phenolic compounds. They are characterized by a unique chemical structure that includes a heptadienone chain connected by two aryl groups, attributing to their significant biological activities (Kotha RR. and Luthria DL., 2019). These compounds impart a vivid yellow color, commonly used in food and medicinal products. Recognized for their safety by the Food and Drug Administration, curcuminoids have demonstrated potential in clinical studies, even at high doses.

Turmeric's utility extends beyond culinary uses, serving as a natural dye, antimicrobial agent (Moghadamtousi SZ. et al., 2014), and insect repellent. It has been traditionally employed in treating wounds, respiratory issues, liver disorders, and skin conditions (Araújo CC. and Leon LL., 2001; Goel A. et al., 2008). Notably, curcuminoids have garnered attention for their wide-ranging pharmacological effects, including antioxidant, anti-inflammatory, gastrointestinal, anticancer, cardiovascular, antidiabetic, antimicrobial activities, photoprotection, hepatoprotection, and in treating Alzheimer's disease and inflammatory and edematous disorders (Araújo CC. and Leon LL., 2001; Goel A. et al., 2008; Anand P. et al., 2007).

Despite these promising attributes, curcuminoids are challenged by issues of solubility, bioavailability, and pharmacokinetics, hindering their therapeutic potential. Consequently, the scientific community emphasizes the need for more rigorous clinical trials to substantiate health claims and elucidate the mechanisms behind turmeric's beneficial effects. This research is vital for developing

standardized, effective, and safe turmeric-based products (Kotha RR. and Luthria DL., 2019).

2.2.1 Pharmacological effects

Curcuminoids have attracted significant scientific interest due to their extensive pharmacological properties. These compounds interact with a multitude of biological targets, exhibiting activities against a range of diseases (Prasad S. et al., 2014; Anand P. et al., 2007; Gupta SC. et al., 2012). Presented below is an overview of the most significant activities of curcuminoids:

1. Antioxidant and anti-inflammatory activities.
   Curcuminoids exert their antioxidant activity by neutralizing free radicals, such as reactive oxygen and nitrogen species, thereby preventing oxidative stress, a major cause of cellular damage and aging. These compounds enhance the body's endogenous antioxidant defenses by upregulating the expression of several antioxidant enzymes, including superoxide dismutase (SOD), catalase (CAT), and glutathione peroxidase (GPx). This dual antioxidant mechanism, both direct and indirect, underscores their effectiveness in mitigating oxidative stress-related pathologies (Shahrajabian MH. and Sun W., 2023; Santosh K. et al., 2007; Manju M. et al., 2008).

   Similarly, the anti-inflammatory properties of curcuminoids are of considerable significance. They mitigate inflammation by downregulating pro-inflammatory cytokines and enzymes, thereby offering therapeutic potential in chronic conditions like arthritis, cardiovascular diseases, and neurodegenerative disorders. Curcuminoids specifically inhibit the activity of key molecules involved in inflammation, such as NF-κB, a transcription factor crucial in regulating the immune response to infection. By inhibiting NF-κB activation, they reduce the expression of pro-inflammatory cytokines (e.g., tumor necrosis factor-alpha (TNF-α), interleukins (IL-1, IL-6, IL-8), enzymes (e.g., cyclooxygenase-2 (COX-2), lipoxygenase (LOX)), and other mediators of inflammation and pain (Shahrajabian MH. and Sun W., 2023; Santosh K. et al., 2007; Kotha RR. and Luthria DL., 2019; Ghosh S. et al., 2015). The confluence of antioxidant and anti-inflammatory actions of curcuminoids underscores their potential as therapeutic agents in the management and prevention of diverse chronic diseases. By mitigating oxidative stress and inflammation, curcuminoids contribute to the reduction of risk factors associated with these diseases, thereby potentially improving health outcomes and enhancing overall quality of life.

2. Anticancer properties.

The anticancer properties of curcuminoids, particularly curcumin, have been the subject of extensive research and documentation in the scientific community. These compounds are recognized for their multifaceted mechanisms, contributing significantly to cancer prevention and treatment. The primary areas of investigation into curcuminoids anticancer efficacy include:

a) Inhibition of cell proliferation: curcuminoids have been shown to impede the proliferation of various cancer cell lines by affecting cell cycle regulation mechanisms. They can induce cell cycle arrest at different phases, contingent upon the type of cancer (Aggarwal BB. et al., 2003; Kunnumakkara AB. et al., 2008; Shahrajabian MH. and Sun W., 2023; Santosh K. et al., 2007; Leyon PV. and Kuttan G., 2003; Anto RJ. et al., 1996; Amalraj A. et al., 2016), showcasing their versatility in targeting cellular proliferation across different cancer models.

b) Induction of apoptosis: through the activation of caspases and the modulation of pro-apoptotic and anti-apoptotic proteins, curcuminoids trigger apoptosis in cancer cells (Sharma RA. et al., 2005; Li D. et al., 2021). This pathway underscores the potential of curcuminoids to systematically eliminate cancerous cells via programmed cell death.

c) Inhibition of angiogenesis: angiogenesis, essential for tumor growth and metastasis, is notably inhibited by curcuminoids. These compounds target vascular endothelial growth factor (VEGF) and other angiogenesis-related signaling pathways, thereby constraining the vascular support necessary for tumor expansion (Kunnumakkara AB. et al., 2008; Shahrajabian MH. and Sun W., 2023; Leyon PV. and Kuttan G., 2003; Amalraj A. et al., 2016).

d) Anti-inflammatory effects: given the recognized role of chronic inflammation in promoting tumorigenesis, curcuminoids mitigate this risk by inhibiting the NF-κB pathway. This action reduces the production of pro-inflammatory cytokines and enzymes involved in the cancer progression process (Aggarwal BB. et al., 2003; Sharma RA. et al., 2005; Santosh K. et al., 2007; Ghosh S. et al., 2015).

e) Antioxidant activity: by combating oxidative stress, which can lead to DNA damage and mutations, curcuminoids play a crucial role in cancer prevention. Their antioxidant properties facilitate the scavenging of

free radicals, thereby protecting cells from oxidative damage (Shahrajabian MH. and Sun W., 2023).

f) Modulation of cancer signaling pathways: curcuminoids exert influence over numerous signaling pathways pivotal to cancer progression, including those regulating the cell cycle and apoptosis, such as p53, Bcl-2, Wnt/β-catenin, and PI3K/Akt/mTOR (Shahrajabian MH. and Sun W., 2023; Kotha RR. and Luthria DL., 2019). This multi-targeted approach highlights the comprehensive potential of curcuminoids in cancer therapy.

3. Neuroprotective effects.

The neuroprotective effects of curcuminoids have been the focus of significant scientific inquiry, highlighting their potential in the prevention and treatment of neurodegenerative disorders such as Alzheimer's and Parkinson's diseases, and multiple sclerosis. These benefits are attributed to their antioxidant, anti-inflammatory, and anti-amyloid properties, which collectively contribute to the inhibition of amyloid-beta aggregation, reduction of oxidative stress, and modulation of signaling pathways involved in neuronal survival and neuroinflammation (Shahrajabian MH. and Sun W., 2023; Santosh K. et al., 2007; Li D. et al., 2021). To elucidate the beneficial impact of curcuminoids on neurological health, it is appropriate to briefly examine their multifunctional capabilities, fundamental to their neuroprotective profile. Curcuminoids effectively counteract oxidative stress, a critical pathogenic factor in neurodegenerative diseases, by neutralizing free radicals and upregulating the expression of antioxidant enzymes, thereby reducing neuronal damage, and improving cognitive function. Moreover, chronic inflammation is a significant driver of neurodegenerative disease progression. Curcuminoids mitigate such inflammation by inhibiting essential inflammatory pathways and cytokines, including NF-κB, thereby protecting neuronal cells from inflammation-induced damage. Specifically, in the context of Alzheimer's disease, curcuminoids have been shown to inhibit the aggregation of amyloid-beta peptides and promote their clearance, targeting a fundamental pathological aspect of the disorder. Additionally, curcuminoids exert a positive influence on the levels and activity of various neurotransmitters, including dopamine and acetylcholine, which play pivotal roles in neurodegenerative diseases. This comprehensive approach not only highlights the multifaceted and complex nature of curcuminoids in countering neurodegeneration but also accentuates their potential as versatile agents in neuroprotective

therapeutic strategies (Shahrajabian MH. and Sun W., 2023; Santosh K. et al., 2007; Amalraj A. et al., 2016).

4. Cardiovascular and metabolic diseases.
   Curcuminoids demonstrate considerable therapeutic promise in combating cardiovascular and metabolic disorders, attributed to their anti-inflammatory, antioxidant, and anti-atherogenic capabilities. These properties are instrumental in addressing key factors implicated in the pathogenesis of such conditions. Sahebkar reported that curcuminoids might reduce circulatory levels of C-reactive protein, a known predictor and independent risk factor for cardiovascular diseases (Sahebkar A., 2013), showcasing their efficacy in combating myocardial infarction and atherosclerosis (Kotha RR. and Luthria DL., 2019). Moreover, curcuminoids are reported to enhance endothelial function, alleviate arterial stiffness, and reduce blood pressure, thereby offering protective measures against cardiovascular diseases. They also beneficially modulate lipid metabolism, evidenced by reduced levels of LDL cholesterol and triglycerides, alongside an increase in HDL cholesterol, collectively diminishing the risk of atherosclerosis (Kunnumakkara AB. et al., 2016; Kotha RR. and Luthria DL., 2019). In the realm of metabolic disorders, curcuminoids have demonstrated efficacy in enhancing insulin sensitivity, regulating glucose levels, and affecting the metabolism of carbohydrates and fats. These effects make them valuable in the management of diabetes and obesity (Arun N. and Nalini N., 2002; Kotha RR. and Luthria DL., 2019). Their capability to influence various signaling pathways, notably those associated with inflammation, oxidative stress, and energy metabolism, underpins their therapeutic potential in these diseases.

2.2.2 Bioavailability

The bioavailability and pharmacokinetics of curcuminoids present substantial hurdles to their therapeutic efficacy. These challenges stem from curcuminoids' poor solubility, rapid metabolism, and swift elimination from the gastrointestinal tract, all of which contribute to their notably low bioavailability (Anand P. et al., 2007). At a physiological pH of 7.2 and a temperature of 37°C, curcumin is quickly metabolized, predominantly through reduction and conjugation pathways (Kotha RR. and Luthria DL., 2019).

Reduction processes lead to the formation of di-, tetra-, and octahydrocurcumin derivatives via enzymes such as NADPH-dependent reductase and alcohol

dehydrogenase (Anand P. et al., 2007; Schneider C. et al., 2015). Conjugation, involving glucuronidation and sulfonation, mainly occurs at the phenolic oxygen of curcumin through the action of enzymes (Priyadarsini KI., 2014) like human phenol sulfotransferase isoenzymes SULT1A1, SULT1A3, and UDP-glucuronosyltransferase, further complicating its stability and bioactivity in the body (Ireson CR. et al., 2002; Hoehle SI. et al., 2007).

Curcumin's half-life is remarkably brief, with reports indicating it to be less than 10 minutes (Nelson KM. et al., 2017), emphasizing the rapid degradation and metabolism that significantly reduce its systemic availability. Degradation occurs via solvolysis and photodegradation pathways (Grynkiewicz G. et al., 2012), playing a pivotal role in this process. Solvolysis, involving nucleophilic substitution or elimination by solvent molecules, leads to substantial curcumin degradation in aqueous alkaline conditions, resulting in various degradation products, including vanillin and ferulic acid (Anand P. et al., 2007; Nelson KM. et al., 2017; Priyadarsini KI., 2014). Autoxidation introduces oxygen into curcumin through a radical chain reaction, producing bicyclopentadione (Nelson KM. et al., 2017; Priyadarsini KI., 2014; Schneider C. et al., 2015Furthermore, the natural molecule is sensitive to light, necessitating protective measures against light exposure to mitigate photodegradation, which can yield degradation products similar to those of solvolysis (Priyadarsini KI., 2014), including ferulic acid, ferulic aldehyde, vanillin, and vanillic acid (Nelson KM. et al., 2017; Priyadarsini KI., 2014).

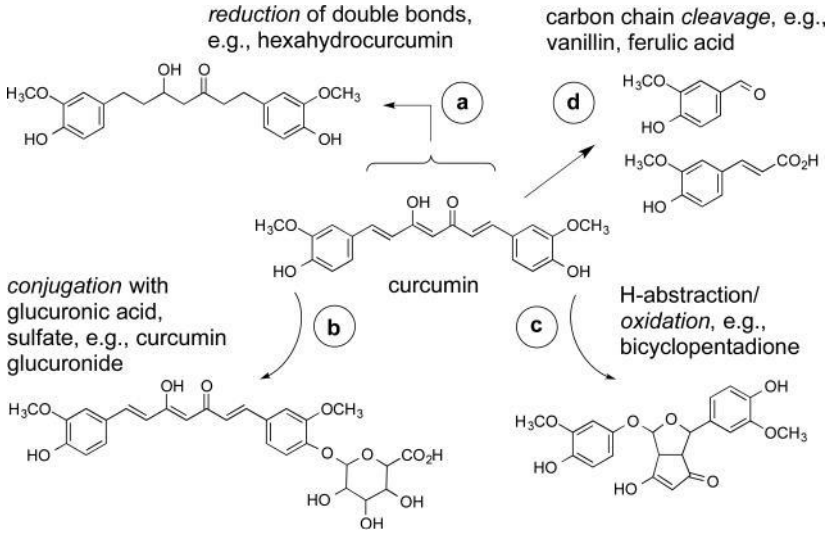


Figure 6. The metabolic pathways and degradation mechanisms of curcumin: **a**, reduction; **b**, conjugation; **c**, oxidation; and **d**, cleavage (Schneider C. et al., 2015).

These insights underscore the complexity of curcuminoids' bioavailability and pharmacokinetics, highlighting the necessity for innovative approaches to enhance their therapeutic potential.

2.2.3 Formulation and challenges

Despite their promising therapeutic effects, the clinical application of curcuminoids is limited due to their poor bioavailability, which is attributed to their low solubility in water, rapid metabolism, and systemic elimination. Curcuminoids are quickly metabolized and eliminated from the body, reducing their bioactive concentration in target tissues. This has led to skepticism about their potential as drug leads, notwithstanding their promising pharmacological profile.

To address these challenges, various strategies have been investigated to improve the bioavailability and therapeutic efficacy of curcuminoids. These include the utilization of adjuvants (e.g., piperine), liposomal encapsulation, polymer conjugation, and formulation with cyclodextrins, aiming to enhance absorption, offer target specificity, and increase therapeutic efficacy (Amalraj A. et al., 2016; Anand P. et al., 2007; Mirzaei H. et al., 2017).

The ongoing research highlights the potential of curcuminoids as multi-targeted therapeutic agents. Future efforts should focus on elucidating their molecular mechanisms of action, improving their bioavailability, and conducting extensive clinical trials to validate their efficacy and safety in human subjects.

In summary, curcuminoids represent a promising category of natural compounds with a wide range of therapeutic applications. The advancements in pharmaceutical sciences and nanotechnology offer new opportunities to overcome existing challenges, thus unlocking the full therapeutic potential of curcuminoids in clinical practice.

2.2.4 Curcumin and derivatives

Curcumin is the predominant curcuminoid found in turmeric (77%, contrasting with the lesser quantities of demethoxycurcumin (17%) and bisdemethoxycurcumin (3-6%)) (Prasad S. et al., 2014). Its discovery dates to 1815 with its chemical structure, identified as diferuloylmethane, in 1910.

Curcumin exists in two tautomeric forms, keto and enol, with the keto form predominating at neutral and acidic pH levels but shifting to the enol form under

alkaline conditions. Its keto-enol tautomerism contributes significantly to its pharmacological actions, showing a crucial role in its biological activity and stability (Kotha RR. and Luthria DL., 2019).

The solubility of curcumin in water at room temperature is limited, presenting challenges for its bioavailability. However, it demonstrates solubility in organic solvents, with its absorption peaks varying according to the solvent and pH conditions (Nelson KM. et al., 2017; Kotha RR. and Luthria DL., 2019).

Curcumin possesses three reactive sites: a hydrogen atom donor, Michael acceptor, and metal chelator (Nelson KM. et al., 2017; Priyadarsini KI., 2014). These properties underscore its therapeutic potential against diseases such as Alzheimer's and cancer, particularly through its ability to form complexes with metal ions and inhibit the aggregation of β-amyloid species (Priyadarsini KI., 2014; Baum L. and Ng A., 2004). Additionally, curcumin can reduce heavy metal-induced toxicity (García-Niño WR. and Pedraza-Chaverrí J., 2014) by forming stable complexes with metals and interacting with thiol (-SH) and selenol (-SeH) groups in biological molecules (Kotha RR. and Luthria DL., 2019).

Despite its broad spectrum of biological activities, the clinical application of curcumin is hampered by its low bioavailability, which researchers are attempting to overcome through various formulation strategies, including nanoparticles, liposomes, and complexation with cyclodextrins (Kotha RR. and Luthria DL., 2019; Shahrajabian MH. and Sun W., 2023).

Demethoxycurcumin, bisdemethoxycurcumin, and salicylcurcumin are distinct types of curcuminoids.

While curcumin is characterized by the presence of two methoxy groups on its phenyl rings, demethoxycurcumin and bisdemethoxycurcumin differ from curcumin by the absence of one or two methoxy groups, respectively, influencing their solubility and bioactivity. This structural variation influences their solubility and bioactivity, with bisdemethoxycurcumin exhibiting increased stability relative to curcumin and demethoxycurcumin due to its lack of methoxy groups (Monton C. et al., 2016).

Salicylcurcumin, a synthetic derivative, is less frequently discussed in the scientific literature compared to other curcuminoids. Its chemical structure, detailed as 1,7-Bis(2-hydroxyphenyl)-5-hydroxy-1,4,6-heptatriene-3-one and a molecular formula of $C_{19}H_{16}O_4$ (instead of $C_{21}H_{20}O_6$ of curcumin), lacks methoxy groups on both phenols like bisdemethoxycurcumin, and features hydroxyl groups positioned ortho, similar to salicylates, rather than the para position found in typical curcuminoids. These structural distinctions may potentially affect its solubility, bioavailability, and therapeutic efficacy.

Although not as extensively researched as curcumin, these compounds significantly contribute to turmeric's overall therapeutic potential. They exhibit similar biological activities to curcumin, including antioxidant, anti-inflammatory, and anticancer properties (Shahrajabian MH. and Sun W., 2023). Emerging research suggests that the varied curcuminoids may act synergistically, potentially enhancing the overall effectiveness of turmeric as a therapeutic agent. The stability and bioavailability of these compounds are ongoing research topics, with preliminary studies indicating that chemical modifications could enhance their therapeutic utility (Shahrajabian MH. and Sun W., 2023).

2.3 Phenylpropanoid compounds

Phenylpropanoids constitute a vast class of natural compounds synthesized by plants from either phenylalanine or tyrosine, through a series of enzymatic reactions rooted in the shikimate pathway intermediates. These compounds undergo structural modifications mediated by enzymes such as lyases, transferases, ligases, reductases, and oxygenases, leading to the synthesis and accumulation of a wide array of metabolites across various organs and developmental stages (Vogt T., 2009).

The phenylpropanoid pathway is instrumental in producing critical structural components like lignin, suberin, and condensed tannins, essential for the structural integrity and mechanical strength of plants. Nonetheless, lignin poses significant challenges in biomass conversion for biofuels and bioproducts due to its role in feedstock recalcitrance (Liu Y. et al., 2021). Beyond structural functionalities, phenylpropanoids are crucial for generating anthocyanins for pigmentation, flavonols and flavones for UV protection, flavonoids and isoflavonoids for plant-microbe symbiosis, and phytoalexins for defense against pathogens. These compounds also bear considerable economic value, functioning as nutraceuticals with health benefits and as fundamental components in fragrances, pharmaceuticals, and biopolymers (Lin CY. and Eudes A., 2020).

The biosynthetic diversity of phenylpropanoids underscores their integral role in plant physiology and their wide-ranging applications in various industries (Cesarino I. et al., 2022; Ortiz A. et al., 2023). Environmental stimuli influence phenylpropanoid biosynthesis, impacting plant resilience and antioxidant activity, as evidenced in studies on rice seedlings (Du S. et al., 2021). Research into lignin's structure in rice by-products (Rosado MJ. et al., 2021) aids biomass conversion efforts. Investigations into switchgrass genotypes and the exploration of lignin

biosynthesis and its evolution across plant species (Yao T. et al., 2021) highlight the structural diversity of lignin. The roles of phenoloxidases in the phenylpropanoid pathways (Blaschek L. and Pesquet E., 2021), the tracing of phenylpropanoid biosynthesis from phenylalanine and tyrosine in sorghum (Simpson JP. et al., 2021), and the focus on lignin mutants in Arabidopsis (El Houari I. et al., 2021) and anthocyanins' biosynthesis and health benefits (Cappellini F. et al., 2021) further demonstrate the pathway's significance. Additionally, the study of tannin metabolism genes in nut tree species (Wang J. et al., 2021) indicates the broad impact of phenylpropanoids on agriculture and nutrition.

2.3.1 Vanillin

Vanillin (4-hydroxy-3-methoxybenzaldehyde), with the molecular formula $C_8H_8O_3$, is a phenolic aldehyde renowned for its characteristic vanilla fragrance, making it the predominant component of vanilla bean extract from *Vanilla planifolia* (Figure 7). Its extensive utilization in the food industry as a flavoring agent underscores its significance (Banerjee G. and Chattopadhyay P., 2019; Priefert H. et al., 2001). Beyond its culinary applications, vanillin is also employed in pharmaceuticals and cosmetics, demonstrating its versatility.



Figure 7. Extract from *Vanilla planifolia* (Kamath AK. et al., 2022).

The production of vanillin is primarily achieved through biotechnological approaches, leveraging microbial fermentation or bioconversion of precursors using engineered cells or enzymes. Its biosynthesis encompasses both plant and microbial pathways, with ferulic acid serving as a common precursor (Gallage NJ. et al., 2015). Four principal metabolic pathways facilitate the conversion of ferulic acid to vanillin: a CoA-dependent transformation in microorganisms, a CoA-

independent conversion, a two-step bioconversion process involving fungi, and a one-step synthetic pathway within plant cells. Microbial transformation requires specific enzymes, such as feruloyl-CoA synthetase and enoyl-CoA hydratase, underscoring the complexity and adaptability of vanillin biosynthesis across different biological systems (Jiang W. et al., 2023).

In its natural state within vanilla pods, vanillin is found as a glycoside, which serves to shield the plant from vanillin's potentially toxic effects (Hansen EH. et al., 2009). The enzyme vanillin synthetase (VpVAN) plays a pivotal role in the biosynthesis of vanillin from endogenous ferulic acid, particularly in *Vanilla planifolia* and *Glechoma hederacea* (Gallage NJ. et al., 2015). Although plant-based production of vanillin, including through genetic modification to enhance yield, presents challenges such as environmental variability and high costs, biotechnological advancements have led to notable increases in vanillin content. However, these methods still face difficulties in fully satisfying market demand.

2.3.2 Vanillic acid

Vanillic acid, a naturally occurring organic compound with the molecular formula $C_8H_8O_4$, is classified within the family of phenolic acids. Structurally akin to vanillin, vanillic acid is distinguished by the presence of a carboxylic acid group, in contrast to the aldehyde group characteristic of vanillin. This compound is sourced from various plants and is present in a range of foods, including wine, vinegar, and vanilla extract, where it contributes to the flavor profile and offers potential health benefits.

In the realm of biotechnological applications, vanillic acid functions as a precursor or intermediate in the biosynthesis and biodegradation of more complex molecules, including vanillin, via biotransformation processes (Girawale SD. et al., 2022). The bioconversion of vanillic acid to vanillin represents a focal point for the flavor and fragrance industry, offering a more sustainable alternative to conventional synthetic methods of vanillin production (Banerjee G. and Chattopadhyay P., 2019). Furthermore, vanillic acid is recognized for its diverse bioactivities, including antioxidant, anti-inflammatory, and antimicrobial properties. These attributes render it a subject of interest across various disciplines, such as food science, nutrition, pharmacology, and environmental science. Notably, vanillic acid has been associated with protective effects against a range of diseases, including cardiovascular diseases and neurodegenerative disorders (Jiang W. et al., 2023).

2.3.3 Ferulic acid

Ferulic acid is a phenolic compound prevalent in plants, particularly within the seeds of cereals such as wheat, rice, and oats. It serves as a crucial active ingredient in numerous traditional Chinese medicinal formulations. Ferulic acid is renowned for its array of biological activities, notably its protective effects against oxidative stress, inflammation, vascular endothelial damage, fibrosis, apoptosis, and platelet aggregation (Li D. et al., 2021). As a prominent cinnamic acid derivative, ferulic acid shares this classification with other compounds including caffeic, p-coumaric, sinapinic, syringic, and vanillic acids, highlighting its significance among phenolic substances (Bezerra G. et al., 2017).

Distinguished by its superior bioavailability and prolonged presence in the bloodstream compared to other phenolic acids, ferulic acid exhibits low toxicity and a wide range of physiological functions. These include anti-inflammatory, antimicrobial, and anticancer properties (targeting lung, breast, colon, and skin cancers), in addition to anti-arrhythmic, antithrombotic, antidiabetic, immunostimulatory effects, and neuroprotective activities that may aid in cell repair. Its extensive utilization spans the pharmaceuticals and food industries, underpinning its versatility. Furthermore, ferulic acid is incorporated into skincare formulations as a photoprotective agent in sunscreens, a preventive measure against photoaging, and a skin-brightening agent. Despite its beneficial attributes, the application of ferulic acid is constrained by its propensity for rapid oxidation, posing challenges to its stability and efficacy in some contexts (Bezerra G. et al., 2017; Tee-ngam P. et al., 2013; Moldovan M. et al., 2017).

2.3.4 Caffeic acid

Caffeic acid, a naturally occurring compound within the class of hydroxycinnamic acids, is distinguished by its phenolic and acrylic functional groups, integrating the structural characteristics of both phenols and acrylics (Khan F. et al., 2021; Pavlíková N., 2022). Predominantly found in coffee, caffeic acid is also present in a variety of fruits and vegetables, contributing to the nutritional and health-promoting profiles of these foods.

This compound is recognized for its broad spectrum of biological activities, including antioxidant, anti-inflammatory, anticancer, and cardioprotective effects. These properties highlight the role of caffeic acid in enhancing the health benefits associated with the consumption of certain foods, underscoring its potential

therapeutic and preventative applications in addressing various health conditions (Khan F. et al., 2021).

2.3.5 Chicoric acid

Discovered in 1958, chicoric acid has gained attention for its health-promoting properties. It is found in a wide array of plants across at least 63 different genera and species (Lee J. et al., 2013), with *Echinacea purpurea (L.)* Moench (Figure 8) being the most notable natural source (Yang M. et al., 2022). However, given the limited knowledge regarding alternative natural sources, there is a recognized need to expand production methods through chemical synthesis, biosynthesis, and the exploration of other plant sources.



Figure 8. *Echinacea purpurea (L.)* Moench; East USA (Asteraceae) Botanical Garden of Fribourg, Guy Waterval.

As a derivative of caffeic acid, chicoric acid, with the molecular formula $C_{22}H_{18}O_{12}$, features two chiral carbon atoms in this structure. This structural complexity results in three stereoisomers: levorotatory-chicoric acid (L-chicoric acid), dextrorotatory-chicoric acid (D-chicoric acid), and meso-chicoric acid.

Its application in medicinal products, nutritional supplements, and health foods is primarily attributed to its diverse bioactivities. It has been shown to modulate glucose and lipid metabolism effectively and exhibits anti-inflammatory, antioxidant, antimicrobial, neuroprotective, and anti-aging properties (Peng Y. et

al., 2019). These multifaceted health benefits underscore the potential of chicoric acid as a valuable compound in various health-related applications.

2.3.6 Rosmarinic acid

Rosmarinic acid, a phenolic compound resulting from the esterification of caffeic acid with 3,4-dihydroxyphenyllactic acid, is predominantly found within the *Boraginaceae* family and the *Nepetoideae* subfamily of the *Lamiaceae*. Additionally, its presence extends to various other plant families, along with certain ferns and hornworts, underscoring its widespread occurrence in the plant kingdom (Petersen M. and Simmonds MS., 2003). The compound was initially isolated from *Rosmarinus officinalis L.* (Figure 9), with its nomenclature reflecting the source plant's name (Al-Dhabi NA. et al., 2014).



Figure 9. *Rosmarinus officinalis L.*; United States National Arboretum, Washington D.C., David J. Stang.

Renowned for its extensive pharmacological and biological activities, natural rosmarinic acid exhibits antioxidative, anti-inflammatory, antibacterial, and antiviral properties (Al-Dhabi NA. et al., 2014; Gamaro GD. et al., 2011; Shahhamzehei N. et al., 2022). It is particularly effective against *Herpes simplex* virus infections, leveraging its antiviral efficacy in extracts from *Melissa officinalis*. The anti-inflammatory action of rosmarinic acid is attributed to its ability to inhibit lipoxygenases and cyclooxygenases, as well as its interactions with the complement cascade. Although it is rapidly cleared from the bloodstream (with a half-life of approximately 9 minutes) following intravenous administration, rosmarinic acid is characterized by low toxicity. Furthermore, it is credited with

enhancing the antioxidant properties of cosmetic plants like *Rosmarinus officinalis* and *Sanicula europaea*.

In addition to its antimicrobial and anti-inflammatory effects, rosmarinic acid has been recognized for its anti-diabetic properties, demonstrating efficacy in mitigating diabetes-related disorders and complications (Ngo YL. et al., 2018).

2.3.7 Salvianolic acid

Salvia miltiorrhiza (Figure 10), commonly referred to as red sage or Chinese sage, is highly regarded in traditional medicine for treating a wide range of diseases, including cardiovascular diseases, hepatitis, hepatocirrhosis, stomachache, chronic renal failure, and dysmenorrhea (He G. et al., 2023; Ianni A. et al., 2022).

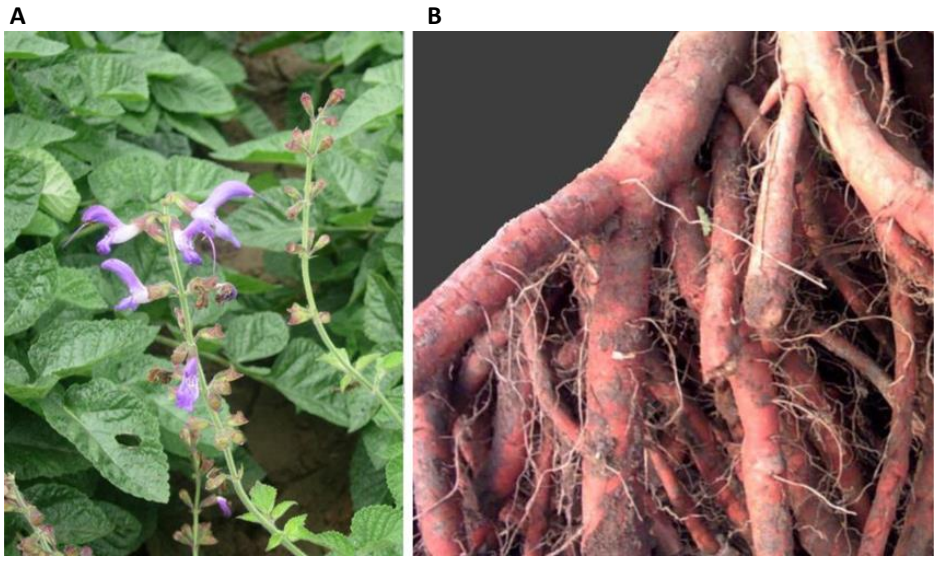


Figure 10. A) *Salvia miltiorrhiza*. **B)** Roots of *S. miltiorrhiza* (Rupasinghe HP. et al., 2016).

Within *S. miltiorrhiza*, researchers have identified two pharmacologically active fractions: lipophilic diterpenoids known as tanshinones, and water-soluble phenolic acids (Wang BQ., 2010). Recent studies have particularly focused on the phenolic acid fraction, from which twenty-five compounds have been isolated and identified. Notably, Salvianolic acid B (SalB) emerges as the most abundant, constituting 3–5% of the herb's total dried weight (Zhao GR. et al., 2008). SalB is acclaimed for its extensive pharmacological effects, especially regarding cardiovascular protection. It exhibits remarkable antioxidant capabilities, scavenging reactive oxygen species and thus protecting cardiomyocytes against

drug-induced toxicity. This effect has been demonstrated in mouse models of doxorubicin-induced cardiotoxicity, where SalB notably reduces myocardial oxidative stress (Ho JHC. et al., 2011). In vascular health, SalB has been found to mitigate leukocyte-endothelial cell adherence, a preliminary stage in atherosclerosis. It reduces the expression of vascular cell adhesion molecule-1 (VCAM-1) and intercellular adhesion molecule-1 (ICAM-1) without altering E-selectin expression, acting through anti-inflammatory mechanisms by inhibiting the activation of the NF-κB pathway induced by TNF-α. Moreover, SalB influences the expression of metalloproteinases, essential in cardiovascular injury and atherosclerosis. It suppresses the genetic and protein expression of cyclooxygenase-2 (COX-2) and matrix metalloproteinases (MMP-2 and MMP-9), pivotal enzymes in cardiovascular diseases and tumor cell invasiveness, by inhibiting specific kinase phosphorylation. This suggests its role in averting the involvement of vascular smooth muscle cells in atherosclerosis pathogenesis and modulating MMP-9 function in human MDA-MB-231 breast cancer cells, which depend significantly on MMPs (Ianni A. et al., 2022). Additionally, SalB acts as an immunomodulator, inhibiting the protein-protein interactions mediated by SH2 domains of Src-family kinases and CD36, a receptor for oxidized low-density lipoproteins (oxLDL), thereby playing a role in immune response modulation within cardiovascular protection (Ho JHC. et al., 2011). The therapeutic potential, safety profile, suitability for combination therapy, new dosage forms, and innovative drug delivery routes of SalB have been thoroughly reviewed, highlighting its broad applicability in addressing various organ-specific and systemic diseases, including its anti-tumor and anti-inflammatory properties (He G. et al., 2023).

Chapter III

Materials and methods

3.1 Reagents

SARS-CoV-2 3CL Protease was purchased from Sigma-Aldrich (*https://www.sigmaaldrich.com/Italy*). 3CL Protease Substrate, 3CL Protease Assay Buffer, and 3CL inhibitor GC376 were purchased from Vinci Biochem (Firenze, Italy). Dithiothreitol (DTT) and dimethyl sulfoxide (DMSO) were purchased from Sigma-Aldrich Chemical Co. (Saint Louis, MO, USA). Dulbecco's modified Eagle medium (DMEM)/Ham's F-12 50/50 Mix (with 2 mM L-glutamine and 15 mM Hepes) was purchased from Corning Life Sciences (Manassas, VA, USA). Fetal bovine serum (FBS), and horse serum (HS) were from EuroClone (Pero, MI, Italy). Penicillin-streptomycin was from TermoFisher Scientific (Carlsband, CA, USA). Trypan-blue assay and other reagents were from Sigma-Aldrich Chemical Co. (Saint Louis, MOi, USA). Lichen secondary metabolites (Table 3), isolated from lichens collected in various Chilean regions including the Chilean Antarctic Territory, were donated by Prof. Marisa Piovano (Universidad Técnica Federico Santa María, Valparaíso, Chile). Salycilcurcumin and Chicoric acid (Table 2) were purchased from Cayman Chemical (Ann Arbor, Michigan). Curcumin, Bisdemethoxycurcumin, Demethoxycurcumin, Vanillin, Vanillic acid, Caffeic acid, Ferulic acid, Salvianolic acid, and Rosmarinic acid (Table 1) were purchased from Sigma-Aldrich (https://www.sigmaaldrich.com/Italy).

3.2 Spectrofluorimetric assay

SARS-CoV-2 3CL protease activity assay was used to assess the effect of natural compounds on the inhibition of the 3CL protease. The assay was performed according to the manufacturer's protocol (3CL Protease (SARS-CoV-2) Assay Kit, BPS Bioscience), with some modifications. The fluorescence intensity was measured, using the fluorogenic substrate DABCYL-KTSAVLQSGFRKME-EDANS, in

a microtiter plate-reading fluorimeter capable of excitation at a wavelength of 360 nm and detection of emission at a wavelength of 535 nm.

Reactions were performed in a black 96-well microplate with a final volume of 100 µL in each well. Experiments were carried out in the reaction buffer supplied by the manufacturer which requires the addition of dithiothreitol (DTT) to preserve the enzyme integrity in these long-run experiments. DTT was added to 3CL Protease Assay Buffer just before use, with a final concentration of 1 mM. 3CL protease was used at the final concentration of 8,9 nM. The enzyme was preincubated with the inhibitor under examination for 30 min at room temperature in a 96-well microplate. The reaction was started by adding the 3CL substrate solution to each well at a concentration value of 10 µM. The spectrofluorimetric assay was performed by measuring the fluorescence intensities in each well using the Beckman Coulter DTX-880 Multimode Detector microplate reader. The excitation and emission wavelengths were 360 nm and 535 nm, respectively. The percentage of inhibition was calculated as the fractional residual activity of protease 3CL incubated for 30 min with the natural compounds. Additionally, the 3CL inhibitor GC376 was used at a concentration of 100 µM as a positive control and the inhibitor buffer as inhibitor control. A standard curve was produced to convert the relative fluorescence unit (RFU) into the amount of cleaved substrate. The curve was obtained by inducing complete hydrolysis of the substrate with concentrations ranging from 5 and 100 µM (Figure 11).

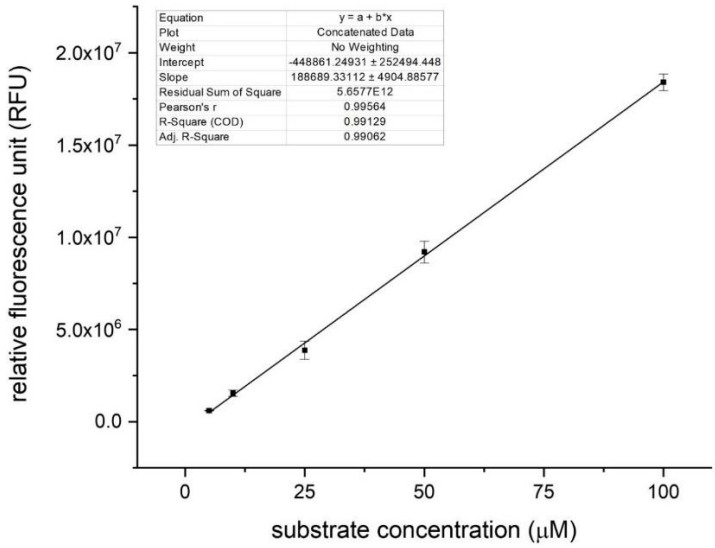


Figure 11. The calibration curve was generated to convert the relative fluorescence unit (RFU) to the amount of the cleaved substrate.

3.3 Determination of kinetic parameters

The kinetic parameters of 3CL SARS-CoV-2 protease were determined by incubating the enzyme as previously described.

The experiment was performed by measuring the initial rates (v_0, RFU/s) of the progress curves that were calculated at less than 10% hydrolysis of the initial substrate concentration. The substrate concentrations used in the experiments range from 5 µM to 100 µM.

The plot was well described by the non-linear fitting of the Hill equation:

$$v_0 = \frac{V_{max}\,[S]^h}{K^h + [S]^h} \qquad \text{equation 1}$$

where *h* is the Hill coefficient, and *K* is related to substrate occupancy at one site on the substrate affinity of the other site. Any deviation from the Michaelis-Menten equation, where *h* is equal to 1, can be easily visualized by the Hanes-Woolf linearization method, where the initial rate v_0 is plotted as $[S]/v_0$ against $[S]$: when *h* is equal to 1, and the plot is represented by a straight line with a coefficient of determination R^2 of the interpolated line close to 1, while for $h \neq 1$, R^2 is far from 1 (Figure 13). Any deviation from the Michaelis-Menten equation, where *h* is equal to 1, can be confirmed by the Hanes-Woolf linearization method, in which the initial rate v_0 is plotted as $[S]/v_0$ against [S]. Briefly, when *h* is equal to 1, the plot is illustrated by a straight line with a coefficient of determination R^2 of the interpolated line close to 1. Otherwise, when *h* is different from 1, R^2 is far from 1.

The kinetic parameters were determined for each set of experiments. The procedure adopted to determine the kinetic parameters is detailed below.

3.3.1 Theoretical basis for approximation to a Michaelis-Menten model

Before proceeding, it is indispensable to know the value of V_{max}, from which the value of k_{cat} can eventually be derived, the value of *K* and *h*.

Determine, as usual, the curve of v_0 as a function of substrate concentration [S], covering the whole range of substrate concentrations to obtain a complete sigmoid curve (Figure 12A). Calculate utilizing a non-linear fit the values of V_{max}, *K,* and the Hill coefficient. Alternatively, it is possible to proceed with the linearisation of the Hill equation, plotting the log $[v_0/(V_{max}-v_0)]$ against the log([S]), obtaining a straight line with slope *h*:

$$log\left(\frac{v_0}{V_{max} - v_0}\right) = h\ log([S]) - h\ log(K)$$ equation 2

Although linearisation is very useful in diagnosing a sigmoid curve pattern and for the "pencil and ruler" estimation of kinetic parameters, its application is limited because the value of V_{max} must be estimated in advance. However, it is always good practice to proceed with the linearisation of the Hill equation, even if a non-linear fitting has been done. Indeed, it still is an excellent method for checking the sigmoidal trend of the curve since a straight line with a good correlation coefficient is diagnostic of the correct application of the model.

To make a correct approximation to a Michaelian enzyme, it is necessary to identify the substrate concentration for which the saturation of possible binding sites is maximum. The best way is to perform the first derivative of the non-linear fitting curve to identify the point where the sigmoidal curve becomes a straight line. The maximum point on the curve, where the second derivative would result in a zero value, represents the value of substrate concentration to be used as reporter substrate in the inactivation studies (Figure 12B). Most common software for data graphing and analysis can perform non-linear regression and the calculation of the first derivatives. In the case where advanced data analysis software is not available and the kinetic parameters have been estimated by linearisation of the Hill equation, it is possible to estimate the maximum value of the derivative by graphing the data on a common spreadsheet using the following formula which is the first derivative of the Hill equation:

$$f'([S]) = \frac{K^h\ V\ h\ [S]^{h-1}}{\left(K_{\square}^h + [S]^h\right)^2}$$

Any value of [S] from which the enzyme can be approximated to a Michaelian enzyme, and the value of K satisfy one of the conditions for the application of equation 3 ([S]≤Km).

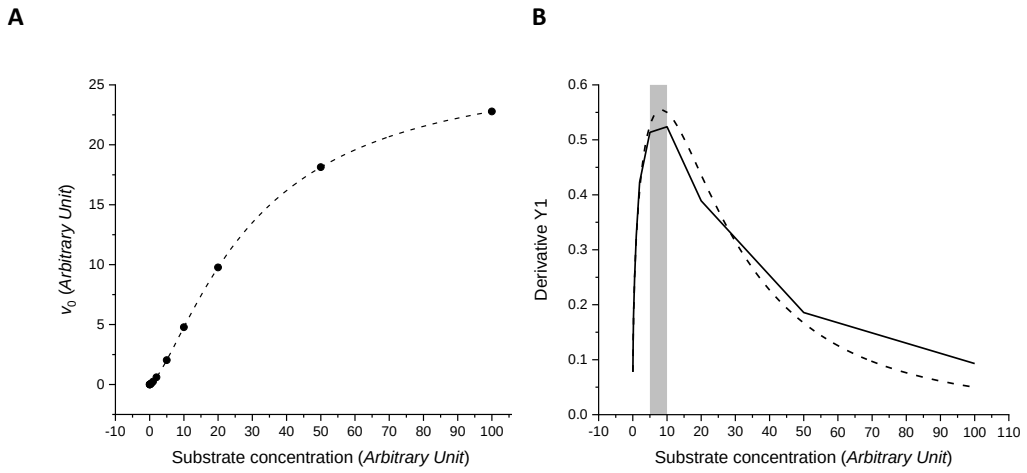


Figure 12. **A)** Plot of the v_0 versus [S] in a simulated cooperative enzyme. The plot is obtained by imposing V_{max}=27 (k_{cat} 2700, E_0 0.01), $K_{0.5}$ 30, h 1.4, as arbitrary units. **B)** Non-linear curve fit of the first derivative.

3.3.1.1 Equation derivation

Derivation of the equation describing the formation of the reaction product only in the presence of slow-binding inactivators and with substrate depletion.

Assumptions:

$$E + S \underset{k_{-1}}{\overset{k_{+1}}{\rightleftarrows}} ES \overset{k_{+2}}{\rightarrow} E + P \qquad \text{scheme 1}$$

$$E + I \underset{k_{off}}{\overset{k_{on}}{\rightleftarrows}} EI \overset{k_{inact}}{\rightarrow} EI^* \qquad \text{scheme 2}$$

The following equation describes the rate of disappearance of the substrate [S].

$$\frac{d[S]}{dt} = -k_{+2}\frac{k_{+1}}{k_{-1} + k_{+2}}[E][S]$$

where, in the context of a generalized reaction scheme, k_{+2} can be approximated to the k_{cat}, and the ratio (k_{-1}+k_{+2})/k_{+1} as the constant of Michaelis, K_m. In the case of cooperative enzymes, it is advisable to use the term K instead of K_m since it represents the enzyme's affinity for the substrate at a specific substrate concentration. Thus:

$$\frac{d[S]}{dt} = -\frac{k_{cat}}{K}[E][S]$$

The mass-balance equation for the enzyme is:

$$[E]_0 = [E] + [EI] + [EI^*] + [ES]$$

It is possible to proceed as follows to solve the mass-balance equation.

I. Solution for the species [EI]

The constant of dissociation of the initial *EI* complex, K_i, can be expressed as

$$K_i = \frac{k_{off}}{k_{on}} = \frac{[E][I]}{[EI]}$$

Over time, the inhibitor concentration can be considered constant when the condition $K_i >> [E]_0$ is verified. Thus, the instantaneous concentration of the inhibitor $[I]$ can be equated to its initial concentration, $[I]=[I]_0$. Under these circumstances, the concentration of the *EI* complex can be described by the following expression:

$$[EI] = \frac{[E][I]_0}{K_i}$$

II. Solution for the species [ES]

The concentration of the species [*ES*] can be obtained by the stationary state assumption:

$$\frac{d[ES]}{dt} = k_{+1}[E][S] - k_{-1}[ES] - k_{+2}[ES] = 0$$

$$[ES] = \frac{k_{+1}}{k_{-1} + k_{+2}}[E][S] = \frac{[E][S]}{K}$$

III. Solution for the species [EI*]

By substituting [*ES*] and [*EI*] to the mass-balance equation:

$$[E]_0 = \left(1 + \frac{[S]}{K} + \frac{[I]_0}{K_i}\right) + [EI^*]$$

Building upon the insights provided by Waley (Waley SG., 1993), in the presence of very slow inhibitors, thereby leading to observable substrate depletion, and in the condition where $[S] \leq K_m$, it might be considered reasonable to omit the term containing [*S*] from the kinetic equation. This simplification, however, results in the loss of any observable dependence on the concentration of reporter substrate used, approximating the value of K_i to its true value. For a better approximation, it is appropriate to keep the term $[S]/K$, expressed as the initial concentration of substrate $[S]_0$, as its value would become irrelevant under the following conditions:

a. for $[S]_0 \leq K$ and $[I]_0 \leq K_i$

b. for $[S]_0 \geq K$ and $[I]_0 \geq K_i$

$$[E] = \frac{[E]_0 - [EI^*]}{1 + \frac{[S]_0}{K} + \frac{[I]_0}{K_i}}$$

The concentration of the EI^* species is obtained by resolving the differential equation:

$$\frac{d[EI^*]}{dt} = k_{inact}[EI] = k_{inact}\frac{[E][I]_0}{K_i}$$

Now it is feasible to replace the free enzyme [*E*] with the equation containing the term [EI^*], and after rearrangement, we obtain:

$$\frac{d[EI^*]}{dt} = \frac{k_{inact}[I]_0([E]_0 - [EI^*])}{K_i^{app} + [I]_0}$$

Where, in competitive inactivators, the constant of inhibition exhibits a dependency on the concentration of the reporter substrate. This relationship is enclosed in the following equation:

$$K_i^{app} = K_i\left(1 + \frac{[S]_0}{K_m}\right)$$

We can describe the k_{obs} as:

$$k_{obs} = \frac{k_{inact}[I]_0}{K_i^{app} + [I]_0}$$

$$\int_0^{[EI^*]} \frac{1}{k_{obs}([E]_0 - [EI^*])} d[EI^*] = \int_0^t dt$$

Integrating for [EI^*], we obtain:

$$[EI^*] = [E]_0(1 - e^{-k_{obs}t})$$

IV. Solution of the differential equation d[S]/dt

The mass-balance equation for the enzyme can be rewritten as:

$$[E]_0 = [E] + [E]\frac{[I]_0}{K_i} + [E]_0(1 - e^{-k_{obs}t}) + [E]\frac{[S]}{K}$$

We solve with respect to [*E*], operating the same approximation done above with respect to the term [*S*] /*K*:

$$[E] = -\frac{[E]_0}{1 + \frac{[S]_0}{K} + \frac{[I]_0}{K_i}} e^{-k_{obs}t}$$

then substitute [E] in the differential equation for the substrate:

$$\frac{d[S]}{dt} = \frac{k_{cat}[E]_0[S]e^{-k_{obs}t}}{K + [S]_0 + \frac{[I]_0 K}{K_i}}$$

$$\int_{[S]_0}^{[S]} \frac{K + [S]_0 + \frac{[I]_0 K}{K_i}}{k_{cat}[E]_0[S]} d[S] = \int_0^t e^{-k_{obs}t} dt$$

The analytical solution for [S] obtained by integration of the differential equation, from $[S]_0$ to [S] and t=0 is:

$$[S] = [S]_0 e^{-\delta(1-e^{-k_{obs}t})}$$

where δ is:

$$\delta = \frac{k_{cat}[E]_0 K_i}{K\, k_{inact}[I]_0}$$

Considering the relationship $[S]_0$=[S]+[P], we can obtain the analytical solution for the concentration of the product during the time:

$$[P] = [S]_0 + \left[1 - e^{-\delta(1-e^{-k_{obs}t})}\right]$$

3.4 Inhibition assay

A preliminary screening process was conducted, employing a combination of computational docking studies, in vitro enzymatic assays, and literature review. Three main groups were selected: lichen secondary metabolites, curcuminoids, and phenylpropanoids. All compounds were initially tested at a standard concentration of 100 µM, to evaluate their potential inhibitory activities against $3CL^{pro}$.

Subsequently, promising candidates were subjected to further investigation. Thus, the inhibition assays were conducted at different inhibitor concentrations. The reactions were performed in a black 96-well microplate as mentioned above.

The irreversibility of the inhibition for salazinic and protocetraric acid was ascertained through the recovery of the enzymatic activity after a 100-fold dilution of the enzyme-inhibitor complex at 50 µM of each inhibitor by microcentrifuge tube filters.

Briefly, the reaction was performed as previously described (spectrofluorimetric assay). After a large dilution of the enzyme-inhibitor complex, it was centrifuged at 5000×g with a temperature of 4°C for about an hour and a half. The retentate was retrieved and after the addition of substrate at 10 µM, the recovery of the enzymatic activity was measured (Figure 15).

To such an extent, it was possible to identify the reaction schemes of the compounds under investigation.

In the reaction scheme for salazinic, protocetraric, fumarprotocetraric, *α*-collatolic, norstictic, ephiphoprellic acids, two kinetic parameters can describe enzyme inactivators: the constant of inhibition, K_i, and the constant rate of inactivation k_{inact}, as well as the k_{inact}/K_i ratio. K_i and k_{inact} are traditionally determined by the simplified version of the well-known Morrison-Walsh equation for slow-binding inhibitors (equation 3) (Waley SG., 1993):

$$E + I \underset{k_{off}}{\overset{k_{on}}{\rightleftarrows}} EI \xrightarrow{k_{inact}} EI^* \qquad \text{scheme 2}$$

$$[P] = \frac{v_i\left(1-e^{-k_{obs}t}\right)}{k_{obs}} \qquad \text{equation 3}$$

where v_i is the initial rate of the progress curve, and k_{obs} are the rate of interconversion between the initial rate v_i and the steady-state v_{ss}, which is equal to zero in the case of an inactivator.

As previously described, the $3CL^{pro}$ exhibits a cooperative behaviour, thus not ascribed to a Michaelian enzyme model. Since the Hill equation is empirical, it is not possible to derive equations describing the enzyme's behaviour in the presence of inhibitors. Using Michaelian models to analyze experimental data would lead to distortions in the results and their misinterpretation. It must also be considered that an essential assumption for the application of equation 3 is that the substrate concentration does not change significantly during the time course. Unfortunately, the very slow binding nature of the inhibitors leads to a consistent depletion of the substrate during the inhibition assays. To overcome substrate depletion, Waley, in 1993, proposed an approach for slow-binding reversible inhibitors (Waley SG., 1993), which can be easily adapted to irreversible inhibitors:

$$[P] = [S]_0 + \left[1 - e^{-\delta\left(1-e^{-k_{obs}t}\right)}\right] \qquad \text{equation 4}$$

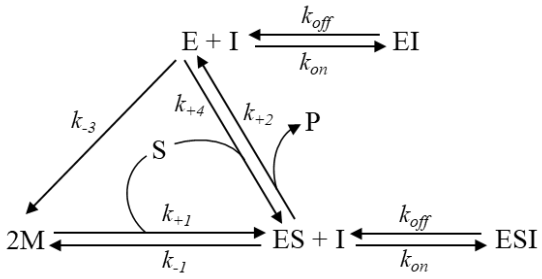
where

$$\delta = \frac{k_{cat}[E]_0\, K_i}{K\, k_{inact}[I]_0}$$ equation 5

$$k_{obs} = \frac{k_{inact}[I]_0}{K_i^{app} + [I]_0}$$ equation 6

One of the main problems in the application of equation 6 lies in that the *K* (*K_m* for Michaelian enzymes) and *k_{cat}* value of the enzyme contained in the *δ* factor must be known. To overcome the problem of the slow nature of the inactivators, we globally analyzed the entire data set at different inhibitor concentrations to obtain the individual values of *K_i^{app}* and *k_{inact}*, by fixing the concentration of the reporter substrate at 10 µM, approximately the minimum concentration where the behaviour of the enzyme can be approximated to a Michaelian model.

The reaction scheme for perlatolinic acid is characterized by a more intricate mechanism, delineated by the constant of inhibition, *K_i*, and the rate constants *k_{on}* and *k_{off}*, as depicted in the following reaction scheme:



scheme 3

In the reaction scheme for curcumin, demethoxycurcumin and salycilcurcumin, two kinetic parameters can describe enzyme inhibitors: the constant of inhibition, *K_i*, and the constant rate of inactivation *k_{inact}*, which are traditionally determined by the simplified version of the well-known Morrison-Walsh equation for slow-binding inhibitors (equation 3) (Waley SG., 1993):

$$E + I \underset{k_{off}}{\overset{k_{on}}{\rightleftarrows}} EI \xrightarrow{k_{inact}} EI^*$$ scheme 2

3.5 Determination of the mechanism of inhibition

The mechanisms of inhibition for salazinic, protocetraric, fumarprotocetraric, alpha-collatolic, and norstictic acids, were ascertained by fixing the concentration of inhibitors and changing the substrate reporter concentration ranging from 10 µM to 100 µM. The rate constant k_{obs} for each substrate concentration were derived by calculating the K_i^{app} and k_{inact} value at each substrate concentration using equation 5 and plotting the derived k_{obs} against the substrate concentration. In competitive inhibitors, the k_{obs} values are expected to decrease as the concentration of the substrate increases. The real value of K_i can be obtained for competitive inhibitors by equation 7. Inhibition assays were performed in triplicates.

$$K_i^{app} = K_i(1 + \frac{[S]_0}{K}) \qquad \text{equation 7}$$

The mechanism of inhibition for perlatolinic acid was first determined through a detailed analysis setting different DynaFit (Kuzmic P., 1996; 2009) scripts, to assess the hypothetical models of inhibition: competitive, noncompetitive, uncompetitive, and mixed types. Equation 8 was used to determine the *alpha* value to identify the binding site of perlatolinic acid.

$$v = \frac{\frac{V_{max}}{\left(1 + \frac{[I]}{\alpha K_i}\right)}[S]}{[S] + K_m\left(\frac{\left(1 + \frac{[I]}{K_i}\right)}{\left(1 + \frac{[I]}{\alpha K_i}\right)}\right)} \qquad \text{equation 8}$$

The theoretical model was experimentally confirmed through the assessment of the kinetic parameters, in particular V_{max} and K, in the presence and absence of perlatolinic acid, achieved by plotting the initial velocity (v_0) versus substrate concentrations (Figures 26A and 26B). The experimental setup involved a series of substrate concentrations (10, 20, 50, and 100 µM) while maintaining perlatolinic acid at a fixed concentration of 25 µM. Inhibition assays were performed in triplicates.

The cooperative behaviour of the 3CL protease was ascertained through the linearization of the Hill equation, by plotting $log(v/(V_{max}-v))$ as a function of $log[S]$

(Figures 26C and 26D). This was performed both in the presence of perlatolinic acid at a concentration of 25 µM and in its absence, determining the R^2 and h values.

The mechanism of inhibition for curcuminoids was ascertained by fixing the concentration of inhibitors and changing the substrate reporter concentration ranging from 10 µM to 100 µM. The rate constant k_{obs} for each substrate concentration were derived using equation 5 and plotting the k_{obs} against the substrate concentration. In competitive inhibitors, the k_{obs} values are expected to decrease as the concentration of the substrate increases. The real value of K_i can be obtained for competitive inhibitors by equation 7. Inhibition assays were performed in triplicates.

3.6 Molecular docking

3.6.1 Molecular docking: salazinic and protocetraric acids

From protein and ligand preparation, receptor grid generation to molecular docking, the modeling analysis was performed with Maestro module of Schrodinger LLC suite, version 2021-4, Schrödinger, LLC, New York, NY, USA [(L. Schrodinger. Schrodinger Software Suite Schrödinger LLC, New York (2011)].

Inhibitors salazinic acid and protocetraric acids were drawn using the 2D sketcher tool of Maestro, in both cyclic ester form and open conformer, the latter reflecting the effect of the covalent bond with the Cys145 (Figures 17A and 17B) [Maestro, Schrödinger, LLC, New York, NY, USA]. Ligprep utility in the Glide module was used to generate tautomers and isomers of screened ligands. The highest number of conformers to be generated was set to 32 [LigPrep, Schrödinger, LLC, New York, NY, USA) (Chen N. et al., 2020). The ionization states for each conformer were generated at pH 7.0 ± 2.0 with EPIK; ligands were then desalted [Epik, Schrödinger, LLC, New York, NY, USA]. An OPLS3 (Optimised Potentials for Liquid Simulations) force field was used for energy minimization of each compound with default parameters. The so-generated ligands library was then sent to docking using Glide software [Glide, Schrödinger, LLC, New York, NY, USA].
The protein structure CoV-2 main protease (PDB ID: 7RC1) (Holshue ML. et al., 2020; Phan LT. et al., 2020) at a resolution of 1.63 Å was downloaded from the scientific protein data bank (www.rcsb.org) (Fu L. et al., 2020). The downloaded raw protein was then prepared using the protein preparation wizard of GLIDE [Glide, Schrödinger, LLC, New York, NY, USA) (Kim, Y. et al., 2012). Missing hydrogen

atoms were added, bond orders assigned, zero bond order for disulfide bonds defined, and water molecules removed. Missing residues and side chains were added with PRIME [Prime, Schrödinger, LLC, New York, NY, USA]. The H-bond network was created before energy minimisation using the OPLS3 force field with a default constraint of 0.30 Å RMSD (Pedersen NC. et al., 2017).

Receptor Grid Generation wizard in Glide was used for grid generation with default parameters for partial cut-off (0.25) and scaling factor (1.0) (Schrödinger, LLC, New York, NY, USA). The receptor grid defining the active site cavity was generated by selecting the centroid of ligand GRL-0686 binding to CoV-2 main protease (PDB ID: 7RC1) (Phan LT. et al., 2020) as the center of the grid box. The generated grid file defining active site residues was used to dock ligand using Glide software.

3.6.1.1 Docking protocol validation

To validate the designed docking protocol, a covalent docking was performed with the prepared receptor CoV-2 main protease and the ligand GRL-0686 (PDB ID: 7RC1) (Holshue ML. et al., 2020; Phan LT. et al., 2020). The predicted binding orientation of GRL-0686 was then compared with the orientation assumed by GRL-0686 in the x-ray ternary complex RMSD between the docked pose and the crystal structure pose of GRL-0686 of 0,7866 strongly supports the designed procedure.

3.6.1.2 Extra Precision (XP) and Covalent Docking (CovDOCK)

A library of 13 ligands, prepared from the closed and the open conformation of inhibitors salazinic and protocetraric acids was docked in the active site of SARS-CoV main protease using GLIDE Extra Precision XP (non-covalent docking) and CovDock modes (Schrödinger, LLC, New York, NY, USA) (Kim, Y. et al., 2012; Wang Z. et al., 2021).

For cyclic esters conformers, molecular docking was conducted both in extra precision mode (XP mode) and covalent mode (CovDOCK mode) (Figure 17A). For open conformers (Figure 17B), docking was run only in CovDOCK mode. For covalent docking, the residue Cys145 was set as the active residue to covalently bind the ligand: nucleophilic addition to a double bond was selected as the reaction type. For the validation procedure and covalent docking, 'Virtual Screening (Fast)' was selected as docking mode in the CovDock module. The default 0.8 scaling factor (vdW) and 0.15 potential charge cut-off for XP docking were set. Post-docking analysis and visualization were executed using Pymol

(PyMOL Molecular Graphics System, Version 2.5 Schrödinger) (Owen DR. et al., 2021).

3.6.2 Molecular docking: perlatolinic acid

Perlatolinic acid was submitted to docking calculations towards $3CL^{pro}$ to investigate its binding mode and the major receptor-ligand interactions. Crystallographic structures of SARS-CoV-2 and SARS-CoV $3CL^{pro}$ available in Protein Data Bank (PDB) (*https://www.rcsb.org/*) were collected and ranked according to resolution, structure integrity and the presence of a co-crystallized ligand. Both SARS-CoV and SARS-CoV-2 were considered as they show 96% sequence identity, with only 12 variant residues out of 306, none of them involved in any major roles in the enzymatic activity of the protein (Goyal B. and Goyal D., 2020). Given the noncompetitive inhibition of perlatolinic acid, the research has been narrowed to targets co-crystallized with inhibitors within the active site. For this purpose, the X-ray structure of the SARS-CoV main protease covalently bound to indole Chloropyridinyl Ester-Derived inhibitor (PDB ID: 7RC1) was selected (Ghosh et al., 2021). Before docking, the protein structure was prepared while using the Protein Preparation Wizard in Maestro (Schrödinger LLC suite, version 2022–2, NY, USA), ionized at a pH of 7.4 using PROPKA, minimized using the OPLS4 force field and converging the heavy atoms to a RMSD of 0.30 Å. Water molecules, metals and the cognate ligand were removed. Perlatolinic acid was built via 2D sketcher panel in Maestro, then it was submitted to ligand preparation by LigPrep module, including conversion of 2D structure to 3D ones, hydrogens addition, partial charges computation and structure optimization at a pH of 7.0 ± 2.0 using Epik.

To predict the target druggability and identify the potential allosteric binding sites, the prepared protein was submitted to SiteMap (SiteMap, Schrödinger, LLC, New York, NY, 2022), looking for binding sites on the entire protein structure, including shallow sites. The definition of hydrophobicity used in the calculation was set to “more restrictive”, and a fine grid was selected. Binding sites were then selected from all identified sites, and all output values were recorded.

Having identified the top-ranked binding sites, perlatolinic acid was submitted to docking simulations. In the rigid docking mode, the grid was generated and centered on the binding site from SiteMap calculations; the Receptor Grid Generation module was carried out with default parameters, while serines 139, 144 and 147 were set as rotatable. The ligand was then docked both with Glide SP and XP protocol. To further investigate the binding mode of the ligand and allow

a certain degree of flexibility at the dimer interface, perlatolinic acid was docked in an induced-fit mode (Induced Fit Docking protocol; Glide, Schrödinger, LLC, New York, NY, 2022; Prime, Schrödinger, LLC, New York, NY, 2022). The grid was centered on Arg4, Lys5, Lys137 and Glu288, residues lining the pocket previously identified by SiteMap. The extra-precision (XP) protocol was adopted using a maximum number of poses equal to five, refining residues within 5.0 Å of ligands and automatically trimming the side chains based on the B-factor.

3.6.3 Molecular docking: fumarprotocetraric acid

The computational investigation of fumarprotocetraric acid began with a preliminary molecular docking study. To predict the molecular interactions between the ligand and the 3CL protease, SwissDock (*http://www.swissdock.ch.*) (Grosdidier A. et al., 2011a; 2011b) served as the initial platform for assessing the binding affinities and potential inhibition mechanisms of fumarprotocetraric acid, with Accurate Docking Type without flexibility as extra parameters.

The protein structure CoV-2 main protease (PDB ID: 7RC1) (Holshue ML. et al., 2020; Phan LT. et al., 2020) at a resolution of 1.63 Å was downloaded from the scientific protein data bank (www.rcsb.org) (Fu L. et al., 2020).

Following the preliminary docking assessments, detailed analyses were conducted using the Chimera software package (*https://www.rbvi.ucsf.edu/chimera*). This step involved a thorough examination of the docking poses, interaction energies, and the potential binding sites identified during the initial SwissDock simulations. Specific attention was given to elucidating the molecular interactions that underpin the observed binding affinities, with a focus on hydrogen bonding, hydrophobic contacts, and electrostatic interactions.

3.7 Cell culture and viability assay

TM4 (ATCC® CRL1715™) mouse Sertoli cells were obtained from the American Type Culture Collection. Cells were initially seeded at a density of 1×10^4 cells/cm^2 and regularly maintained in DMEM/F-12 50/50 Mix supplemented with 5% HS (horse serum), 2.5% FBS (fetal bovine serum), 100 IU/mL penicillin, and 100 µg/mL streptomycin until they reached a confluence of about 80%. Proliferation and viability rates were evaluated using a Trypan blue exclusion assay. Cells were maintained at 37 °C in a humidified atmosphere containing 5% CO_2. Cells were

seeded at a density of 1×10^4 cells/cm^2 and maintained in standard conditions for 24 hours before treatments. Afterward, cells were exposed to perlatolinic acid at concentrations ranging from 0 to 80 µM for 24 and 48 hours, and to protocetraric and salazinic acid at concentrations ranging from 1 to 80 µM for 24 and 48 hours.

3.8 Statistics and data analysis

All experiments were performed in triplicate. The parameters, experimental errors, and non-linear fitting were assessed and calculated using Microsoft Excel and OriginPro 8.5.1. The analysis to determine the kinetic inhibition parameters was performed using the software DynaFit ver 4.09.047 by Petr Kuzmic (BioKin Ltd).

The modelling analysis for salazinic and protocetraric acids was performed with Maestro module of Schrodinger LLC suite, version 2021-4, Schrödinger, LLC, New York, NY, USA.

The modeling analysis for perlatolinic acid was performed with Schrödinger LLC suite, version 2022–2, NY, USA. Figures were generated using Pymol (Pymol Molecular Graphics System, Version 2.0 Schrödinger, LLC).

The modeling analysis for fumarprotocetraric acid was performed with SwissDock (*http://www.swissdock.ch.*) and Chimera software package (*https://www.rbvi.ucsf.edu/chimera*).

Capitolo IV

Results

4.1 Determination of the kinetic parameters

The plot of the initial rate (v_0) versus the substrate concentration for the $3CL^{pro}$ enzyme is well described by the Hill equation for a cooperative enzyme (Figure 13A). Kinetic parameters were systematically determined across each series of experiments, subsequently, they were explicitly used for the analysis of the experimental data. For simplicity, in this section, the mean values, derived from the aggregated dataset obtained through a number of experiments, are reported. The V_{max} value is 4457 ± 290 RFU s^{-1}, equivalent to 0.0235 µM s^{-1} with a k_{cat} value of 2.73 s^{-1}. The enzyme's affinity for the substrate, K, is calculated as 31.5 ± 3.8 µM and the Hill coefficient h is equal to 1.43 ± 0.14. The deviation from the Michaelian behaviour of the enzyme is confirmed by the Hanes–Woolf linearization of the Michaelis–Menten equation (Figure 13B). Any deviation from the hyperbolic kinetic can be easily assessed by examining the coefficient of determination R^2 of the interpolated line, which is equal to 0.7260, providing a clear indication of the enzyme's non-Michaelian behaviour.

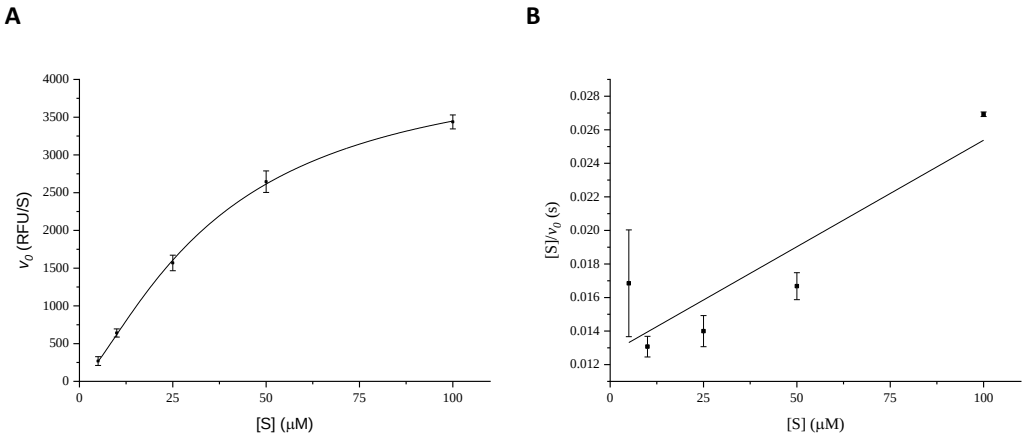


Figure 13. Determination of the kinetic parameters of 3CL protease. **A)** Plot of the non-linear fit of the initial rates versus five different substrate concentrations fitting the Hill equation for cooperative enzymes. **B)** Hanes-Woolf linearisation of the initial rates versus several substrate concentrations to verify the non-Michaelian behaviour of the enzyme. In this case, the coefficient of determination R^2 of the interpolated line is equal to 0.7260, which excludes the Michaelian model.

4.2 Screening of natural compounds

The initial phase of this doctoral research involves a comprehensive screening process aimed at identifying natural compounds with potential inhibitory properties against the SARS-CoV-2 3CL protease. This preliminary stage adopts a comprehensive, multifaceted approach, integrating computational docking studies, *in vitro* enzymatic assays, and an extensive review of existing literature to methodically assess the antiviral capabilities of a broad spectrum of natural compounds.

Various natural compounds are evaluated for their potential to inhibit the SARS-CoV-2 3CL protease, with a particular focus on three primary groups: lichen secondary metabolites, curcuminoids, and phenylpropanoids. This selection is based on their distinct chemical structures and documented biological activities, which suggest a promising groundwork for their antiviral properties.

Subsequent to their identification, all compounds are subjected to initial testing at a standardized concentration of 100 µM. This phase is pivotal in determining their potential inhibitory actions against $3CL^{pro}$, thereby paving the way for more detailed analyses of promising candidates.

Within the curcuminoids group, tested at a concentration of 100 µM, bisdemethoxycurcumin does not exhibit any inhibitory activity against the enzyme. Conversely, curcumin, salicylcurcumin, and demethoxycurcumin demonstrate potential inhibitory effects, with inhibition fractions observed within the range between 0 and 0.87 (Table 1).

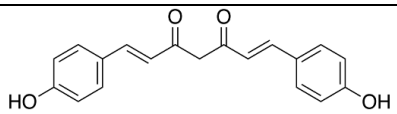
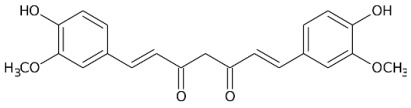
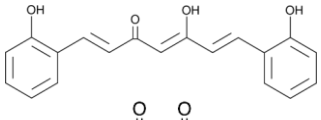
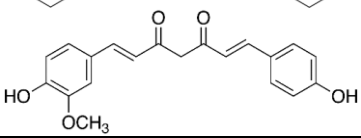
Compound (100 µM)	Structure	v_i/v_0	Inhibited Fraction
Bisdemethoxycurcumin		1	0
Curcumin		0.13	0.87
Salicylcurcumin		0.25	0.75
Demethoxycurcumin		0.15	0.85

Table 1. Results of the preliminary screening experiment for curcuminoids. The structures, the fractional residual activity (v_i/v_0) and the fraction of inhibition are reported.

At the tested concentration of 100 µM, the investigated phenylpropanoid compounds exhibit limited or absent inhibitory activity against the 3CL protease, as demonstrated in Table 2. The ratio of v_i/v_0 ranged between 0.72 and 1, indicating, considering the tested concentration, a lack of significant impact on the enzyme's activity.

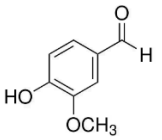
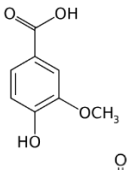
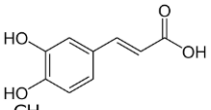
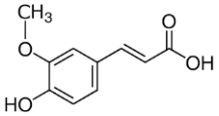
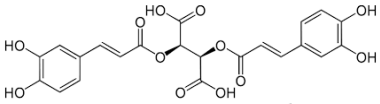
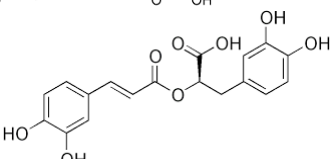
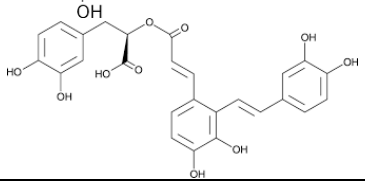
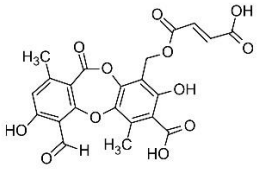
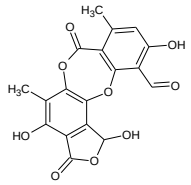
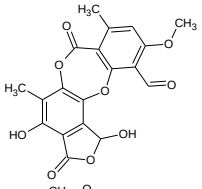
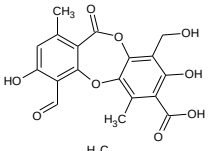
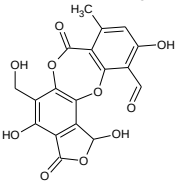
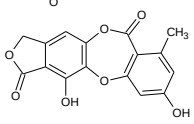
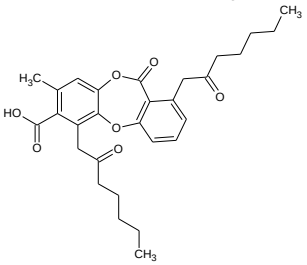
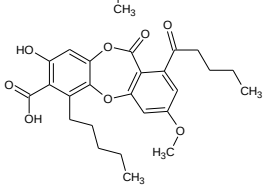
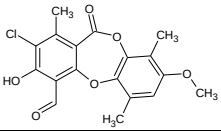
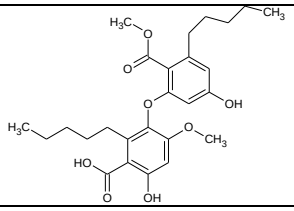
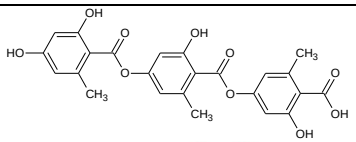
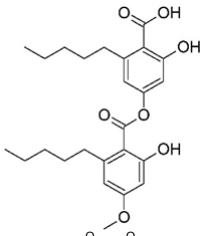
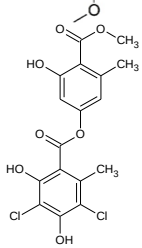
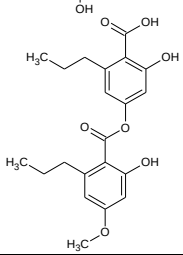
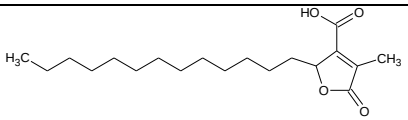
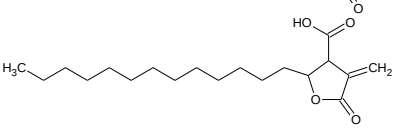
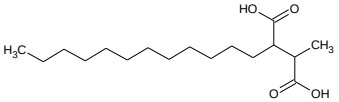
Compound (100 µM)	Structure	v_i/v_0	Inhibited Fraction
Vanillin		0.76	0.24
Vanillic acid		0.93	0.07
Caffeic acid		0.82	0.18
Ferulic acid		1	0
Chicoric acid		1	0
Rosmarinic acid		0.72	0.28
Salvianolic acid		1	0

Table 2. Results of the preliminary screening experiment for phenylpropanoid compounds. The structures, the fractional residual activity (v_i/v_0) and the fraction of inhibition are reported.

Lichen secondary metabolites demonstrate promising results in their activity against the SARS-CoV-2 protease, with the majority showing good inhibitory effects, regardless of group. The inhibition percentage observed ranges from 67% to 99% (Table 3).

Lichen Compound (100µM)	Structure	v_i/v_0	Inhibited Fraction
Depsidones			
Fumarprotocetraric acid		0.09	0.91
Norstictic acid		0.25	0.75
Stictic acid		0.28	0.72
Protocetraric acid		0.16	0.84
Salazinic acid		0.11	0.89
Variolaric acid		0.22	0.78
Alpha-collatolic acid		0.02	0.98
Lobaric acid		0.87	0.13
Pannarin		0.95	0.05

Lichen Compound (100µM)	Structure	v_i/v_0	Inhibited Fraction
Pseudo-depsidones			
Ephiphorellic acid		0.02	0.98
Depsides			
Gyrophoric acid		0.15	0.85
Perlatolinic acid		0.01	0.99
Tumidulin		0.17	0.83
Divaricatic acid		0.21	0.79
Paraconic acids			
Lichesterinic acid		0.20	0.80
Protolichesterinic acid		0.33	0.67
Roccellic acid		0.89	0.11

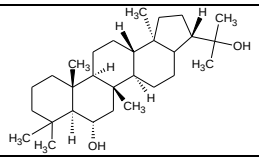
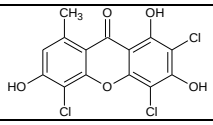
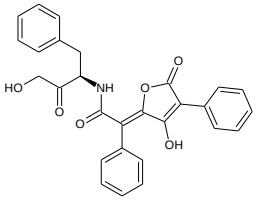
Lichen Compound (100μM)	Structure	v_i/v_0	Inhibited Fraction
Triterpenes			
Zeorin		0.26	0.74
Xanthones			
Arthotelin		0.23	0.77
Diphenyl-butenolides			
Rhizocarpic acid		0.13	0.87

Table 3. Results of the preliminary screening experiment for lichen secondary metabolites. The structures, the fractional residual activity (v_i/v_0) and the fraction of inhibition are reported. Lichen secondary metabolites are divided in groups, based on their specific structure.

Given the outcomes of the research, phenylpropanoid compounds, are excluded from further investigation due to their lack of significant activity in relation to the objectives of this work. In contrast, lichen secondary metabolites and curcuminoids, which demonstrate promising inhibitory effects against the SARS-CoV-2 $3CL^{pro}$, are selected for more in-depth analysis.

4.3 Detailed results from in-depth investigations

In this section, attention will be directed towards the detailed presentation of results derived from the in-depth analysis of the two primary compounds investigated, lichens and curcuminoids. Below is the detailed analysis of each compound concerning, where available, the inhibition assay, molecular docking, and cell proliferation and viability in TM4 epithelial cells.

4.3.1 Lichen secondary metabolites

4.3.1.1 Salazinic and protocetraric acids

Inhibition Assay. The time-course plots at inhibitor concentrations ranging from 5 µM to 100 µM are consistent with a slow-binding inactivator for protocetraric acid (Figure 14A) and salazinic acid (Figure 14B).

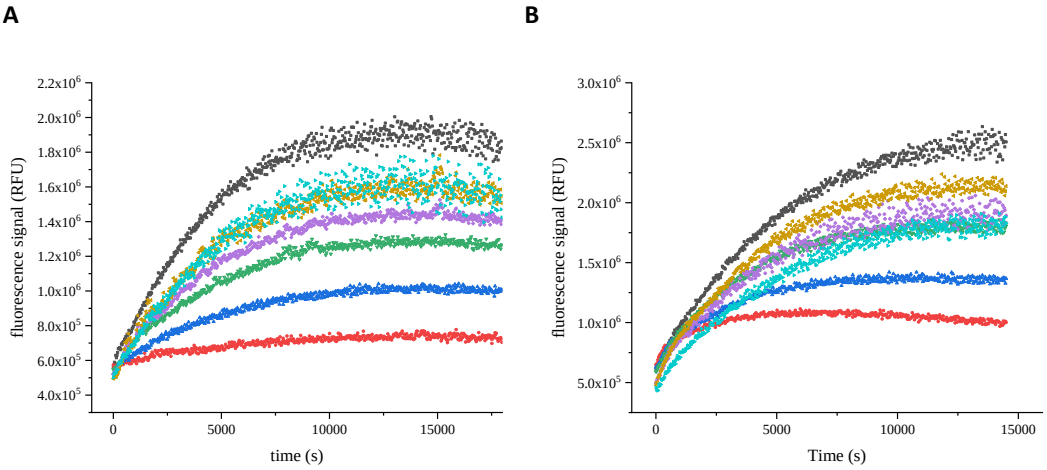


Figure 14. Time course at various Inhibitor concentrations. **A)** Protocetraric acid; **B)** Salazinic acid. Black, positive control; light blue, 5 µM; yellow, 10 µM; magenta, 25 µM; green, 50 µM; blue, 75 µM; red, 100 µM. RFU, relative fluorescence unit.

The irreversibility of the inhibition is confirmed by measuring the recovery of the enzymatic activity after a large dilution of the enzyme-inhibitor complex at 50 µM of each inhibitor. The results, plotted in Figure 15, indicate the absence of enzymatic activity recovery after dilution of the inhibitors, suggesting the formation of a stable enzyme-inhibitor complex. This outcome supports the classification of these inhibitors as inactivators. The described mode of action of the inhibitors conforms to the scheme of reaction reported in scheme 2, where the initial *EI* complex, characterized by a k_{on} and k_{off} rate constants, is slowly followed by the formation of a stable EI^* adduct, characterized by an inactivation rate constant, k_{inact}.

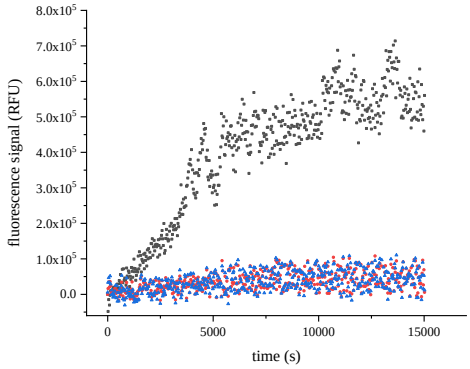


Figure 15. The irreversibility of the inhibition is ascertained through the recovery of the enzymatic activity. Black, positive control; red, protocetraric acid 50 µM; blue, salazinic acid 50 µM.

To overcome the substrate depletion effect, the time-course curves at different inhibitor concentrations are fitted to equation 4. The K_i^{app} and k_{inact} values are estimated by analyzing the entire set of data. The results from this analysis are reported in Table 4. Both compounds behave in the same way with almost equal K_i^{app} and k_{inact} values.

Compound	k_{inact} (s^{-1})	K_i^{app} (µM)	K_i (µM)	k_{inact}/K_i (s^{-1} $µM^{-1}$)
Protocetraric acid	$1.19\times10^{-4}\pm2.1\times10^{-6}$	5.22±0.07	3.95	3.01×10^{-5}
Salazinic acid	$1.33\times10^{-4}\pm3.0\times10^{-6}$	4.98±0.09	3.77	3.53×10^{-5}

Table 4. Estimation of inhibition parameters at 10 µM of substrate.

The investigation of the inhibition mechanism is clarified by determining the k_{obs} values from the K_i^{app} and k_{inact} determined at a fixed concentration of inhibitor, 75 µM for both compounds, varying the concentration of the reporter substrate. As depicted in Figure 15, both compounds act competitively with the substrate since the k_{obs} value decreases as the substrate concentration increases. The determination of a competitive mechanism of inhibition allows the determination of the real K_i^{app} value by applying equation 7. The K_i value for both compounds is lower than 4 µM (Table 4).

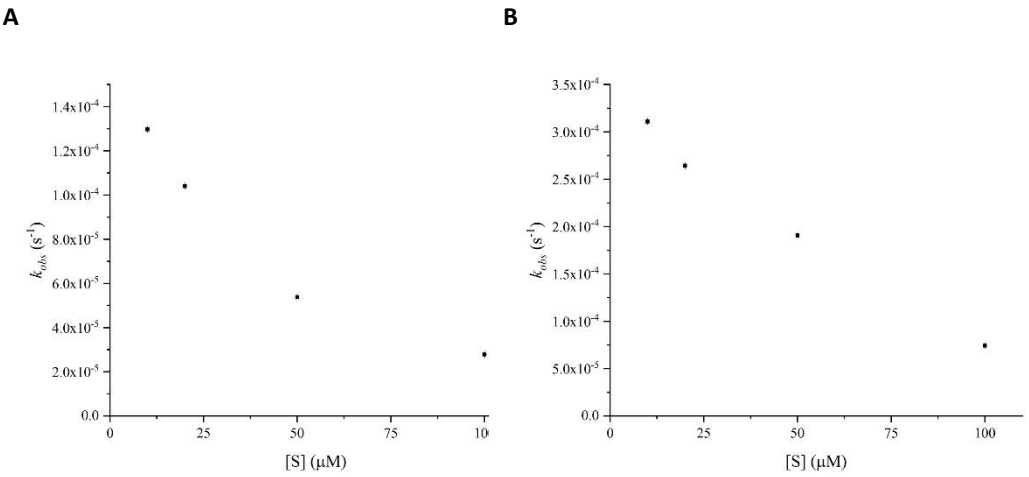


Figure 16. Plot of the k_{obs} versus the substrate reporter, ranging from 10 μM to 100 μM, at a concentration of inhibitors at 75 μM for the determination of the mechanism of inhibition. **A)** Protocetraric acid; **B)** salazinic acid.

Molecular docking. A preparative docking analysis is performed exclusively on cyclic ester conformers using the extra precision mode (XP mode, non-covalent docking), to validate their compatibility with the active site of the $3CL^{pro}$. This docking simulation suggest that the ligands are well-suited for the active site, forming numerous interactions with adjacent residues (data not shown).
Subsequently, covalent docking (CovDOCK) is conducted on salazinic and protocetraric acids in both their open and closed conformations (Figure 17).

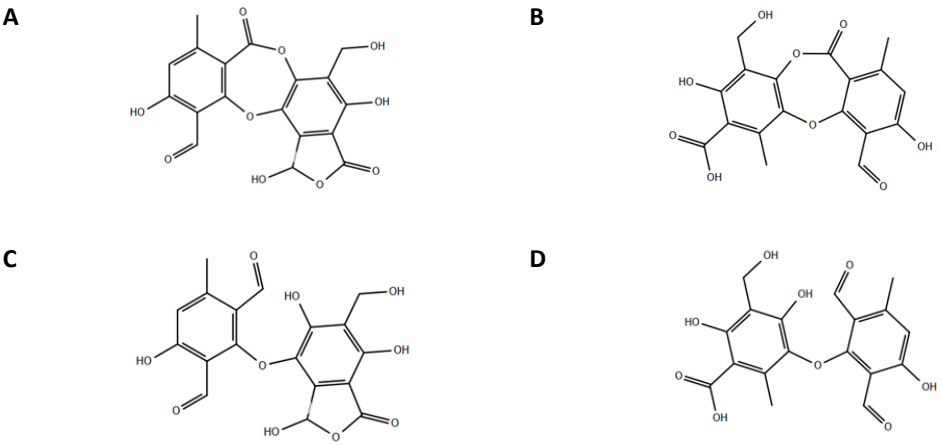


Figure 17. Molecule structures. **A)** Salazinic acid and **B)** protocetraric acid: the cyclic ester conformers (closed) docked against SARS-CoV-2 main protease are represented. **C)** Salazinic acid and **D)** protocetraric acid: the open conformers docked against SARS-CoV-2 3CL protease are represented. All the molecules are drawn using 2D sketcher tool of Maestro [Maestro, Schrödinger, LLC, New York, NY, USA].

This analysis depicts the formation of a covalent interaction, corroborating the results of kinetic analyses. The findings indicate that both ligands are well accommodated within the active site. The complex predicted between enzyme and inhibitor is primarily guided by the covalent bond with the Cys145, a key reactive residue within the active site, and is further reinforced by specific interactions, including hydrogen bonds, salt bridges, and π-π interactions (Figures 18-20).

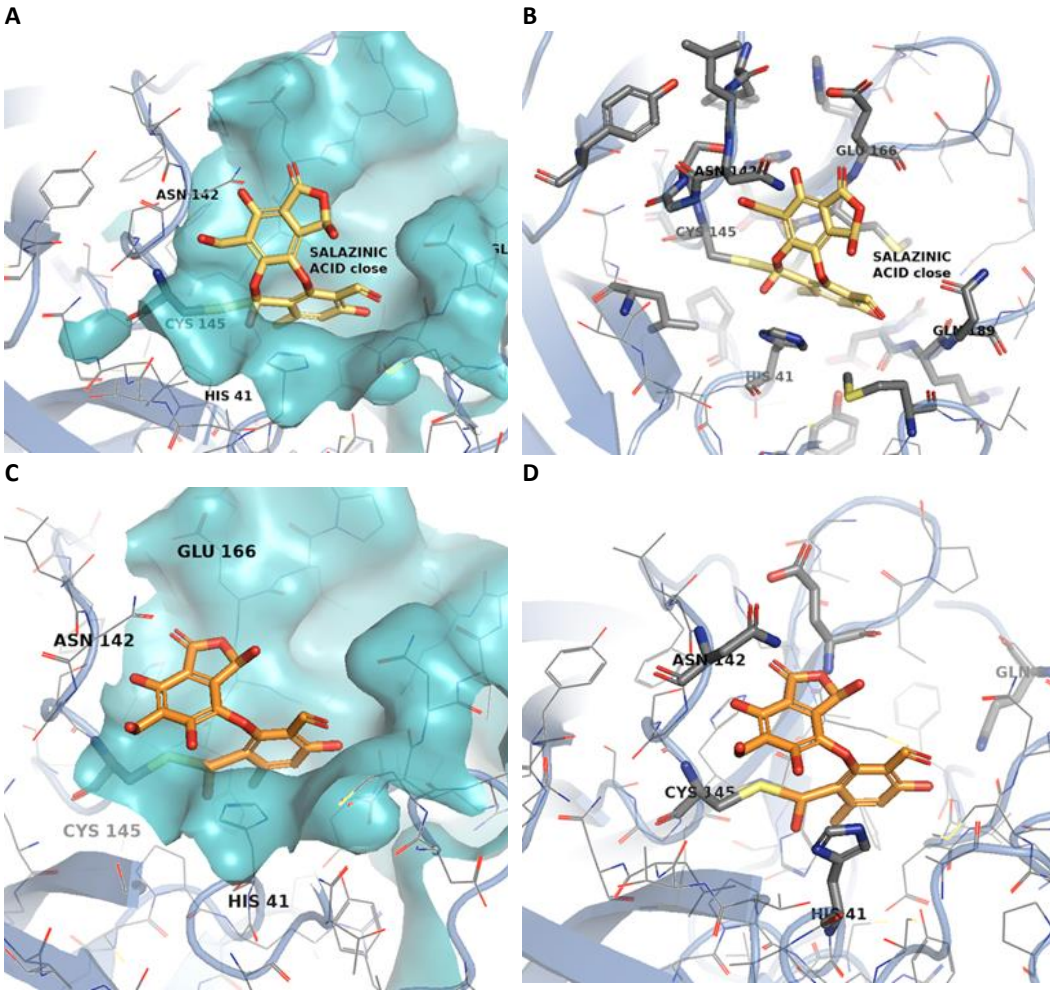


Figure 18. A-B) Cyclic ester salazinic acid covalently bound to SARS-CoV-2 $3CL^{pro}$. **C-D)** Open salazinic acid conformer covalently bound to CoV-2. Cys145, His41, and Glu166, residues essential for the enzymatic activity of $3CL^{pro}$, are highlighted. All the figures are prepared with PyMOL (PyMOL Molecular Graphics System, Version 2.5 Schrödinger, LLC).

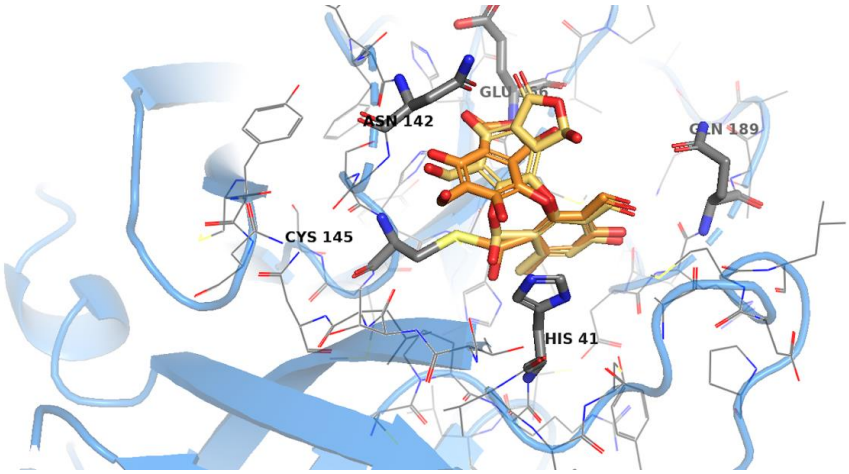


Figure 19. Comparison between open (orange) and closed (dark yellow) conformation for salazinic. The benzofuranone ring rearranges and makes a hydrogen bond with Glu166. Figures are prepared with PyMOL **(**PyMOL Molecular Graphics System, Version 2.5 Schrödinger, LLC).

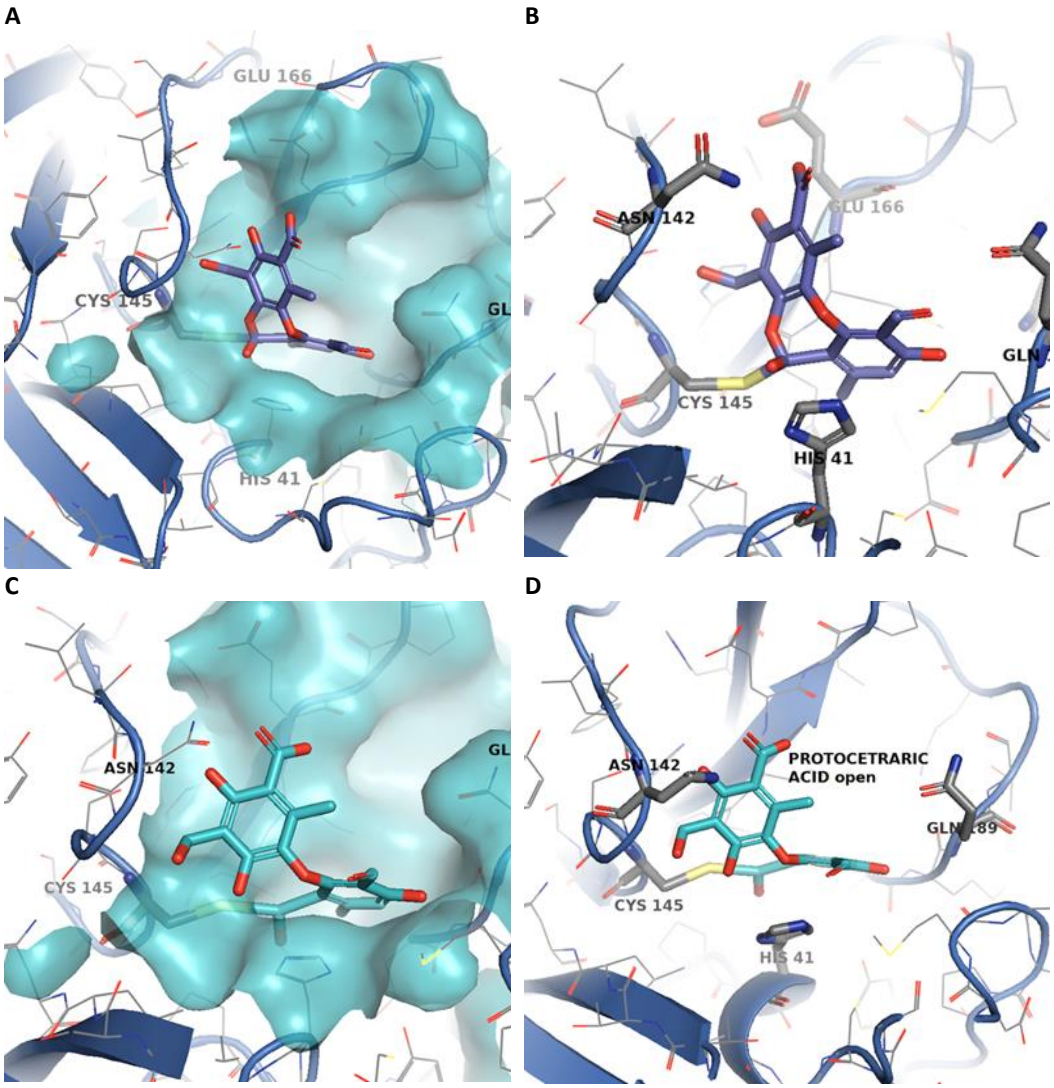


Figure 20. A-B) Cyclic ester protocetraric acid covalently bound to SARS-CoV-2 $3CL^{pro}$. **C-D)** Open protocetraric acid conformer covalently bound to SARS-CoV-2 $3CL^{pro}$. Cys145, His41, and Glu166, residues essential for the enzymatic activity of $3CL^{pro}$, are highlighted. All the figures are prepared with PyMOL (PyMOL Molecular Graphics System, Version 2.5 Schrödinger, LLC).

Noteworthy, the nucleophilic attack mediated by the Cys145 involves ligands at their cyclic ester, one of the possible but not exclusive reactive points within the molecules.

Delving further into specifics, the binding prediction for salazinic acid in its cyclic ester form (closed conformer) (Figures 18A and 18B) confirms that the catalytic Cys145 forms a covalent bond with the ester carbon carbonyl. The aromatic ring forms a π-π stacking with His41 and the hydroxyl group of the adjacent ring interacts by H-bond with Gly143 and Leu141 (Figure 21).

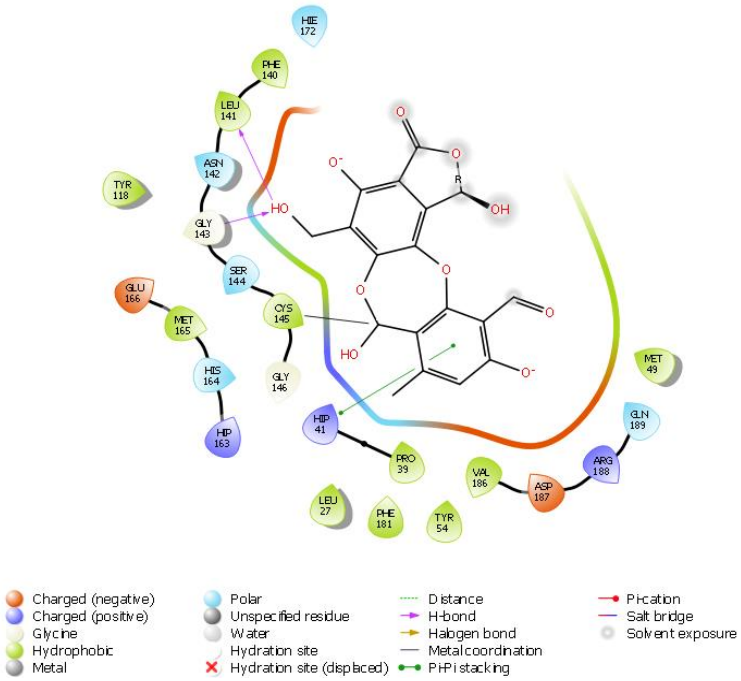


Figure 21. Cyclic ester salazinic acid conformer covalently bound to CoV-2: detailed interactions. Figures are prepared with PyMOL (PyMOL Molecular Graphics System, Version 2.5 Schrödinger, LLC).

In the binding prediction for salazinic acid carrying the hydrolyzed ester (open conformer) (Figures 18C and 18D), the Cys145 initiates a covalent attack, as previously mentioned, and the molecule takes advantage of the higher conformational freedom due to its open form. As a result, the molecule can tune some established interactions with the surrounding active site residues as it slightly rearranges in the binding site. The aromatic side ring maintains the π-π stacking with His41, which additionally forms a salt bridge interaction with the bicycle hydroxyl. The dihydro benzofuranone hydroxyl establishes two H-bond interactions with Ser144 and Gly143. Furthermore, the furanone forms an additional H-bond with Glu166 (Figure 22).

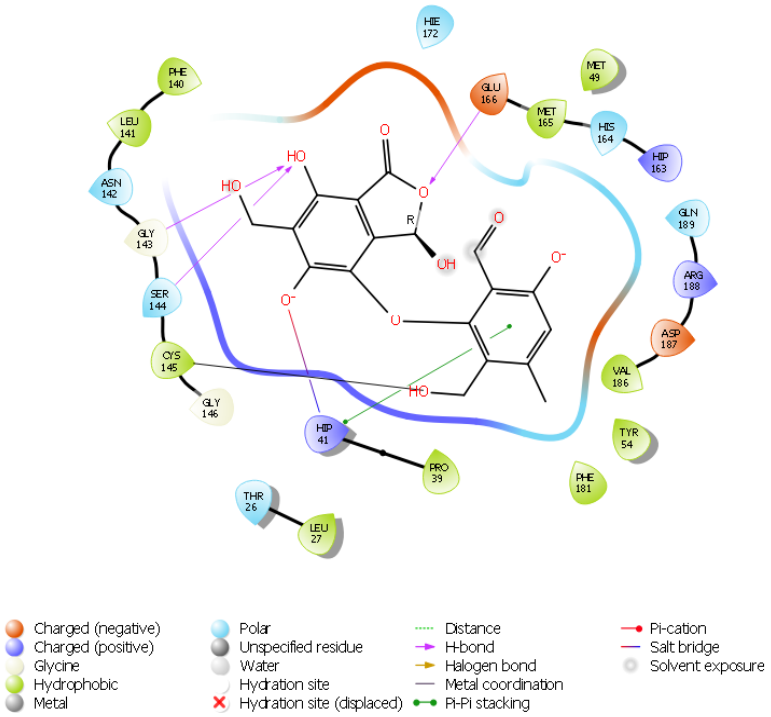


Figure 22. Open salazinic acid conformer covalently bound to CoV-2: detailed interactions. Figures are prepared with PyMOL **(**PyMOL Molecular Graphics System, Version 2.5 Schrödinger, LLC).

The binding energy of the salazinic acid in its cyclic ester is consistent (docking score -5.982). After its rearrangement in the active site allowing a better orientation of the bulky benzo furanone rings, the open conformation demonstrates a more favorable energy profile (docking score -7.007). Additionally, the number of allowed docking poses from closed to open conformations increases remarkably (52 respect to 82) (Figure 19).

In the binding prediction for protocetraric acid as a cyclic ester (closed conformer) (Figures 20A and 20B), as already seen for salazinic acid, the carbonyl carbon of the cyclic ester undergoes a nucleophilic attack by the catalytic Cys145 and result covalently bonded to it. The side aromatic ring forms a π-π stacking with His41. The aromatic carboxylic acid is involved in an H-bond with Asn142. The ligand seems stabilized further in the active site, mainly by apolar interactions (Figure 23).

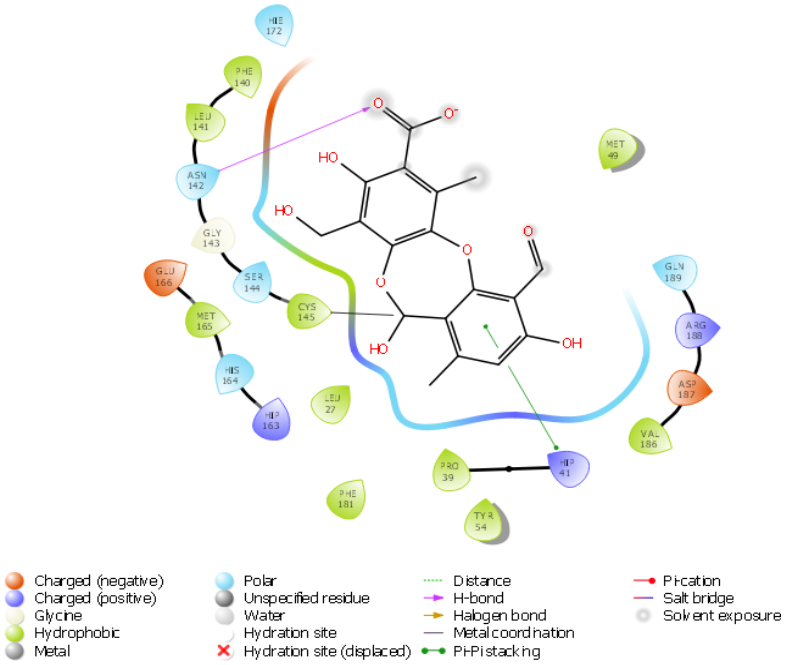


Figure 23. Cyclic ester protocetraric acid conformer covalently bound to CoV-2: detailed interactions. Figures are prepared with PyMOL (PyMOL Molecular Graphics System, Version 2.5 Schrödinger, LLC).

The open protocetraric acid conformer is predicted to undergo a covalent attack by the Cys145 as well; moreover, the cleaved cyclic ester slightly rearranges in the binding site thanks to the gained conformational freedom as also seen for the open salazinic acid conformer (Figures 20C and 20D). As a matter of fact, this adjustment results in the loss of interaction with Asn143 but facilitates the formation of new interactions with residues within the active site: the aromatic hydroxyl methyl group interacts by H-bonds with Gly143, while the aromatic carboxylic group establishes an H-bond with Glu166. The aromatic ring maintains its π-π stacking with His41, which is also involved in a hydrogen bond with the vicinal carbonyl group carried by the ligand (Figure 24). Few hydrophobic residues in the proximity further stabilize the complex. The improvement in the binding is confirmed by increasing the docking score and the number of allowed orientations for each conformer.

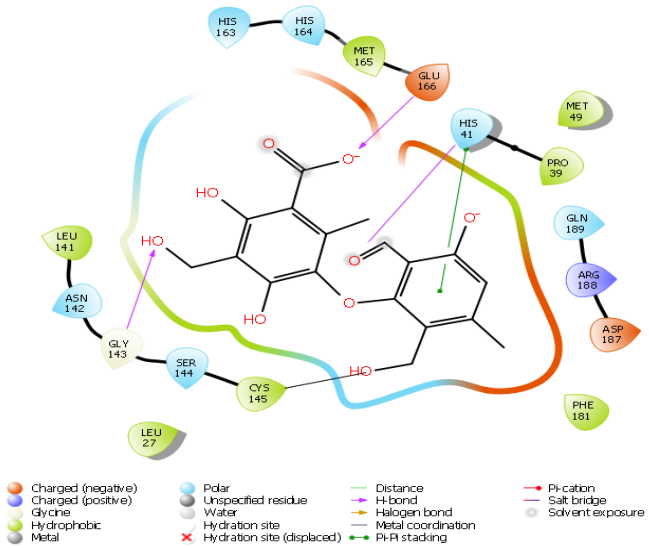


Figure 24. Open protocetraric acid conformer covalently bound to CoV-2: detailed interactions. Figures were prepared with PyMOL (PyMOL Molecular Graphics System, Version 2.5 Schrödinger, LLC).

Cell proliferation and viability in TM4 epithelial cells. The trypan-blue exclusion assays do not reveal any cytotoxic effects induced by protocetraric acid and salazinic acid on TM4 cells at the tested doses, ranging from 1 to 80 µM, up to 48h exposure (data not shown). It could not be possible to explore higher concentrations since the poor solubility of the compounds would increase the toxic effect of DMSO.

4.3.1.2 Perlatolinic acid

Inhibition assay. The kinetic analysis, conducted across a range of perlatolinic acid concentrations from 0.5 µM to 50 µM, reveals a slow-binding inhibition mechanism, as depicted by the time-course plots (Figure 25). This phenomenon indicates a time-dependent interaction, characterized by a gradual association rate between the inhibitor and the enzyme. This slow-binding process suggests that the establishment of equilibrium between the inhibitor and enzyme is delayed compared to the turnover rate of the enzyme-catalyzed reaction (Morrison JF. and Walsh CT., 1988).

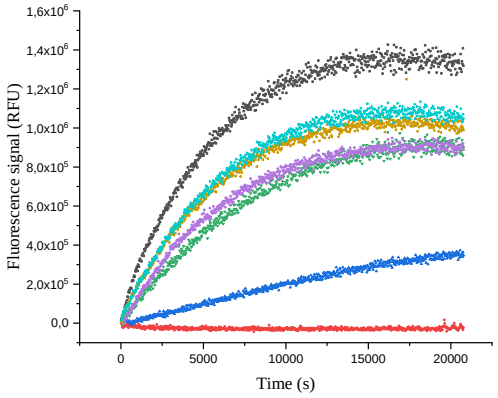


Figure 25. Time-course plots at different inhibitor concentrations. Black, positive control; red, perlatolinic acid 50 µM; blue, 25 µM; green, 10 µM; magenta, 5 µM; yellow, 1 µM; light blue, 0.5 µM.

For this compound, a crucial aspect requiring elucidation is the determination of the mechanism of inhibition which is initially addressed through a detailed analysis setting different DynaFit scripts, to assess the hypothetical models of inhibition: competitive, noncompetitive, uncompetitive, and mixed types. The outcomes of our investigation demonstrate a plausible noncompetitive inhibition model, which is substantially supported by the observed experimental data.

The results of k_{on} and k_{off} values are reported in Table 5.

Compound	k_{on}	k_{off}	K_i (µM)
Perlatolinic acid	$4.56 \times 10^{-5} \pm 8.7 \times 10^{-7}$	$3.04 \times 10^{-5} \pm 1.7 \times 10^{-6}$	0.67

Table 5. Estimation of inhibition parameters at 10 µM of substrate.

Noncompetitive inhibitors can bind the free enzyme and the Michaelis complex, potentially affecting the K_m and/or the V_{max} values, in dependence on the *alpha* value (equation 8). Using this theoretical model, the value of *alpha* has been experimentally determined by evaluating the kinetic parameters both in the presence and absence of the inhibitor. This is made by plotting the initial velocity (v_0) versus different substrate concentrations, both in the absence of perlatolinic acid and with a fixed inhibitor concentration of 25 µM (Figures 26A and 26B).

In this study, noncompetitive inhibition is characterized by a decrease in the apparent maximum velocity (V_{max}) of the reaction, while the value of *K* remains essentially unaffected. Specifically, the *K* parameter remains nearly unaltered, with a value of about 40. V_{max} value exhibits a reduction in the presence of the inhibitor (1932.88 ± 31.51 RFU s^{-1} instead of 2831.13 ± 174.05 RFU s^{-1}). This behaviour is

indicative of a noncompetitive inhibitor with an α value of 1, suggesting that perlatolinic acid can bind equally to both the free enzyme (E) and the enzyme-substrate complex (ES).

Moreover, the results suggest that the enzyme exhibits comparable behaviour regardless of the presence and absence of perlatolinic acid. Furthermore, it is noteworthy that the $3CL^{pro}$ maintains its cooperative behaviour, regardless of the presence of the lichen compound. By linearization of the Hill equation (equation 2) at different inhibitor concentrations, it is possible to demonstrate the permanence of the cooperative behaviour.

Thus, a plot of $log(v/(V_{max}-v))$ versus $log[S]$ should produce a straight line with a slope of h and a y-intercept of $-log(K')$. The verification of our results is obtained with R^2 values almost close to 1, in particular 0.99988 for [I] of 25 µM (Figure 26C) and 0.99935 without perlatolinic acid (Figure 26D). The slope of the straight line provides an estimate of the Hill coefficient h, a value of 1.37±0.02 in the absence of perlatolinic acid and of 1.73±0.01 with a concentration of 25 µM of inhibitor.

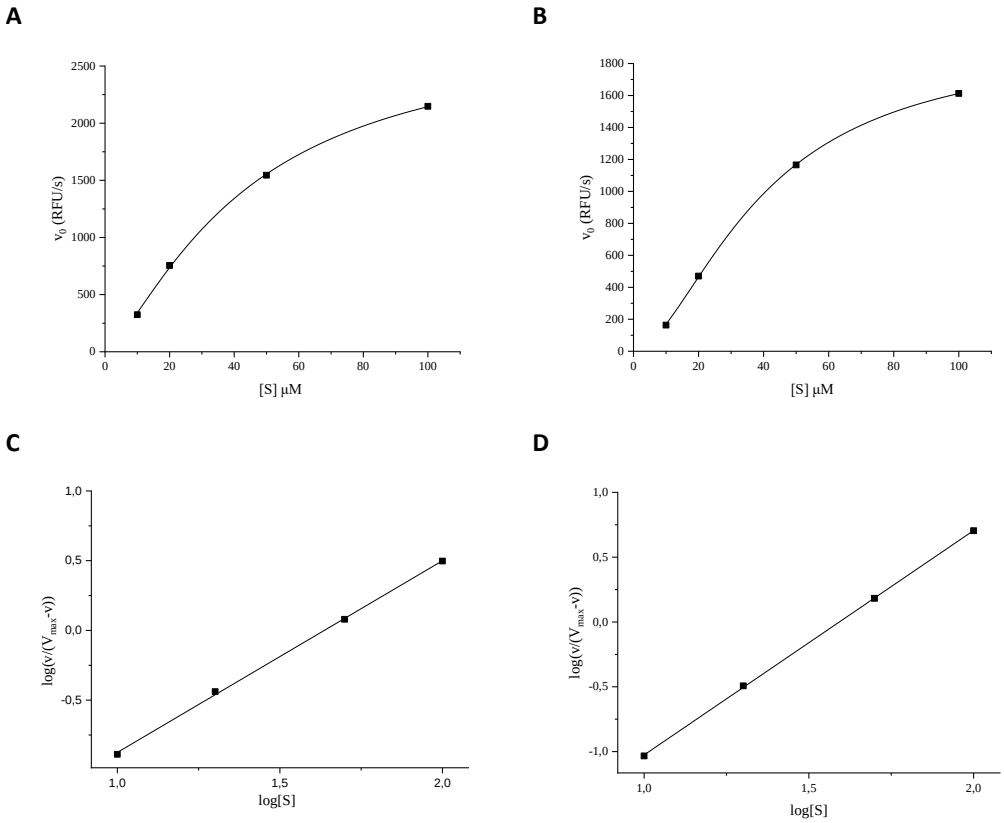


Figure 26. The plot of the initial velocity (v_0) versus substrate concentrations both in the absence (**A**) and presence (**B**) of the inhibitor. **C-D:** The linearization of the Hill equation by plotting $log(v/(V_{max}-v))$ as a function of $log[S]$.

Molecular docking. To elucidate the molecular mechanism of inhibition of SARS-CoV $3CL^{pro}$ by perlatolinic acid, comprehensive docking analyses are carried out. Given the absence of $3CL^{pro}$ - non-competitive inhibitor crystal complexes, a SiteMap analysis of the protein is carried out to determine along target protein accessible binding site for docking studies. This preliminary analysis led to the identification of four available binding sites (Figure 27), including shallow ones, whose scores and volumes are reported and ranked in Table 6. Following the SiteScore criteria, the two best sites, site 1 and Site 2, cover some of the critical residues implicated in the dimerization process and are selected for grid generation and docking. Site 3, despite its favourable score, is excluded as it encompasses the catalytic dyad His41-Cys145, aligning with the results from kinetic analyses. Site 4 is not further investigated due to its poor score and size.

Site	SiteScore	DScore	Volume
Site 2	0.998	1.012	1608.756
Site 1	0.986	1.001	1721.560
Site 3	0.983	1.008	444.056
Site 4	0.546	0.497	35.372

Table 6. Sitemap analyses for $3CL^{pro}$. Sites are ranked according to SiteScore.

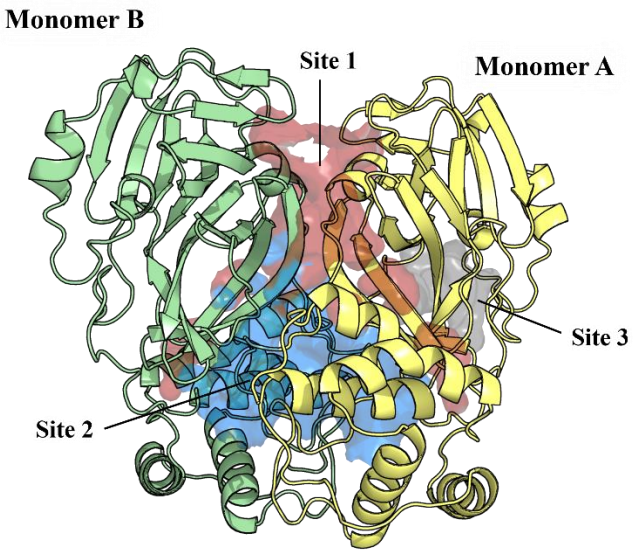


Figure 27. Representative structure of $3CL^{pro}$ dimer with the three main predicted binding sites: Site 1 (red), Site 2 (blue), Site 3 (gray). Site 4 is not included. The protein is shown in cartoons (Chain A in pale yellow and Chain B in pale green) and sites as Connolly surfaces.

Therefore, an initial series of rigid docking simulations is executed in SP and XP mode into the two predetermined sites to evaluate the binding mode and affinity

of the ligand. Notably, perlatolinic acid demonstrates a significantly lower score and better accommodation within Site 2, which is situated at the interface between the two monomers. Conversely, docking within Site 1 produces less favorable scores and exhibits a greater variability among the poses, as depicted in Figure 28.

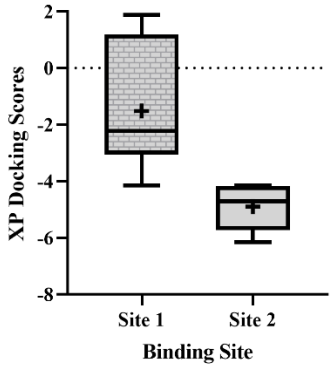


Figure 28. Docking scores from the XP protocol for the two selected binding sites. Each box plot indicates the median value (black line), mean value ("+" symbol), and first and last quartile whereas the whiskers span from minimum to maximum. The box plot graph is generated using GraphPad Prism 9 (GraphPad Software, La Jolla, CA, USA).

Given the encouraging druggability of Site 2 and the low docking scores achieved, perlatolinic acid is sent to Induced Fit docking simulations against Site 2, thus helping to predict ligand binding modes and concomitant structural changes in the target protein complex. Overall, for the predicted enzyme-inhibitor complex, binding is guided by the interaction with Arg4 and Lys5, which are crucial residues for enzyme dimerization and, thereby, its catalytic activity (Goyal B. and Goyal D., 2020; Ferreira JC. et al., 2022; Wei P. et al., 2006). Furthermore, the ligand is stabilized by specific interactions, including hydrogen bonds, salt bridges, and π–cation interactions. These interactions not only ensure optimal accommodation but also steric complementarity within the binding site. Remarkably, the binding at the dimer interface implicates residues belonging to each monomer and, despite the different ligand orientations and the flexibility of the amino acid chains, the residues involved turn out to be constant across poses.

In the predictive analysis for the binding of perlatolinic acid, the phenolic ring H-bonds to Glu288B and forms further π-cation interaction with Arg4A. Additionally, the carboxylic group forms an H-bond/salt bridge network by interacting with Arg4B, Lys5A, and the backbone of Lys5B, thus implicating both monomers in the stabilization of the ligand (Figure 29). Additional hydrophobic interactions between

the two flexible alkyl chains and the Phe3-Phe291- Glu288 side chain from both monomers contribute to ligand accommodation and display symmetry in ligand binding. Furthermore, the aromatic carboxyl ring is further stabilized by apolar contacts with both Lys5 (Figure 30). Perlatolinic acid affinity for the dimer interface is supported by a consistently low docking score (-9.035 kcal/mol).

To evaluate the structural modifications induced by ligand binding, “pre” and “post docking simulations” proteins are superimposed. This approach aligns with the non-competitive mechanism of inhibition, as no alterations are detected at the catalytic site, thus allowing substrate accommodation. Conversely, the binding of perlatolinic acid induces a rearrangement of the residues at the dimer interface, enhancing a better fit and increased stabilization of the ligand. However, such changes result in the disruption of critical interactions between Arg4B-Glu290A and Ser139B-Gln299A, H-bonds and salt bridges, which have been demonstrated to be crucial for dimer formation and its catalytic activity (Chou CY. et al. 2004; Ferreira JC. et al., 2022).

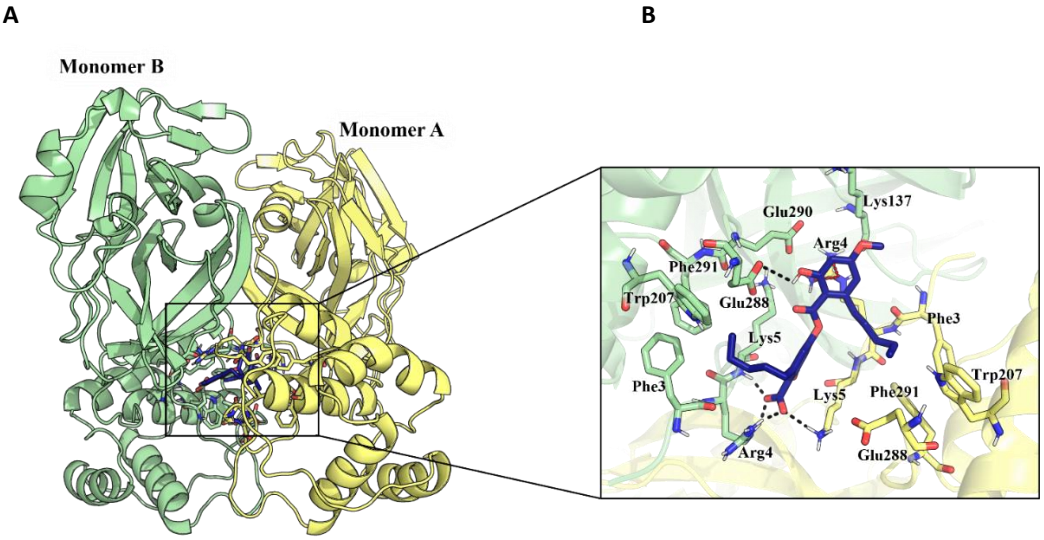


Figure 29. A) Representative structure of 3CL^{pro} dimer with docked ligand. **B)** Docking pose of perlatolinic acid (blue) at the dimer interface, from Induced Fit protocol. The protein is shown in cartoons (Chain A in pale yellow and Chain B in pale green); the ligand (blue) and the residues lining the pocket are displayed in capped sticks. Hydrogen bonds (black) and π-interactions (red) are shown as dashed lines.

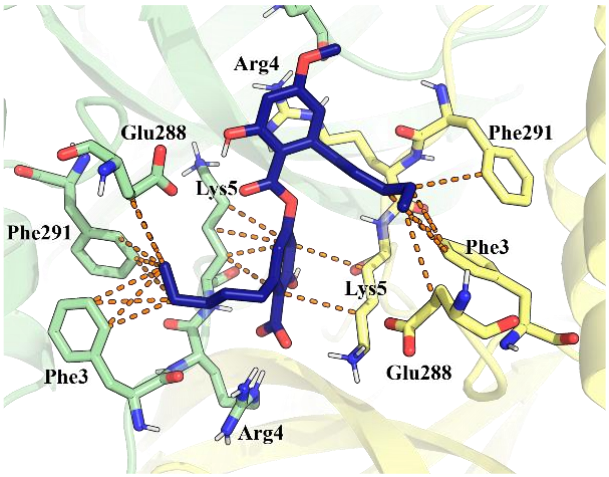


Figure 30. Hydrophobic interactions between the docking pose of perlatolinic acid (blue) and residues at the dimer interface, from Induced Fit protocol. The protein is shown in cartoons (Chain A in pale yellow and Chain B in pale green); the ligand (blue) and the residues lining the pocket are displayed in capped sticks. Hydrophobic interactions are shown as dashed orange lines.

Cell culture and viability assay. The trypan-blue exclusion assay demonstrates the absence of cytotoxic effects elicited by perlatolinic acid on TM4 cells at the tested doses, ranging from 0 to 80 µM, even after exposure for up to 48 hours (Figure 31). The results show an IC_{50} value of 37.7 ± 1.81 and 26.1 ± 0.78 for 24 and 48 hours of exposure, respectively.

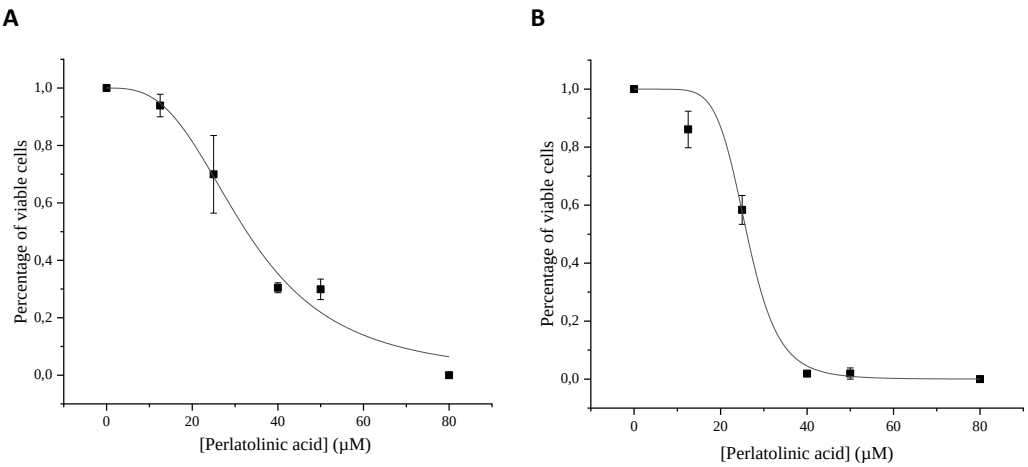


Figure 31. Cell culture and viability assay, with exposure up to 24h (**A**) and 48h (**B**).

4.3.1.3 Fumarprotocetraric acid

Inhibition assay. The time-course plots at inhibitor concentrations ranging from 5 µM to 100 µM are consistent with a slow-binding inhibitor for fumarprotocetraric acid (Figure 31). The IC_{50} value for the compound is about 35 µM.

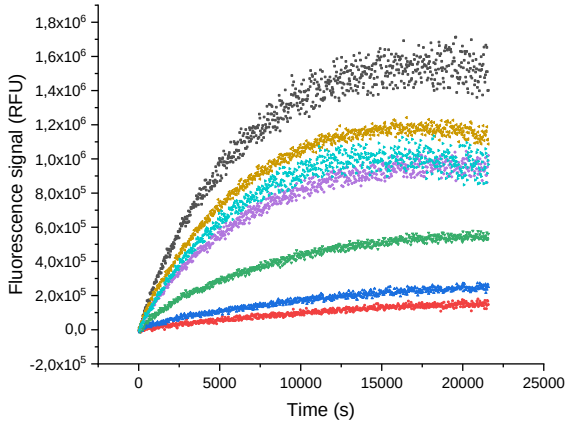


Figure 31. Time-course plots at different inhibitor concentrations. Black, positive control; red, fumarprotocetraric acid 100 µM; blue, 75 µM; green, 50 µM; magenta, 25 µM; light blue,10 µM; yellow 5 µM.

To overcome the substrate depletion effect, the time-course curves are fitted to equation 4. K_i^{app} and k_{inact} values, estimated by analyzing the entire set of data, are reported in Table 7 below.

Compound	k_{inact} (s^{-1})	K_i^{app} (µM)	K_i (µM)	k_{inact}/K_i (s^{-1} μM^{-1})
Fumarprotocetraric acid	$2.11\times10^{-4}\pm5.05\times10^{-6}$	17.5±0.54	13.36	1.58×10^{-5}

Table 7. Estimation of inhibition parameters at 10 µM of substrate.

The last question to be solved concerns the investigation of the mechanism of inhibition, which is initially addressed through a detailed analysis setting different DynaFit scripts. This approach allows us to explore the various hypothetical models of inhibition: competitive, noncompetitive, uncompetitive, and mixed. Our investigations reveal a plausible competitive inhibition model, which is further supported by the observed experimental findings.

The competitivity is also confirmed by calculating the k_{obs} values from the K_i^{app} and k_{inact} determined at a fixed concentration of inhibitor, 50 µM, varying the

concentration of the reporter substrate. As shown in Figure 31, fumarprotocetraric acid acts competitively with the substrate since the k_{obs} value decreases as the substrate concentration increases. This behaviour, diagnostic for a competitive mechanism of inhibition, allows the determination of the real K_i^{app} value by applying equation 7.

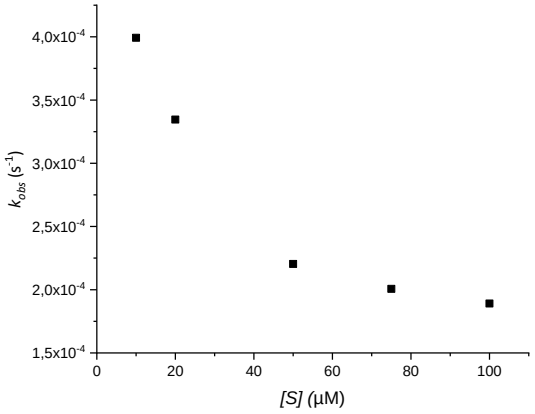


Figure 32. Plot of the k_{obs} versus the substrate reporter, ranging from 10 µM to 100 µM, at a concentration of fumarprotocetraric acid at 50 µM for the determination of the mechanism of inhibition.

Molecular docking. A preliminary docking study is conducted using SwissDock to confirm the ability of fumarprotocetraric acid to complement the active site of the $3CL^{pro}$. The docking predicts that the ligand could fit adequately into the active site by establishing numerous interactions with adjacent residues (Figure 33).

These results demonstrate the ligand's adeptness at engaging with the active site, corroborating the kinetic analysis findings. In detail, the docking predictions highlight that the formation of the enzyme-inhibitor complex is primarily facilitated by covalent bonding with Cys145, a key reactive residue within the active site. This primary association is further bolstered by specific non-covalent interactions, including hydrogen bonds, salt bridges, and π-π interactions, which collectively contribute to the stability and specificity of the binding.

A B

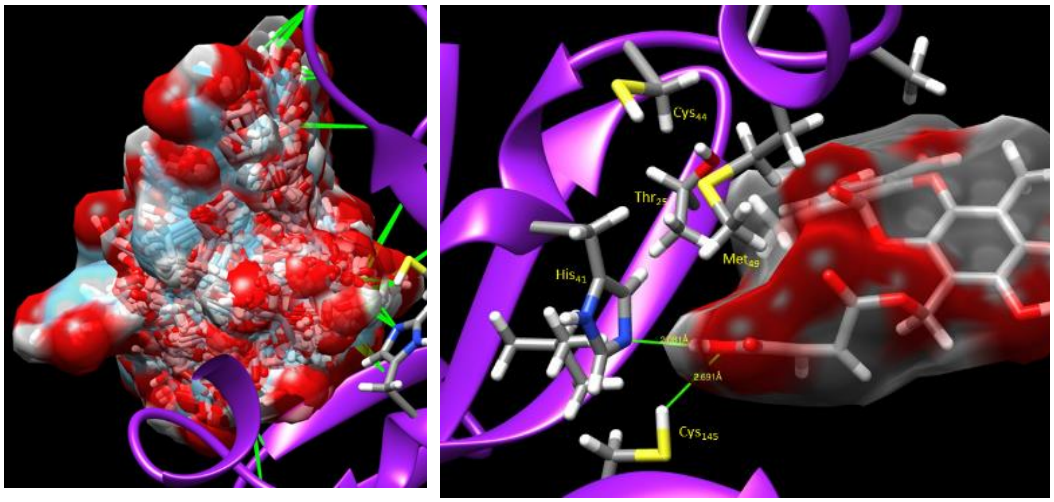


Figure 33. Preliminary docking study of fumarprotocetraric acid. The ligand interacts with residues in the catalytic pocket.

4.3.1.4 Alpha-collatolic acid

Inhibition assay. The time-course plots at inhibitor concentrations ranging from 5 µM to 100 µM are consistent with a slow-binding inhibitor for *α*-collatolic acid, as shown in Figure 34.

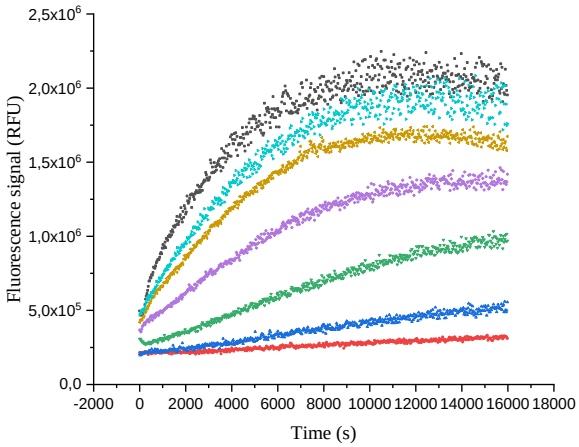


Figure 34. Time-course plots at different inhibitor concentrations. Black, positive control; red, α-collatolic acid acid 100 µM; blue, 75 µM; green, 50 µM; magenta, 25 µM; yellow 10 µM; light blue,5 µM.

K_i^{app} and k_{inact} values, estimated by analyzing the entire set of data as previously described, are reported in Table 8.

Compound	k_{inact} (s^{-1})	K_i^{app} (µM)	*Ki*	k_{inact}/K_i (s^{-1} $µM^{-1}$)
α-collatolic acid	$5.53\times10^{-4}\pm6.7\times10^{-6}$	19.7±0.71	9.56	5.78×10^{-5}

Table 8. Estimation of inhibition parameters at 10 µM of substrate.

The mechanism of inhibition is demonstrated by calculating the k_{obs} values from the K_i^{app} and k_{inact} determined at a fixed concentration of inhibitor, 50 µM, varying the concentration of the reporter substrate. As shown in Figure 35, α-collatolic acid acts as a competitive inhibitor, explained by the diminution of the k_{obs} value as the substrate concentration increases.

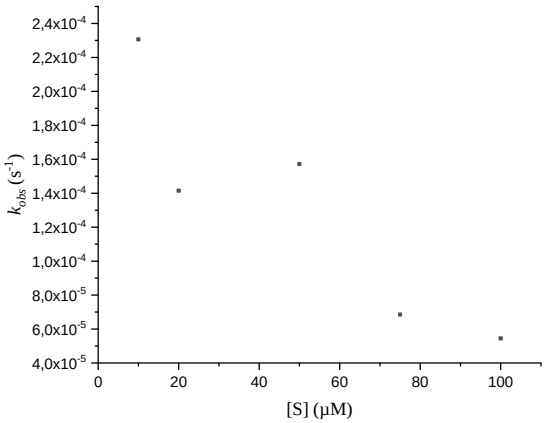


Figure 35. Determination of the mechanism of inhibition. Plot of the k_{obs} versus the substrate reporter, ranging from 10 µM to 100 µM, at a concentration of α-collatolic acid at 50 µM.

4.3.1.5 Norstictic acid

Inhibition assay. The time-course plots at inhibitor concentrations ranging from 5 µM to 100 µM are consistent with a slow-binding inhibitor for norstictic acid (Figure 36).

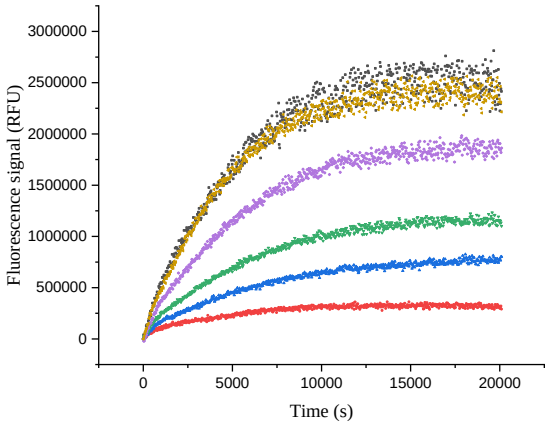


Figure 36. Time-course plots at different inhibitor concentrations. Black, positive control; red, norstictic acid 100 µM; blue, 75 µM; green, 50 µM; magenta, 25 µM; yellow, 5 µM.

The IC_{50} value turns out to be 53.5 µM. K_i^{app} and k_{inact} values, estimated by analyzing the entire set of data as previously described, are reported in Table 9.

Compound	k_{inact} (s^{-1})	K_i^{app} (µM)	K_i (µM)	k_{inact}/K_i (s^{-1} $µM^{-1}$)
Norstictic acid	$1.43\times10^{-4}\pm2.9\times10^{-6}$	43.22±0.47	22.98	6.22×10^{-6}

Table 9. Estimation of inhibition parameters at 10 µM of substrate.

To understand the mechanism of inhibition, a detailed analysis is conducted by setting different DynaFit scripts to explore the hypothetical models of inhibition. Our findings reveal a plausible irreversible competitive inhibition model, further bolstered by kinetics data. That assumption is confirmed by calculating the k_{obs} values from the K_i^{app} and k_{inact} determined at a fixed concentration of inhibitor, 50 µM, varying the concentration of the reporter substrate. As shown in Figure 37, nortistic acid acts competitively with the substrate, as evidenced by the diminution of the k_{obs} value at increasing concentrations of the substrate.

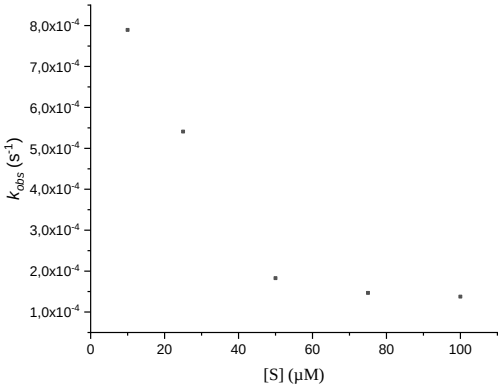


Figure 37. Determination of the mechanism of inhibition. Plot of the k_{obs} versus the substrate reporter, ranging from 10 µM to 100 µM, at a concentration of norstictic acid at 50 µM.

4.3.1.6 Ephiphorellic acid

Inhibition assay. The time-course plots at inhibitor concentrations ranging from 5 µM to 175 µM are consistent with a slow-binding inhibitor for ephiphorellic acid (Figure 38).

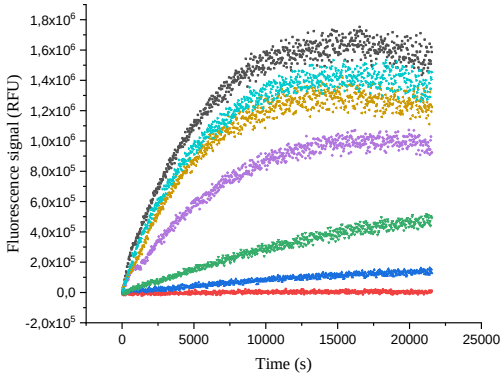


Figure 38. Time-course plots at different inhibitor concentrations. Black, positive control; red, ephiphorellic acid 175 µM; blue, 125 µM; green, 75 µM; magenta, 35 µM; yellow, 15 µM; light blue, 5 µM.

The IC_{50} value is calculated as 25.35 µM. K_i^{app} and k_{inact} values, estimated by analyzing the entire set of data as previously described, are reported in Table 10.

Compound	k_{inact} (s^{-1})	K_i^{app} (µM)	K_i (µM)	k_{inact}/K_i (s^{-1} $µM^{-1}$)
Ephiphorellic acid	$8.13\times10^{-5}\pm3.1\times10^{-6}$	5.57±0.15	2.2	3.69×10^{-5}

Table 10. Estimation of inhibition parameters at 10 µM of substrate.

To determine the mechanism of inhibition, a detailed analysis is conducted by setting different DynaFit scripts to investigate the most suitable model of inhibition. The findings reveal a plausible competitive inhibition.

Further investigations were not conducted due to the limited availability of the compound and issues related to its solubility.

4.3.1.7 Gyrophoric acid, tumidulin and rhizocarpic acid

Inhibition assay. The time-course plots for gyrophoric acid, tumidulin, and rhizocarpic acid are conducted at different inhibitors concentrations, ranging from 10 µM to 100 µM (data not shown). The compounds are consistent with slow-binding inhibitors.

The IC_{50} values are 46.84 µM, 53.18 µM, and 40.36 µM for gyrophoric acid, tumidulin, and rhizocarpic acid, respectively.

Further investigations are not conducted due to the limited availability of the compound and issues related to its solubility.

4.3.1.8 Lichesterinic acid

Inhibition assay. The time-course plots for lichesterinic acid at different inhibitor concentrations, ranging from 5 µM to 110 µM (Figure 39), are consistent with slow-binding inhibitor.

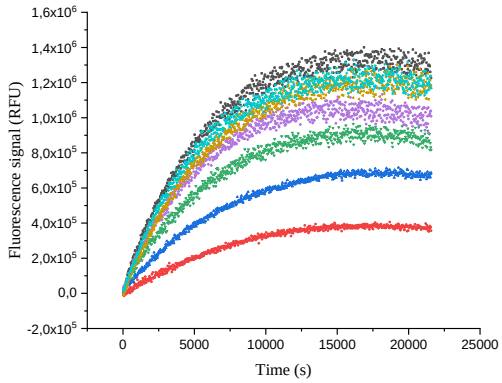


Figure 39. Time-course plots at different inhibitor concentrations. Black, positive control; red, lichesterinic acid 110 µM; blue, 75 µM; green, 50 µM; magenta, 25 µM; yellow, 10 µM; light blu, 5 µM.

The IC_{50} value turns out to be 44.88 µM.

Further investigations are not conducted as it was outside our area of interest, in addition to the limited availability of the compound.

4.3.2 Curcuminoids

Inhibition assay. The time-course plots for curcuminoids are conducted at different inhibitors concentrations, ranging from 10 µM to 100 µM for curcumin, from 2.5 µM to 135 µM for salicylcurcumin, and from 5 µM to 125 µM for demethoxycurcumin (Figure 40).

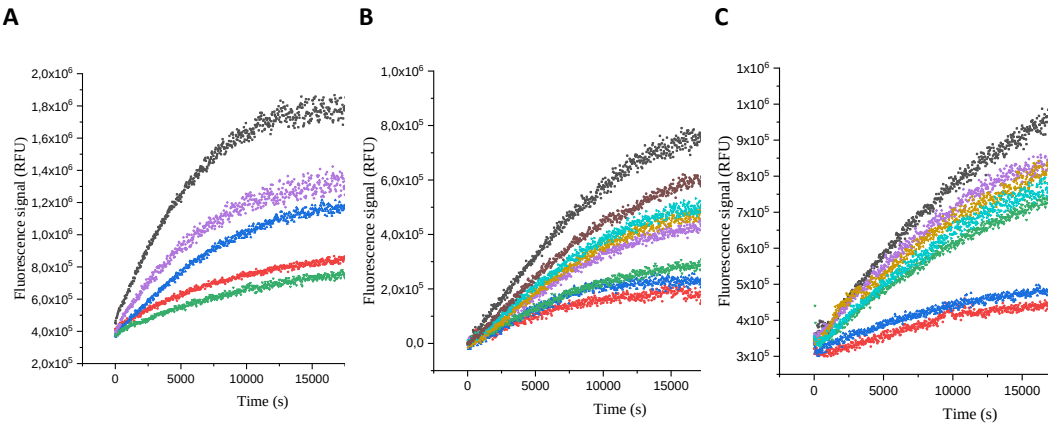


Figure 40. Time-course plots of curcuminoids at different inhibitor concentrations. **A)** Black, positive control; green, curcumin 100 µM; red, 50 µM; blue, 20 µM; magenta, 10 µM. **B)** Black, positive control; red, salicylcurcumin 135 µM; blue, 100 µM; green, 50 µM; magenta, 25 µM; yellow, 10 µM; light blue, 5 µM; brown, 2.5 µM. **C)** Black, positive control; red, demethoxycurcumin 125 µM; blu, 100 µM; green, 50 µM; light blue, 25 µM; yellow, 10 µM; magenta, 5 µM.

From the inhibition assay, it is possible to calculate the IC_{50} values for curcumin, salicylcurcumin, and demethoxycurcumin, which turn out to be 14.64 µM, 18.76 µM, and 49.14 µM, respectively.

K_i^{app}, K_i, and k_{inact} values, estimated by analyzing the entire set of data as previously described, are reported in the table below.

Compound	K_i^{app} (µM)	K_i (µM)	k_{inact} (s^{-1})
Curcumin	4.67	1.18	$6.56\times10^{-5}\pm7.7\times10^{-6}$
Salicylcurcumin	4.5	1.04	$2.18\times10^{-5}\pm3.1\times10^{-6}$
Demethoxycurcumin	4.76	1.21	$1.59\times10^{-5}\pm6.6\times10^{-6}$

Table 11. Estimation of inhibition parameters at 10 µM of substrate.

The mechanism of inhibition demonstrated that inhibitors act competitively with the substrate since the k_{obs} value decreases as the substrate concentration increases, as depicted in Figure 12.

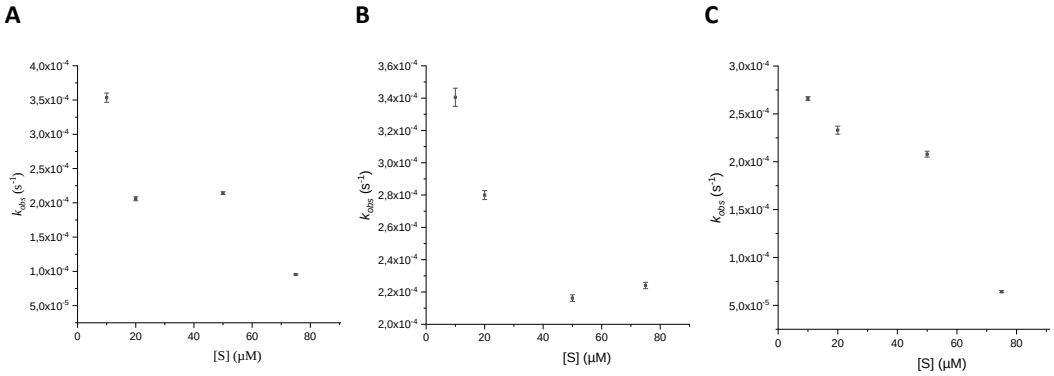


Table 12. Plot of the k_{obs} versus the substrate reporter, ranging from 10 µM to 100 µM, at a fixed concentration of inhibitors (75 µM) for the determination of the mechanism of inhibition. **A)** curcumin; **B)** salicylcurcumin; **C)** demethoxycurcumin.

Capitolo V

Discussion

Two times, between 2002 and 2019, the world grappled with an elusive adversary responsible for widespread mortality and enduring societal disruption. Initially, in late 2002, an unknown coronavirus (HCoV) known as severe acute respiratory syndrome emerged in Guangdong, People's Republic of China. It swiftly spread across Asia and Canada. By early 2003, aggressive containment measures had curbed the spread, yet the outbreak accounted for over 8,000 infections and 800 fatalities (Tseng CT. et al., 2012; World Health Organization). In contrast, December 2019 marked the onset of another crisis with the emergence of a novel coronavirus strain. Originating from Wuhan, Hubei Province, this virus, causing coronavirus disease 2019, quickly escalated into a global pandemic (Chen N. et al., 2020; Holshue ML. et al., 2020). More than four years into the outbreak, the world continues to battle the pervasive impact of this virus.
Since the beginning of the COVID-19 pandemic, due to the ongoing challenges posed by the rapid proliferation of SARS-CoV-2, the attention of the scientific community has notably shifted. While the development of effective vaccines remains a critical avenue of research, the repurposing of existing drugs alongside the exploration of natural compounds is emerging as a particularly promising strategy to counteract the virus.

Among the myriad potential viral targets, considerable attention has been directed towards inhibitors of the 3CL main protease, a key enzyme in the viral life cycle. The vast diversity inherent in the chemical structures of natural substances offers a promising reservoir for the identification of molecular frameworks ideal for the development of effective viral protease inhibitors. This endeavour has predominantly been pursued through the application of virtual screening techniques and dynamic simulations across expansive libraries of natural compounds (Gan C. et al., 2023; Tam NM. et al., 2021; Liu N. et al., 2023; Pennisi R. et al., 2023), facilitating the discovery of natural products with the theoretical capacity to engage the active site of the 3CL protease.

Motivated by the profound impacts and consequences of the COVID-19 pandemic, our research has concentrated on exploring the potential inhibitory effects of natural compounds against SARS-CoV-2's $3CL^{pro}$ enzyme.

Leveraging the well-documented biological activities of natural compounds, our research strategically seeks to exploit this established potential, aligning with the urgent need for innovative solutions in the face of global health issues.

5.1 Lichen secondary metabolites

Our investigations have primarily focused on depsidones, the most abundant secondary metabolites found in lichens (Ureña-Vacas I. et al., 2021). These compounds are biosynthesized from depsides, themselves the result of the condensation of two or more hydroxybenzoic acids. This process involves the esterification of the carboxyl group of one molecule with the phenolic hydroxyl group of another molecule, showcasing a complex and fascinating aspect of natural compound synthesis (Stocker-Wörgötter E. et al., 2013).

The kinetic study conducted elucidated that salazinic, protocetraric, fumarprotocetraric, norstictic, α-collatolic acids act as time-dependent inactivators, a mode of action that aligns with the behaviours observed in other $3CL^{pro}$ inhibitors. This phenomenon of slow binding and time-dependence in inhibition has been corroborated by previous research. For instance, Fu L. et al. have identified Boceprevir and GC376 as time-dependent inhibitors that engage in covalent binding with the catalytic cysteine residue of the SARS-CoV-2 3CL protease. Notably, GC376 exhibits greater potency than Boceprevir, demonstrated by an IC_{50} value of 0.15 µM as opposed to 8.0 µM (Fu L. et al., 2020). However, the presence of substrate competition necessitates caution in directly comparing IC_{50} values to inhibition constants. Consequently, the K_i values for lichen derivatives under investigation are inferred to be within the same order of magnitude as those recorded for Boceprevir and GC376. It is imperative to acknowledge that the most suitable way to measure the inactivator efficacy is the k_{inact}/K_i ratio, which delineates inactivation efficiency. Lichen compounds show limited variances in their inhibition constants which range from 2.2 µM to 22.98 µM (Tables 4, 7, 8, 9). This indicates a level of efficiency in inactivation that aligns with established paradigms within the field of viral protease inhibitors. For example, Boceprevir, a serine protease inhibitor approved for hepatitis C virus (HCV) treatment since 2011, achieves its effect through covalent binding to the NS3 protease (Malcolm BA. et al., 2006). Similarly, GC376 acts as a covalent inhibitor targeting cysteine proteases across a spectrum of viruses, including picornaviruses, noroviruses, and coronaviruses (Kim Y. et al., 2012; Pedersen NC. Et al., 2018). This comparative analysis underscores that the mechanism exhibited by both lichen-derived compounds is consistent with known strategies employed by antiviral protease inhibitors.

The recent introduction of Paxlovid™, an oral antiviral formulation developed by Pfizer Inc., has ignited renewed optimism for the treatment of COVID-19 (Wang Z. et al., 2022; Owen DR. et al., 2021). Paxlovid™ comprises a synergistic combination of two drugs: nirmatrelvir (PF-07321332) and ritonavir[1]. Nirmatrelvir acts as a potent inhibitor of the SARS-CoV-2-3CL protease, directly targeting the virus's replication mechanism. Ritonavir, conversely, is utilized primarily to decelerate the metabolic breakdown of nirmatrelvir, enhancing its efficacy and duration of action (Fishbane S. et al., 2022; Zhao Y. et al., 2022). Like the mechanisms of action observed with Boceprevir, GC376, and the lichen-derived compounds, nirmatrelvir achieves its inhibitory effect by covalently binding to the catalytic Cys145, forming a reversible thioimidate adduct. This interaction has been elucidated through the analysis of a 1.6-Å crystal structure in complex with SARS-CoV-2 $3CL^{pro}$ (Owen DR. et al., 2021).

In this study, the data obtained from our kinetic analysis were further substantiated by molecular docking studies for some depsidones. Specifically, the binding orientations of salazinic and protocetraric acids, characterized in this research as covalent and irreversible inactivators of SARS-CoV-2 protease, were predicted. To mirror the observed inhibitory mechanism, each compound was docked in both its cyclic ester (closed conformation) and hydrolyzed ester (open conformation) forms during the docking process. Intriguingly, our in-silico analysis allowed us to delineate the reaction coordinates: initially, the ligand positions itself within the active site as a cyclic ester (closed conformation, with detailed data not shown here), close to the catalytic Cys145. This arrangement is indicative of the formation of a non-covalent EI complex. Following this, while still in the closed conformer state, the ligand engages in a nucleophilic attack executed by the sulfur atom of Cys145 on the carbonyl carbon of the cyclic ester, leading to the creation of a high-energy intermediate.

The in-silico analyses revealed that the transition to open conformers within the enzyme's active site facilitates energetically favorable ligand rearrangements. These rearrangements are pivotal, serving as the driving force for the conversion of the high-energy transition intermediate into a more stable EI* complex. This process is depicted in the accompanying reaction scheme, highlighting the critical steps of ligand transformation. Within this enzymatic context, the molecules present multiple potential sites for nucleophilic attack by Cys145. From a pharmacological perspective, the most probable target is the carbonyl carbon within the ester bond of the central cyclic ester, a feature common to both molecules. Additionally, the carbonyl carbon of the hydroxyfuranone ring,

[1] Pfizer's Novel COVID-19 Oral Antiviral Treatment Candidate Reduced Risk of Hospitalization or Death by 89% in Interim Analysis of Phase 2/3 EPIC-HR Study|Pfizer. Available online: https://www.pfizer.com/news/press-release/press-release-detail/pfizers-novel-covid-19-oral-antiviral-treatment-candidate (accessed on 31 January 2022).

exclusive to salazinic acid, emerges as another potential site, albeit not in protocetraric acid. Remarkably, despite the presence of several other electrophilic centers within these inhibitors, the nucleophilic attack by the catalytic Cys145 predominantly targets the cyclic ester in both salazinic and protocetraric acids. This specificity is underscored by the kinetic data on inhibition and the observed molecular behavior, which collectively discount the hydroxyfuranone ring as a viable pharmacophore. This conclusion is further bolstered by in-silico findings, identifying the central cyclic ester as the preferred site for cysteine's attack.

In addition to the exploration of the compounds previously discussed, a preliminary molecular docking study was conducted for fumarprotocetraric acid. This investigation provided insights into the ligand's capacity to adequately fit within the 3CL protease's active site, facilitating numerous interactions with adjacent residues. This finding is in harmony with the results derived from kinetic analysis, further validating the inhibitory potential of fumarprotocetraric acid. Similar to the other depsidones examined, fumarprotocetraric acid achieves enzyme inhibition through interaction with the catalytic residue Cys145. This mode of action is expected, considering the structural resemblance of fumarprotocetraric acid with protocetraric acid, which has been extensively analyzed previously. The structural parallels between fumarprotocetraric acid and protocetraric acid underscore the consistency in their mechanisms of interaction with the 3CL protease, reinforcing the predictive value of molecular docking in identifying potential inhibitors based on structural criteria.

The findings from our in-silico study align with the outcomes of co-crystallization studies on SARS-CoV-2 3CL protease inhibitors conducted by other researchers (Zhang L. et al., 2020; Lockbaum GJ. Et al., 2021; Ma C. et al., 2020; Dai W. et al., 2020). These corroborative studies have demonstrated that the residues within the catalytic pocket, which interact with protocetraric and salazinic acids, are also implicated in the binding mechanisms of other inhibitors. Notably, His41, Gly143, and Glu166 are identified as key residues that may play a crucial role in the stabilization of the inhibitor within the catalytic pocket.

In summary, the convergence of data from the in-silico study and kinetic analysis, which characterized salazinic, fumarprotocetraric, and protocetraric acids as irreversible inactivators of the enzyme, supports the hypothesis of covalent bond formation between the inhibitors and the catalytic cysteine. This assumption is grounded in the observed behaviours and interactions, underpinning the mechanism of inhibition.

This research extended its inquiry to assess the potential cytotoxic effects of protocetraric and salazinic acids on TM4 cells, a model widely recognized for drug cytotoxicity testing (Reis MM. et al., 2015; Petricca S., et al., 2019). Prior studies have documented the antiproliferative properties of these compounds across various tumoral cellular models, including those of colorectal and melanoma

cancers, without reporting adverse effects on normal cell cultures (Ingelfinger R. et al., 2020; Manojlovic NT. Et al., 2012; Alexandrino, C.A.F., et al., 2019; de Paz GA. Et al., 2010). Consistent with these findings, our experimental results corroborated the absence of significant cytotoxic effects attributable to the compounds over 48 hours of exposure at the administered doses.

The investigation into *alpha*-collatolic and norstictic acids enhances our comprehension of depsidones as inhibitors of the SARS-CoV-2 3CL protease and contributes to the expanding arsenal of potential antiviral agents derived from natural products. Despite the insightful revelations derived from kinetic analysis, the lack of molecular docking data marks a significant gap in our understanding. This deficiency hampers our ability to fully elucidate the intricate mechanisms of action and the efficiency of binding of these compounds, which are critical for the rational design of more potent inhibitors. Comparative analysis reveals that, akin to other depsidones previously examined, both *alpha*-collatolic and norstictic acids exhibit a similar competitive mode of inhibition against the 3CL protease. This consistent mechanism, characterized by the formation of a complex with the catalytic cysteine, highlights the intrinsic potential of depsidone compounds to serve as competitive inhibitors. However, the unavailability of computational docking studies for these latter compounds restricts a thorough understanding of their precise binding orientations and interactions within the active site of the 3CL protease. This limitation emphasizes the need for future research, where computational methodologies could be instrumental in delineating the structural determinants critical for potent inhibition. Nevertheless, this mode of inhibition not only suggests a promising pathway for developing therapeutic agents capable of effectively halting viral replication by targeting a key enzymatic function of SARS-CoV-2 but also prompts intriguing inquiries into the interplay between molecular structure and inhibitory efficacy. The observed variances in inhibitory potency, as suggested by kinetic parameters such as the K_i and the k_{inact}/K_i ratio, underscore the nuanced and complex relationship between molecular architecture and functional activity within depsidone compounds. These findings imply that minor structural modifications could dramatically influence the antiviral efficacy of these natural products as antiviral agents. The focused examination of *alpha*-collatolic and norstictic acids not only broadens our understanding of depsidones as viable antiviral agents against SARS-CoV-2 but also signals the potential for discovering additional potent inhibitors within this class. By delving into the structural nuances that govern their inhibitory actions and exploring a broader spectrum of depsidones, it could uncover additional candidates with potent inhibitory activities, contributing to the understanding of mechanistic diversity within this class of natural inhibitors. This could pave the promising way by pointing toward a more personalized approach in the development of antiviral strategies and

consequently toward exploiting the full therapeutic potential of natural compounds, marking a significant step forward in the fight against viral pandemics.

The exploration of lichen-derived secondary metabolites in the search for potent antiviral agents has unveiled promising prospects also within the realms of pseudo-depsidones, depsides, and diphenyl-butenolides, although contingent upon more detailed research is required. These compounds, characterized by their diverse chemical structures and biological activities, represent a rich reservoir of potential for the development of novel therapeutic agents. Kinetic studies have played a crucial role in this exploration, shedding light on the inhibitory capabilities of specific metabolites against the SARS-CoV-2 3CL protease, identifying epiphorellic acid, gyrophoric acid, rhizocarpic acid, perlatolinic acid, and tumidulin as slow-binding inhibitors of the M^{pro}. The significance of these findings is twofold. Firstly, it broadens the spectrum of natural compounds under consideration for antiviral drug development, beyond the more commonly studied classes of metabolites. Secondly, it highlights the importance of kinetic studies to unravel the dynamics of enzyme inhibition, providing insights that are crucial for the rational design of inhibitors.

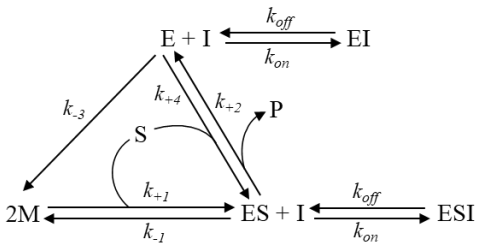
The findings elucidated to date have demonstrated how the natural compounds can inhibit the 3CL protease competitively.

Nevertheless, the catalytic site does not represent the only enzymatic target. For example, a wealth of research has conclusively demonstrated that the enzymatic activity of 3CL protease is contingent upon its dimerization, a process initiated by the binding of a substrate (Goyal B. and Goyal D., 2020). This binding results in a subsequent structural transformation, culminating in the protease activation.

A study conducted by Wang et al. (Wang G. et al., 2024) delved into the G11S mutation, a naturally occurring variant in the SARS-CoV-2 3C-like protease, on the dimer interface. Their research hypothesizes that the strategic inhibition of the dimer interface could serve as a potent mechanism against the proliferation of SARS-CoV-2 variants. This underscores the critical role of inhibitors designed to destabilize the 3CL dimer, thereby impeding its enzymatic functionality. Furthermore, the study accentuates the pivotal importance of targeting protein-protein interactions (PPIs) with specific inhibitors as a novel therapeutic avenue.
Subsequent investigations have shed light on the therapeutic potential of intervening at the 3CL protease dimer interface as a means of counteracting SARS-CoV-2 replication. A key strategy within this approach involves the deployment of inhibitors that are capable of binding to this interface, thereby neutralizing the protease's enzymatic activity essential for viral replication. Investigations have identified several natural compounds, including extracts from *Ginkgo biloba* (Zhang YN: et al., 2020), *Aloe* spp. (Hicks EG. et al., 2022) or *Citrus*

japonica (Panagiotopoulos AA. et al., 2021) as efficacious in inhibiting 3CL dimerization. This line of inquiry not only reinforces the feasibility of targeting the dimer interface for therapeutic intervention but also highlights the potential of natural products as a reservoir for the development of novel antiviral agents.
This mechanism of action, divergent from targeting the active site, induces conformational alterations within the enzyme, thereby debilitating its functionality without engaging in direct competition with the substrate. This paradigm of noncompetitive inhibition harbors considerable promise, as it offers strategic leverage in overcoming resistance induced by viral mutations, a prevalent hurdle in the realm of antiviral drug development.

Based on the results obtained for perlatolinic acid, we can propose a general reaction scheme that illustrates, as experimentally demonstrated, a noncompetitive inhibition mechanism (scheme 3).



scheme 3

As delineated by Goyal B. et al. (Goyal B. and Goyal D., 2020), the enzymatic function of 3CL protease is contingent upon substrate interaction. This interaction initiates with the substrate binding to the inactive monomeric form of 3CL (denoted as M), triggering a conformational transformation that culminates in the enzyme's activation. In the overarching reaction schema, substrate (S) association with the inactive monomer (M) leads to the formation of the Michaelis complex, thereby engendering the active enzyme form (E). However, the intricate process governing the transition from the initial substrate-monomer encounter to the Michaelis complex (ES) formation remains insufficiently elucidated. This gap in detailed mechanistic insight renders the transition phase a 'black box' in the context of understanding the inhibition mechanism, underscoring the complexity of the enzymatic activation process.

It is postulated that the allosteric modifications induced by substrate binding to the monomeric form of the enzyme, which leads to the transition to its active state (E), do not dissipate immediately upon initiation of the catalytic cycle. This allows the “E state” to persist for the time required to initiate a subsequent catalytic cycle. From a kinetic perspective, this phenomenon is reflected in the rate constants, with k_{+4} being approximately equivalent, or marginally surpassing, than k_{-3}. This observation is congruent with a noncompetitive inhibition model,

characterized by an *alpha* value of 1. This theoretical framework is bolstered by in-silico simulations, which elucidate the inhibitor's strategic positioning at the interface between the two monomers, thereby substantiating the proposed mechanism of inhibition. The implications and nuances of these in-silico findings are explored further in subsequent discussions.

While the formation of the enzyme-substrate-inhibitor (ESI) complex can be conceptually straightforward, the elucidation of the enzyme-inhibitor (EI) complex formation poses a greater challenge. This complexity arises, as extensively documented in the literature and prior analyses, from the substrate-induced dimerization process. The hypothesis suggesting the persistence of an “E state” during the catalytic cycle offers a resolution to this apparent paradox. Specifically, under steady-state conditions, where k_{+4} is approximately equal to k_{-3} - a scenario we term the “E persistence condition”- the possibility of inhibitor binding at the interface between monomers gains credence.

Although the precise mechanism underlying substrate binding to monomers, followed by the transition to the active enzyme within the Michaelis complex (ES) conformation, remains partially undefined, this limitation does not necessarily detract from the interpretation of the overarching results.

Significantly, the 3CL protease exhibits consistent cooperative behaviour in the presence of the perlatolinic acid, suggesting an unaltered functional mechanism. This observation prompts the hypothesis that perlatolinic acid exhibits a preferential binding affinity for the enzyme post-dimerization. Such a mechanism implies that perlatolinic acid does not disrupt the enzyme's native cooperative dynamics but rather interacts with the enzyme in its dimeric form, offering insights into the specificity of inhibitor-enzyme interactions and the potential for targeted therapeutic development.

In-silico analyses have elucidated the capability of perlatolinic acid to specifically target the site at the dimer interface of the enzyme, without perturbing the active site, thereby achieving symmetrical binding to both monomeric units. Within the scope of our investigation, perlatolinic acid underwent Induced Fit docking simulations directed at the dimer interface. The resultant low docking scores, coupled with the delineated binding modes, suggest a pronounced affinity of perlatolinic acid for this specific site. Notably, the binding dynamics are predominantly facilitated by interactions with Arg4 and Lys5, residues that are crucial to the dimerization process and, by extension, the enzyme's catalytic function.

Our research further delineates the intricate mechanism by which perlatolinic acid interacts with the dimer interface of the enzyme, engaging residues from both monomeric units. This engagement results in a symmetrical binding configuration that is instrumental for its inhibitory action. Specifically, the attachment of

perlatolinic acid to residues Glu288B and Arg4A, accompanied by the establishment of a H-bond/salt bridge network involving Arg4B, Lys5A, and Lys5B, unveils a complex interplay of interactions at the dimer interface. Such a network is pivotal for maintaining the ligand's stability and proper alignment within the binding site, consequently leading to the perturbation of critical interactions that are foundational for dimer formation.

Our investigation into the interaction of perlatolinic acid with the 3CL enzyme's dimer interface serves as a complementary extension to the seminal work by Wang et al. (Wang G. et al., 2024). They identified that a mutation from Gly to Ser at the dimer interface markedly compromises the dimer's stability, diminishing it by an estimated 600-fold. Our findings not only corroborate the pivotal role of the dimer interface in enzyme stability but also reinforce the concept of noncompetitive inhibition as embodied by perlatolinic acid. Notably, the binding of this ligand does not induce significant alterations at the catalytic site, thereby not obstructing substrate access.

This observation is particularly salient in the context of Wang et al.'s discovery, as it underscores the feasibility of targeting the dimer interface as a strategic approach for inhibitor design. Such inhibitors, by not directly engaging with the active site, preserve the site's ability to accommodate substrates while concurrently diminishing enzyme stability. Therefore, our study affirms the viability of exploiting the dimer interface for the development of inhibitors that leverage noncompetitive mechanisms to circumvent enzymatic activity, offering a nuanced pathway for therapeutic intervention against viral replication.

A critical dimension of our study's outcomes is the observed low cytotoxicity of perlatolinic acid, particularly evident in its interaction with epithelial TM4 cells. Remarkably, the cytotoxicity assessments reveal that, across the administered dosages, perlatolinic acid exhibited no detrimental effects on these cells. This aspect of our findings underscores the compound therapeutic potential, emphasizing its safety profile in biological contexts. Furthermore, the comparative analysis of the IC_{50} to the inhibition constant K_i value for perlatolinic acid presents an intriguing insight. The IC_{50} value, being approximately 43 times higher than the K_i value, suggests a significant inhibitory efficacy against the target enzyme, while maintaining a minimal impact on cell viability. This ratio highlights perlatolinic acid as a noteworthy natural compound, offering a promising balance between therapeutic efficacy and cytotoxicity.

A recent investigation conducted by Desmarets et al. explored the antiviral properties of various natural compounds, highlighting 28 secondary metabolites derived from lichens (Desmarets L. et al., 2023). Among these, perlatolinic acid emerged as the most potent inhibitor against both alpha and betacoronaviruses, specifically HCoV-229E and SARS-CoV-2. Notably, the study revealed that perlatolinic acid effectively inhibits the viral replication process. It is no coincidence that the 3CL protease is involved precisely in the replication process.

Nevertheless, its favorable safety profile and antiviral activity are indispensable for advancing toward clinical applications, positioning perlatolinic acid as a viable candidate for further pharmacological development. This profile is not only pivotal for its application in combating viral infections but also indicative of the broader pharmacological promise held by lichen-derived compounds. Historically, these substances are celebrated for their bioactive potential, often emphasizing their minimal cytotoxic effects on human cells (Ureña-Vacas I. et al., 2021; Ingelfinger R. et al., 2020; A. Méndez-Vilas, 2010). This trend reinforces the therapeutic viability of perlatolinic acid and similar compounds, suggesting a valuable avenue for the development of antiviral therapies with reduced risk profiles.

The identification of perlatolinic acid as a potent noncompetitive inhibitor specifically targeting the 3CL protease dimer interface marks a major advance in the search for innovative therapeutic strategies against SARS-CoV-2. Our findings elucidate that perlatolinic acid effectively binds to the dimer interface, thereby disrupting essential interactions required for the enzymatic dimer's formation and stability. This unique mechanism of action offers a strategic advantage by providing an alternative to conventional active site-targeted drugs, which frequently encounter challenges due to viral mutation-induced drug resistance.

The promising results obtained by lichen-derived compounds not only showcase their ability to inhibit key viral enzymes but could also offer a substantial advantage in the realm of drug development, particularly in the context of antiviral therapeutics. This attribute has the potential to streamline the clinical trial process, significantly reducing both the time and resources necessary for the development phase. Consequently, this efficiency could accelerate the introduction of efficacious treatments against formidable viral infections, including COVID-19, to the market.

In an era where the swift mitigation of emerging viral threats is crucial, the rapid deployment of such treatments could be a game-changer in global health management.

However, the journey from identifying potential inhibitors to the development of clinically viable antiviral agents is complex and fraught with challenges. The vast, yet largely untapped, repository of lichen secondary metabolites represents a frontier of opportunity for discovering bioactive compounds with novel antiviral properties. The promising results obtained for our lichen compounds underscore the necessity for further research to fully harness their vast potential, optimize their inhibitory properties, and assess their safety and efficacy in biological systems, rigorously evaluating their pharmacological attributes in comprehensive preclinical and clinical frameworks. By harnessing the rich biodiversity of lichens and translating these natural resources into viable therapeutic solutions, the scientific community stands on the cusp of a new era in antiviral treatment.

5.2 Curcuminoids

Our investigation into the inhibitory potential of natural compounds on the viral 3-chymotrypsin-like protease gains further significance considering existing literature. Curcuminoids, with their well-documented anti-inflammatory and antioxidant properties, have demonstrated promising inhibitory activities that could be leveraged for antiviral therapeutic development.

The kinetic assays conducted in our study are in harmony with existing research. Previous studies (Guijarro-Real C. et al., 2021; Ryu YB. et al., 2010; Mandal A. et al., 2021) have shown that curcumin can inhibit SARS-CoV with observed discrepancies in IC_{50} values across studies, including 15.74 µg/mL, 75 µg/mL, 23.5 µM and 40 µM. Our current research contributes to this body of knowledge, suggesting that the differences in IC_{50} values may be attributed to variations in experimental conditions, compound purity (e.g. naturally extracted and commercial curcumin), and possible differences in viral enzyme isoforms, and in case of competitive inhibition, in reporter substrate concentration. The broader antiviral efficacy of curcuminoids observed in literature and their varied IC_{50} values against SARS-CoV and SARS-CoV-2 reflect the complexity of their interaction with viral proteases. The discrepancies in these values are a reminder of the necessity for precise, controlled experimental conditions and the standardization of curcuminoid sources to achieve reliable and reproducible results.

However, our findings further delineate curcumin's inhibitory profile. In alignment with previous findings, our study positions curcumin as an effective inhibitor of SARS-CoV-2 $3CL^{pro}$ with an IC_{50} value of 14.64 µM and a K_i value of 1.18 µM, thereby reinforcing its potential as a therapeutic agent.

While the precise inhibitory mechanism of curcumin on SARS-CoV-2 $3CL^{pro}$ remains to be fully elucidated (Ryu YB. et al., 2010), computational studies have consistently reported low binding energy values, signifying a strong affinity between curcumin and the viral protease (Bahun M. et al., 2022; Sharma A. et al., 2020). Such low binding energies suggest that curcumin likely forms a stable complex with $3CL^{pro}$, corroborated by evidence indicating curcumin's localization at the enzyme's active site (Bahun M. et al., 2022).

To date, to the best of our knowledge, no previous studies have investigated the mechanism of inhibition of SARS–CoV–2 $3CL^{pro}$ by curcumin experimentally *in-vitro*. Consequently, there appears to be a gap in the literature regarding the experimental investigation of curcumin's mechanism of inhibition on SARS-CoV-2 $3CL^{pro}$ *in vitro*. Thus, our study seeks to bridge this gap by providing experimental data that elucidates curcumin's inhibitory mechanism. The significance of our research lies in its potential to enrich the current understanding with concrete experimental evidence, offering a clearer picture of how curcumin interacts with and impedes the function of $3CL^{pro}$. The journey of scientific discovery often

involves piecing together a puzzle where each study contributes a vital piece. In this context, our findings aim to add a crucial piece to the puzzle, enhancing collective knowledge and setting the stage for future research endeavours to build upon.

In accordance with computational studies that illustrate the curcumin's affinity for the active site of M^{pro}, our research undertook experimental investigations into the molecular mechanism, elucidating that the inhibition mechanism employed by curcumin is competitive.

Recognizing the substantial potential that curcumin holds in combating SARS-CoV in general, our research endeavours have expanded to delve into the inhibitory capabilities of related compounds. Specifically, this study has directed the focus toward assessing the potential antiviral activities of demethoxycurcumin, bisdemethoxycurcumin, and salicylcurcumin. This strategic pivot in our study is driven by the premise that these structurally related curcuminoids may offer similar, if not enhanced, therapeutic benefits against SARS-CoV-2 due to their unique chemical properties. By broadening our investigational scope to include these compounds, we aim to uncover a more comprehensive understanding of curcuminoids' antiviral mechanisms and their collective potential in antiviral therapy development. This choice was further validated by in-silico studies, showing that bisdemethoxycurcumin and demethoxycurcumin exhibit minimal binding energies, greater than -7 Kcal/mol, towards both SARS-CoV-2 $3CL^{pro}$ and endoribonuclease (NSP15) proteins (Sharma A. et al., 2020). They formed significant interactions with the viral proteins, including five hydrogen bonds with amino acid residues Lys-290, Gly-248, His-235, Thr-341, and Glu-340 by bisdemethoxycurcumin and one hydrogen bond with His-163 by demethoxycurcumin.

The antiviral activity of curcumin and its analogues against a range of viruses, such as hepatitis viruses, influenza viruses, and emerging arboviruses like Zika virus (ZIKV) and chikungunya virus (CHIKV), has been documented, highlighting their broad-spectrum antiviral capabilities (Ardebili A. et al., 2021; Jennings MR. et al., 2020; Goh VSL. et al., 2020; Mounce et al., 2017; von Rhein et al., 2016). In addition to their roles as metabolites, anti-neoplastic, and anti-inflammatory agents as described in the PubChem database, these analogues exhibit enhanced chemical stability at physiological pH.

The comprehensive docking study underscores that plant-derived compounds, including demethoxycurcumin and bisdemethoxycurcumin, emerge as potential drug candidates against the main protease of SARS-CoV-2. This exploration not only reinforces the therapeutic prospects of curcumin and its derivatives against SARS-CoV-2 but also broadens the horizon for their application in treating a variety of viral infections, further substantiating their importance in the development of antiviral strategies.

In this context, the present study has concentrated on examining the potential inhibitory activity of bisdemethoxycurcumin, demethoxycurcumin, and salicylcurcumin against $3CL^{pro}$.

Despite demonstrating favorable docking scores, bisdemethoxycurcumin was excluded from further investigation due to its poor or even non-existent inhibitory activity in preliminary screening studies at 100 µM. This decision illustrates the well-documented challenge of translating in-silico predictions into actual biological efficacy, underscoring the essential role of empirical validation in the drug discovery process. It reaffirms the notion that, despite sophisticated computational models offering promising leads, the ultimate test for any compound's therapeutic potential lies in its performance in real-world biological assays. This is not a novel observation but a recurring theme in pharmacological research, where the intricacies of biological systems often defy straightforward predictions based on molecular docking scores alone.

Conversely, the other two compounds, demethoxycurcumin and salicylcurcumin, have undergone more detailed scrutiny based on their promising initial results. They both exhibit strong inhibitory capabilities, as clearly evidenced by our kinetic studies, showing K_i values of 1.21 and 1.04 µM. Moreover, demethoxycurcumin and salicylcurcumin appear to exhibit enhanced inhibitory activity against SARS-CoV-2. This observation from our kinetic studies suggests that these compounds could be more potent than initially anticipated, potentially offering significant advantages in the development of antiviral therapies. Their performance not only confirms the promising in-silico predictions but also highlights the critical importance of empirical research in identifying viable candidates for combating viral infections.

In addition, it should be considered that the IC_{50} values are comparable to those of the compounds that were identified as the top five SARS–CoV–2 $3CL^{pro}$ inhibitors among the 3987 US Food and Drug Administration approved drugs (Mody V. et al., 2021).

As experimentally demonstrated through our above-mentioned kinetic studies for curcumin, and supported by in-silico research outlined in the literature that showcases binding interactions with residues within the M^{pro} active site, our kinetic analyses on bisdemethoxycurcumin and salicylcurcumin have experimentally confirmed the competitive inhibition mechanism of these compounds. This empirical evidence solidifies the notion that the structural interaction between these curcuminoids and specific active site residues is crucial for their inhibitory action. The competitive nature of this inhibition, established through meticulous kinetic experimentation, aligns seamlessly with theoretical predictions, thereby reinforcing the critical role of direct active site engagement in the mechanism of action of these compounds. Our findings not only validate the competitive inhibitory mechanism suggested by in-silico models but also

contribute significantly to the existing body of knowledge by providing concrete experimental proof of this mode of action in the context of viral protease inhibition.

The distinct inhibitory activities observed among curcuminoids can largely be attributed to their structural differences, which affect their interaction with the SARS-CoV-2 enzyme. This variance in activity underscores the significance of molecular architecture in determining the efficacy of these compounds as viral protease inhibitors. Curcumin, along with its derivatives demethoxycurcumin and salicylcurcumin, exhibits a core chemical structure that is crucial for bioactivity. The slight variations in the placement and number of methoxy and hydroxyl groups across these molecules play a pivotal role in their ability to interact with specific amino acid residues within the active site of the viral protease.

These functional groups are key to establishing hydrogen bonds and hydrophobic interactions with the enzyme, which are essential for effective inhibition. It is the nuanced arrangement of these groups that might afford demethoxycurcumin and salicylcurcumin a superior fit within the active site of the enzyme compared to curcumin, potentially leading to their increased inhibitory potency. The specific positioning and presence of methoxy and hydroxyl groups could influence the binding affinity through more precise interactions, leveraging the structural complementarity to disrupt the viral protease activity effectively.

On the contrary, bisdemethoxycurcumin's structure, characterized by the absence of one or more methoxy groups found in its counterparts, significantly impacts its inhibitory activity. This structural modification detracts from the compound's hydrophobic character and its capacity to form critical hydrogen bonds with the $3CL^{pro}$ enzyme, which are vital for robust binding. Consequently, this alteration leads to a diminished fit within the enzyme's active site, reflecting its reduced or non-existent inhibitory effect. The absence of these methoxy groups not only affects the overall molecular stability and interaction with the enzyme but also highlights the delicate balance between molecular structure and biological function.

In essence, the activity of these curcuminoids against SARS-CoV-2 vividly illustrates the complex interplay between molecular structure and antiviral efficacy. While demethoxycurcumin, salicylcurcumin, and curcumin have emerged as more potent inhibitors due to their optimal structural alignment with the enzyme's active site, bisdemethoxycurcumin's altered molecular architecture limits its ability to engage effectively with the viral target. This analysis not only sheds light on the structural basis of their inhibitory action but also paves the way for the rational design of more effective antiviral agents by leveraging structural modifications to enhance bioactivity.

Through meticulous structural analysis and understanding of the nuanced interactions between these molecules and their viral targets, the scientific

community can further refine this approach to identifying and optimizing potent antiviral agents.

In conclusion, the current study, alongside the corroborative findings from the literature, underscores the potential of curcuminoids as promising candidates for the development of new antiviral agents targeting $3CL^{pro}$. The varying degrees of inhibitory efficacy and binding energies reported necessitate further research to optimize these compounds for clinical use. Extensive *in vivo* studies and clinical trials remain imperative to confirm their practical applicability and therapeutic efficacy.

5.3 Phenylpropanoid compounds

As previously stated, the ongoing COVID-19 pandemic has prompted a significant amount of research into the potential activity of natural compounds as possible inhibitors of the main protease of SARS-CoV-2.

The ongoing quest to find effective treatments against SARS-CoV-2 has led researchers to explore a variety of natural compounds, among which phenylpropanoids and polyphenols have emerged as candidates with significant potential. This research has extended the exploration towards the potential of phenylpropanoids, with the main objective of assessing the effectiveness of these compounds in blocking the enzyme's activity, aiming to pave the way for the development of new antiviral treatments.

Phenylpropanoids, recognized for their diverse structures and extensive range of biological activities, initially showed promise in this area. Recent in-silico docking studies have stated that certain phenylpropanoids exhibit strong inhibitory activity against the 3CL protease of SARS-CoV-2 (Shahhamzehei N. et al., 2022), aligning with the hypothesis that natural compounds can be effective in combating viral infections. Further, these investigations have revealed that such phenylpropanoids are not only effective against the main protease but also exhibit promising interactions with the spike protein, both vital components for the virus's replication and lifecycle, as evidenced by relatively low docking scores, hinting at their capacity to serve as potent inhibitors.

For instance, rosmarinic acid and quercetin exhibited impressive docking scores of -7.8 and -9.2 kcal/mol, respectively, indicating stronger or comparable binding affinities to the well-known inhibitor GC376. In addition, such findings suggest these natural compounds' potential as dual inhibitors, capable of targeting both

the M^{pro} and the spike protein of SARS-CoV-2, which is a promising avenue for therapeutic development.

Salvianolic acid also emerged as a noteworthy candidate based on its potent docking scores against both targets (Elebeedy D. et al., 2021). However, previous experimental studies on SARS-CoV indicated salvianolic acid as a weak inhibitor at a concentration of 200 µM (Park JY. et al., 2012), a discrepancy that underscores the complexity and challenges of translating in-silico efficacy into biological activity. Considering the notable homology between SARS-CoV and SARS-CoV-2, the absence of inhibitory activity on SARS-CoV-2 observed in our kinetic studies aligns with expectations.

Despite the optimism generated by the computational studies, the transition to kinetic analyses has painted a more complex picture. The *in vitro* cytotoxicity evaluations, particularly on Vero E6 cells, demonstrated that compounds like rosmarinic and salvianolic acids did not exhibit significant inhibitory activity against the $3CL^{pro}$. This discrepancy underscores a critical challenge in drug discovery: the gap between theoretical in-silico predictions potential in effective *in vitro* and *in vivo* outcomes.

Although a previous study has suggested that rosmarinic acid exhibits inhibitory effects on the 3CL protease (Shahhamzehei N. et al., 2022), our results show that the compound, when tested at a concentration of 100 µM, can inhibit the enzyme by only 28%.

Within our research framework, chicoric acid, with a docking score of -7.7 kcal/mol, stood out as another noteworthy compound due to its ability to bind at the active site of the catalytic dyad (His41 and Cys145), suggesting its potential as a SARS-CoV-2 inhibitor. However, alongside other phenylpropanoids, our kinetic analysis revealed a completely different scenario, since the compound, at a concentration of 100 µM, demonstrates ineffectiveness in inhibiting the protease activity.

Also caffeic (Ali S. et al., 2022; Souid I. et al., 2022) and ferulic acid can interact with the M^{pro}, with moderate docking scores of -5.05 and -5.55 kcal/mol, respectively (Bahun M. et al., 2022; Souid I. et al., 2022; Antonopoulou I. et al., 2022). However, despite these interactions, our kinetic results demonstrated their limited or negligible capability to inhibit the mail protease, mirroring the disparity observed with other compounds.

In a previous work, vanillin derivatives were explored (Law WY. et al., 2020) through a ligand-based pharmacophore modeling approach, broughting to light their significant antiviral activity as M^{pro} inhibitors of SARS-CoV-2. This finding underscores the potential utility of these compounds in combating COVID-19,

suggesting that they could play a role in the development of therapeutic strategies against the virus. The pharmacophore model's predictive capacity elucidated the structural features essential for interaction with the SARS-CoV-2 main protease, laying the groundwork for identifying potent inhibitors among the vanillin derivatives. However, vanillic acid, despite a docking score of approximately -5 kcal/mol against M^{pro} (Elsbaey M. et al., 2021; Antonopoulou I. et al., 2022), demonstrated minimal inhibitory activity towards the 3CL protease in our experimental studies, as well as vanillin with an effect of about 20% when tested at 100 µM.

This exploration into the realm of natural compounds against SARS-CoV-2, spanning from in-silico predictions to *in vitro* outcomes, elucidates the complex and multifaceted nature of drug discovery, revealing the intricate balance required to transition theoretical inhibitors into practical therapeutic effectiveness of natural compounds for advancing potential COVID-19 treatments. This divergence between computational predictions and laboratory results is not uncommon in drug discovery and underscores the complexities involved in identifying effective inhibitors, emphasizing the need for a holistic approach in drug development.

Such an approach should consider not only the molecular interactions but also the pharmacokinetic and pharmacodynamic profiles of potential therapeutics. The real-world efficacy of these compounds is influenced by a myriad of factors, including bioavailability, cellular uptake, and the dynamic environment of biological systems, highlighting the critical need for experimental validation of computational predictions.

The apparent contradiction between the in-silico potential and *in vitro* efficacy of phenylpropanoids as 3CL protease inhibitors prompts a critical evaluation of the methodologies used in both approaches. It underscores the importance of integrating computational predictions with empirical evidence, reminding us of the limitations inherent in each method. While docking studies provide valuable insights into the possible interactions between molecules and their targets, they do not account for the dynamic nature of proteins in a biological environment, nor do they consider the pharmacokinetic properties that influence a compound's bioavailability and metabolism *in vivo*.

Our findings, though not culminating in the desired outcome, contribute to the broader scientific endeavour to harness the antiviral potential of natural compounds against COVID-19, providing a broader understanding of the structural diversity within natural compounds that may confer inhibitory activity against SARS-CoV-2.

Moreover, our research emphasizes the indispensable need for a multidisciplinary approach, combining computational chemistry, biochemistry, and pharmacology, to overcome the hurdles in identifying effective antiviral agents.

Future research should not only continue to explore the vast chemical space of natural compounds but also invest in understanding their mechanism of action, optimizing their pharmacological properties, and validating their efficacy in more complex biological models, crucial steps in moving promising candidates towards clinical application. The future and new directions might include refining docking models to better mimic biological conditions, exploring structural analogues of phenylpropanoids with enhanced properties, or employing alternative *in vitro* assays that may capture the nuances of enzyme inhibition more effectively.

This multifaceted approach is crucial for advancing promising candidates towards clinical application, contributing to the foundational knowledge necessary for developing effective treatments against COVID-19 and future viral threats.

The continuous improvement in technological capabilities, coupled with the extensive array of available natural compounds, highlights the critical need to further delve into the chemical space of natural compounds. This exploration is essential for identifying and utilizing specific compounds as foundational scaffolds in the development of new therapeutic agents.

5.4 Final remarks

There is one critical observation to underscore. Some of the recent investigations into 3CL protease inhibition have encountered methodological challenges. A primary concern is the non-Michaelian behaviour of the enzyme, a phenomenon documented since 2006 for the SARS-CoV equivalent enzyme (Bacha U. et al., 2004; Xia B. and Kang X., 2011; Muramatsu T. et al., 2016; Cheng SC. et al., 2010). Many studies fail to account for this enzyme's cooperative behaviour, rendering traditional Michaelian analysis ineffective for interpreting inhibition data (Eberle RJ. et al., 2021).
Furthermore, the handling of slow inactivators, such as Boceprevir and GC376, which undergo substrate depletion, presents another methodological hurdle (Fu L. et al., 2020). The methodology adopted in our study addresses these pivotal issues, facilitating the accurate determination of kinetic parameters of inhibition. This approach is effective even in the context of a non-Michaelian enzyme and for slow-binding inhibitors, marking a significant methodological advancement in the field.

Conclusion

COVID-19, a novel infectious disease caused by a single-stranded positive-sense RNA virus, has posed a serious worldwide public health emergency. Despite lessons learned from past coronaviruses outbreaks like SARS and MERS, the global community remains underprepared for effectively managing such infectious diseases. This underscores the urgent need for discovering effective therapeutic agents and vaccine candidates to combat COVID-19. The extensive research efforts mobilized in response to the COVID-19 pandemic have significantly advanced our understanding of the SARS-CoV-2 3CL protease, a pivotal target for antiviral intervention.

The present study contributes significantly to this burgeoning field, spotlighting the extraordinary potential of natural products as viable inhibitors of this critical enzyme, heralding a promising avenue for the development of novel antiviral agents, and marking a substantial contribution to enhancing global health security. Our findings not only enrich the existing body of knowledge on therapeutic strategies against SARS-CoV-2, underscoring the utility of natural compounds in crafting safe and efficacious treatments but also add an important piece to the mosaic of the already numerous biological activities of natural compounds, highlighting their promise as a source of novel, safe antiviral agents.

A hallmark of this study is the employment of a dual inhibition strategy, which underscores the innovative approach to antiviral drug development.

A significant breakthrough in this research is the identification of perlatolinic acid as a potent noncompetitive inhibitor targeting the protease dimer interface. This discovery represents a pivotal advancement in developing innovative therapeutic strategies against SARS-CoV-2, offering the potential for highly specific and effective treatments. The mode of action, targeting a site distinct from the active site, induces conformational changes in the enzyme, impairing its function without directly competing with the substrate. Such noncompetitive inhibition is particularly promising as it suggests a promising strategy to bypass viral mutation-induced drug resistance, a common challenge in antiviral drug development.

As the global community continues to grapple with COVID-19 and emerging viral threats, the insights garnered from our research highlight the indispensable role of innovative scientific inquiry in developing resilient and adaptable therapeutic responses.

Our research reaffirms the invaluable role of natural products in combating emerging viral diseases, advocating for ongoing exploration of the natural world for health solutions. The path forward, while fraught with challenges, is rich with the potential for breakthrough discoveries that could revolutionize our approach to viral pandemics, offering hope and concrete solutions amid global health crises.

Our findings, particularly regarding lichen secondary metabolites and curcuminoids, demonstrate promising inhibitory effects against the SARS-CoV-2 protease, highlighting the potential of these natural compounds in antiviral therapy. To fully realize the therapeutic potential of these findings, extensive *in vivo* studies and clinical trials are essential.

References

Aggarwal BB, Kumar A, Bharti AC. Anticancer potential of curcumin: preclinical and clinical studies. Anticancer Res. 2003 Jan-Feb;23(1A):363-98. PMID: 126802389

Ahad AM, Goto Y, Kiuchi F, Tsuda Y, Kondo K, Sato T. Nematocidal principles in "oakmoss absolute" and nematocidal activity of 2,4-dihydroxybenzoates. Chem Pharm Bull (Tokyo). 1991 Apr;39(4):1043-6. doi: 10.1248/cpb.39.1043. PMID: 1893489

Ahmad B, Batool M, Ain QU, Kim MS, Choi S. Exploring the Binding Mechanism of PF-07321332 SARS-CoV-2 Protease Inhibitor through Molecular Dynamics and Binding Free Energy Simulations. Int J Mol Sci. 2021 Aug 24;22(17):9124. doi: 10.3390/ijms22179124. PMID: 34502033; PMCID: PMC8430524

Ahmadjian V. 1993.The lichen symbiosis. 250 pp. Chichester: John Wiley & Sons. Ann Bot. 1995 Jan;75(1):101–2. doi: 10.1016/S0305-7364(05)80015-0. PMCID: PMC3023656

Al-Dhabi NA, Arasu MV, Park CH, Park SU. Recent studies on rosmarinic acid and its biological and pharmacological activities. EXCLI J. 2014 Oct 30;13:1192-5. PMID: 26417331; PMCID: PMC4464312

Alexandrino, C.A.F.; Honda, N.K.; Matos, M.D.F.C.; Portugal, L.C.; de Souza, P.R.B.; Perdomo, R.T.; Guimarães, R.D.C.A.; Kadri, M.C.T.; Silva, M.C.B.L.; Bogo, D. Antitumor effect of depsidones from lichens on tumor cell lines and experimental murine melanoma. Rev. Bras. Farmacogn. 2019, 29, 449–456

Ali S, Alam M, Khatoon F, Fatima U, Elasbali AM, Adnan M, Islam A, Hassan MI, Snoussi M, De Feo V. Natural products can be used in therapeutic management of COVID-19: Probable mechanistic insights. Biomed Pharmacother. 2022 Mar;147:112658. doi: 10.1016/j.biopha.2022.112658. Epub 2022 Jan 20.

Amalraj A, Pius A, Gopi S, Gopi S. Biological activities of curcuminoids, other biomolecules from turmeric and their derivatives - A review. J Tradit Complement Med. 2016 Jun 15;7(2):205-233. doi: 10.1016/j.jtcme.2016.05.005. PMID: 28417091; PMCID: PMC5388087

Anand K, Ziebuhr J, Wadhwani P, Mesters JR, Hilgenfeld R. Coronavirus main proteinase (3CLpro) structure: basis for design of anti-SARS drugs. Science. 2003 Jun 13;300(5626):1763-7. doi: 10.1126/science.1085658. Epub 2003 May 13. PMID: 12746549

Anand P, Kunnumakkara AB, Newman RA, Aggarwal BB. Bioavailability of curcumin: problems and promises. Mol Pharm. 2007 Nov-Dec;4(6):807-18. doi: 10.1021/mp700113r. Epub 2007 Nov 14. PMID: 17999464

Angelini MM, Akhlaghpour M, Neuman BW, Buchmeier MJ. Severe acute respiratory syndrome coronavirus nonstructural proteins 3, 4, and 6 induce double-membrane vesicles. mBio. 2013 Aug 13;4(4):e00524-13. doi: 10.1128/mBio.00524-13. PMID: 23943763; PMCID: PMC3747587

Anto RJ, George J, Babu KV, Rajasekharan KN, Kuttan R. Antimutagenic and anticarcinogenic activity of natural and synthetic curcuminoids. Mutat Res. 1996 Sep 13;370(2):127-31. doi: 10.1016/0165-1218(96)00074-2. PMID: 8879271

Antonopoulou I, Sapountzaki E, Rova U, Christakopoulos P. The Inhibitory Potential of Ferulic Acid Derivatives against the SARS-CoV-2 Main Protease: Molecular Docking, Molecular Dynamics, and ADMET Evaluation. Biomedicines. 2022 Jul 25;10(8):1787. doi: 10.3390/biomedicines10081787. PMID: 35892687; PMCID: PMC9329733

Araújo CC, Leon LL. Biological activities of Curcuma longa L. Mem Inst Oswaldo Cruz. 2001 Jul;96(5):723-8. doi: 10.1590/s0074-02762001000500026. PMID: 11500779

Ardebili A, Pouriayevali MH, Aleshikh S, Zahani M, Ajorloo M, Izanloo A, et al. Antiviral Therapeutic Potential of Curcumin: An Update. Molecules. 2021 Nov 19;26(22):6994. doi: 10.3390/molecules26226994. PMID: 34834089; PMCID: PMC8617637.

Armaleo D. 1993 Proceedings of the International Botanical Congress, Tokyo-Yokohama, abstract 15

Arun N, Nalini N. Efficacy of turmeric on blood sugar and polyol pathway in diabetic albino rats. Plant Foods Hum Nutr. 2002 Winter;57(1):41-52. doi: 10.1023/a:1013106527829. PMID: 11855620

Arya R, Kumari S, Pandey B, Mistry H, Bihani SC, Das A, Prashar V, Gupta GD, Panicker L, Kumar M. Structural insights into SARS-CoV-2 proteins. J Mol Biol. 2021 Jan 22;433(2):166725. doi: 10.1016/j.jmb.2020.11.024. Epub 2020 Nov 24. PMID: 33245961; PMCID: PMC7685130

Asahina, Y. 1936. Microchemischer Nachweis der Flechtenstoffe (I). J Jap Bot 12:516-525

Asplund J, Wardle DA. How lichens impact on terrestrial community and ecosystem properties. Biol Rev Camb Philos Soc. 2017 Aug;92(3):1720-1738. doi: 10.1111/brv.12305. Epub 2016 Oct 11. PMID: 27730713

Bacha U, Barrila J, Velazquez-Campoy A, Leavitt SA, Freire E. Identification of novel inhibitors of the SARS coronavirus main protease 3CLpro. Biochemistry. 2004 May 4;43(17):4906-12. doi: 10.1021/bi0361766. PMID: 15109248

Bachmann H. and Portmann P., 1981, Agent for oxidative dyeing of hair, Ger. Offen. DE 2939303, pp. 18

Bahun M, Jukić M, Oblak D, Kranjc L, Bajc G, Butala M, Bozovičar K, Bratkovič T, Podlipnik Č, Poklar Ulrih N. Inhibition of the SARS-CoV-2 3CLpro main protease by plant polyphenols. Food Chem. 2022 Mar 30;373(Pt B):131594. doi: 10.1016/j.foodchem.2021.131594. Epub 2021 Nov 14. PMID: 34838409; PMCID: PMC8592230

Banerjee A, Kulcsar K, Misra V, Frieman M, Mossman K. Bats and Coronaviruses. Viruses. 2019 Jan 9;11(1):41. doi: 10.3390/v11010041. PMID: 30634396; PMCID: PMC6356540

Banerjee G, Chattopadhyay P. Vanillin biotechnology: the perspectives and future. J Sci Food Agric. 2019 Jan 30;99(2):499-506. doi: 10.1002/jsfa.9303. Epub 2018 Sep 27. PMID: 30094833

Bannwarth L, Rose T, Dufau L, Vanderesse R, Dumond J, Jamart-Grégoire B, Pannecouque C, De Clercq E, Reboud-Ravaux M. Dimer disruption and monomer sequestration by alkyl tripeptides are successful strategies for inhibiting wild-type and multidrug-resistant mutated HIV-1 proteases. Biochemistry. 2009 Jan 20;48(2):379-87. doi: 10.1021/bi801422u. PMID: 19105629

Barrila J, Bacha U, Freire E. Long-range cooperative interactions modulate dimerization in SARS 3CLpro. Biochemistry. 2006 Dec 19;45(50):14908-16. doi: 10.1021/bi0616302. PMID: 17154528; PMCID: PMC2570436

Baum L, Ng A. Curcumin interaction with copper and iron suggests one possible mechanism of action in Alzheimer's disease animal models. J Alzheimers Dis. 2004 Aug;6(4):367-77; discussion 443-9. doi: 10.3233/jad-2004-6403. PMID: 15345806

Behera BC, Verma N, Sonone A, Makhija U. Antioxidant and antibacterial activities of lichen Usnea ghattensis in vitro. Biotechnol Lett. 2005 Jul;27(14):991-5. doi: 10.1007/s10529-005-7847-3. PMID: 16132842

Bellio P, Segatore B, Mancini A, Di Pietro L, Bottoni C, Sabatini A, Brisdelli F, Piovano M, Nicoletti M, Amicosante G, Perilli M, Celenza G. Interaction between lichen secondary metabolites and antibiotics against clinical isolates methicillin-resistant Staphylococcus aureus strains. Phytomedicine. 2015 Feb 15;22(2):223-30. doi: 10.1016/j.phymed.2014.12.005. Epub 2014 Dec 19. PMID: 25765826

Bellio P, Di Pietro L, Mancini A, Piovano M, Nicoletti M, Brisdelli F, Tondi D, Cendron L, Franceschini N, Amicosante G, Perilli M, Celenza G. SOS response in bacteria: Inhibitory activity of lichen secondary metabolites against Escherichia coli RecA protein. Phytomedicine. 2017 Jun 15;29:11-18. doi: 10.1016/j.phymed.2017.04.001. Epub 2017 Apr 8. PMID: 28515022

Bezerra G, Pereira M, Ostrosky E, Barbosa E, Moura M, Ferrari M, Aragão C, Gomes A: Compatibility study between ferulic acid and excipients used in cosmetic formulations by TG/DTG, DSC and FTIR. J Therm Anal Calorim 2017; 127: 1683–1691

Bhattarai HD, Paudel B, Hong SG, Lee HK, Yim JH. Thin layer chromatography analysis of antioxidant constituents of lichens from Antarctica. J Nat Med. 2008 Oct;62(4):481-4. doi: 10.1007/s11418-008-0257-9. Epub 2008 Jun 17. PMID: 18553181

Blaschek L, Pesquet E. Phenoloxidases in Plants-How Structural Diversity Enables Functional Specificity. Front Plant Sci. 2021 Oct 1;12:754601. doi: 10.3389/fpls.2021.754601. PMID: 34659324; PMCID: PMC8517187

Bradburne AF, Bynoe ML, Tyrrell DA. Effects of a "new" human respiratory virus in volunteers. Br Med J. 1967 Sep 23;3(5568):767-9. doi: 10.1136/bmj.3.5568.767. PMID: 6043624; PMCID: PMC1843247

Brisdelli F, Perilli M, Sellitri D, Bellio P, Bozzi A, Amicosante G, Nicoletti M, Piovano M, Celenza G. Protolichesterinic acid enhances doxorubicin-induced apoptosis in HeLa cells in vitro. Life Sci. 2016 Aug 1; 158:89-97. DOI: 10.1016/j.lfs.2016.06.023. Epub 2016 Jun 27. PMID: 27363900

Burkholder PR, Evans AW, McVeigh I, Thornton HK. Antibiotic Activity of Lichens. Proc Natl Acad Sci U S A. 1944 Sep 15;30(9):250-5. doi: 10.1073/pnas.30.9.250. PMID: 16588653; PMCID: PMC1078706

Burlando B, Ranzato E, Volante A, Appendino G, Pollastro F, Verotta L. Antiproliferative effects on tumour cells and promotion of keratinocyte wound healing by different lichen compounds. Planta Med. 2009 May;75(6):607-13. doi: 10.1055/s-0029-1185329. Epub 2009 Feb 6. PMID: 19199230

Calcott MJ, Ackerley DF, Knight A, Keyzers RA, Owen JG. Secondary metabolism in the lichen symbiosis. Chem Soc Rev. 2018 Mar 5;47(5):1730-1760. doi: 10.1039/c7cs00431a. PMID: 29094129

Cappellini F, Marinelli A, Toccaceli M, Tonelli C, Petroni K. Anthocyanins: From Mechanisms of Regulation in Plants to Health Benefits in Foods. Front Plant Sci. 2021 Oct 28;12:748049. doi: 10.3389/fpls.2021.748049. PMID: 34777426; PMCID: PMC8580863

Carabelli, A.M., Peacock, T.P., Thorne, L.G. et al. SARS-CoV-2 variant biology: immune escape, transmission and fitness. Nat Rev Microbiol 21, 162–177 (2023). https://doi.org/10.1038/s41579-022-00841-7

Cardarelli M, Serino G, Campanella L, Ercole P, De Cicco Nardone F, Alesiani O, Rossiello F. Antimitotic effects of usnic acid on different biological systems. Cell Mol Life Sci. 1997 Aug;53(8):667-72. doi: 10.1007/s000180050086. PMID: 9351470

Cardinale M, Grube M, Castro JV Jr, Müller H, Berg G. Bacterial taxa associated with the lung lichen Lobaria pulmonaria are differentially shaped by geography and habitat. FEMS Microbiol Lett. 2012 Apr;329(2):111-5. doi: 10.1111/j.1574-6968.2012.02508.x. Epub 2012 Feb 13. PMID: 22268428

Celenza G, Segatore B, Setacci D, Perilli M, Brisdelli F, Bellio P, Piovano M, Garbarino JA, Amicosante G, Nicoletti M. Antibacterial activity of selected metabolites from Chilean lichen species against methicillin-resistant staphylococci. Nat Prod Res. 2013;27(17):1528-31. doi: 10.1080/14786419.2012.730043. Epub 2012 Oct 2. PMID: 23030591

Cesarino I, Eudes A, Urbanowicz B, Xie M. Editorial: Phenylpropanoid Systems Biology and Biotechnology. Front Plant Sci. 2022 Mar 3;13:866164. doi: 10.3389/fpls.2022.866164. PMID: 35310632; PMCID: PMC8928430

Cha HJ, Park MT, Chung HY, Kim ND, Sato H, Seiki M, Kim KW. Ursolic acid-induced down-regulation of MMP-9 gene is mediated through the nuclear translocation of glucocorticoid receptor in HT1080 human fibrosarcoma cells. Oncogene. 1998 Feb 12;16(6):771-8. doi: 10.1038/sj.onc.1201587. PMID: 9488041

Chen CC, Yu X, Kuo CJ, Min J, Chen S, Ma L, Liu K, Guo RT. Overview of antiviral drug candidates targeting coronaviral 3C-like main proteases. FEBS J. 2021 Sep;288(17):5089-5121. doi: 10.1111/febs.15696. Epub 2021 Feb 1. PMID: 33400393

Chen H, Wei P, Huang C, Tan L, Liu Y, Lai L. Only one protomer is active in the dimer of SARS 3C-like proteinase. J Biol Chem. 2006 May 19;281(20):13894-8. doi: 10.1074/jbc.M510745200. Epub 2006 Mar 24. PMID: 16565086; PMCID: PMC7990651

Chen N, Zhou M, Dong X, Qu J, Gong F, Han Y, Qiu Y, Wang J, Liu Y, Wei Y, Xia J, Yu T, Zhang X, Zhang L. Epidemiological and clinical characteristics of 99 cases of 2019 novel coronavirus pneumonia in Wuhan, China: a descriptive study. Lancet. 2020 Feb 15;395(10223):507-513. doi: 10.1016/S0140-6736(20)30211-7. Epub 2020 Jan 30. PMID: 32007143; PMCID: PMC7135076

Chen S, Chen L, Tan J, Chen J, Du L, Sun T, Shen J, Chen K, Jiang H, Shen X. Severe acute respiratory syndrome coronavirus 3C-like proteinase N terminus is indispensable for proteolytic activity but not for enzyme dimerization. Biochemical and thermodynamic investigation in conjunction with molecular dynamics simulations. J Biol Chem. 2005 Jan 7;280(1):164-73. doi: 10.1074/jbc.M408211200. Epub 2004 Oct 26. PMID: 15507456; PMCID: PMC7982548

Cheng SC, Chang GG, Chou CY. Mutation of Glu-166 blocks the substrate-induced dimerization of SARS coronavirus main protease. Biophys J. 2010 Apr 7;98(7):1327-36. doi: 10.1016/j.bpj.2009.12.4272. PMID: 20371333; PMCID: PMC2849084

Chou CY, Chang HC, Hsu WC, Lin TZ, Lin CH, Chang GG. Quaternary structure of the severe acute respiratory syndrome (SARS) coronavirus main protease. Biochemistry. 2004 Nov 30;43(47):14958-70. doi: 10.1021/bi0490237. PMID: 15554703

Choudhary MI, Saima Jalil A and Atta-ur-Rahman (2005) Bioactive phenolic compounds from a medicinal lichen, Usnea longissima. Phytochem 66:2346–2350

Cohen PA, Hudson JB, Towers GH. Antiviral activities of anthraquinones, bianthrones and hypericin derivatives from lichens. Experientia. 1996 Feb 15;52(2):180-3. doi: 10.1007/BF01923366. PMID: 8608821

Coleman CM, Frieman MB. Coronaviruses: important emerging human pathogens. J Virol. 2014 May;88(10):5209-12. doi: 10.1128/JVI.03488-13. Epub 2014 Mar 5. PMID: 24600003; PMCID: PMC4019136

Corman VM, Muth D, Niemeyer D, Drosten C. Hosts and Sources of Endemic Human Coronaviruses. Adv Virus Res. 2018;100:163-188. DOI: 10.1016/bs.aivir.2018.01.001. Epub 2018 Feb 16. PMID: 29551135; PMCID: PMC7112090

Crittenden PD, Porter N. Lichen-forming fungi: potential sources of novel metabolites. Trends Biotechnol. 1991 Dec;9(12):409-14. doi: 10.1016/0167-7799(91)90141-4. PMID: 1367745

Cui J, Li F, Shi ZL. Origin and evolution of pathogenic coronaviruses. Nat Rev Microbiol. 2019 Mar;17(3):181-192. doi: 10.1038/s41579-018-0118-9. PMID: 30531947; PMCID: PMC7097006

Culberson, C.F. 1969. Chemical and botanical guide to lichen products (Durham; University of North Carolina Press)

Culberson, C.F. 1970. Supplement to 'Chemical and Botanical Guide to Lichen Products'. Bryologist 73:177-377

Culberson, C.F. and Armaleo, D. 1992. Induction of a complete secondary-product pathway in cultures of a lichen fungus. Exp Mycol 16:52-63.

Culberson, C.F., Culberson, W.L., and Johnson, A. 1977. Second Supplement to 'Chemical and Botanical Guide to Lichen Products'. (St. Louis; American Bryological and Lichenologial Society, Missouri Botanical Garden)

Dai W, Zhang B, Jiang XM, Su H, Li J, Zhao Y, et al. Structure-based design of antiviral drug candidates targeting the SARS-CoV-2 main protease. Science. 2020 Jun 19;368(6497):1331-1335. doi:10.1126/science.abb4489. Epub 2020 Apr 22. PMID: 32321856; PMCID: PMC7179937

Dayan FE, Romagni JG (2002) Structural diversity of lichen metabolites and their potential for use. In: Upadhyaya R (ed) Advances in microbial toxin research and its biotechnological exploitation. Kluwer Academic/Plenum, New York, pp 151–169

De Groot RJ, Baker SC, Baric RS, Brown CS, Drosten C, Enjuanes L, Fouchier RA, Galiano M, Gorbalenya AE, Memish ZA, Perlman S, Poon LL, Snijder EJ, Stephens GM, Woo PC, Zaki AM, Zambon M, Ziebuhr J. Middle East respiratory syndrome coronavirus (MERS-CoV): announcement of the Coronavirus Study Group. J Virol. 2013 Jul;87(14):7790-2. doi: 10.1128/JVI.01244-13. Epub 2013 May 15. PMID: 23678167; PMCID: PMC3700179

De Paz GA, Raggio J, Gómez-Serranillos MP, Palomino OM, González-Burgos E, Carretero ME, Crespo A. HPLC isolation of antioxidant constituents from Xanthoparmelia spp. J Pharm Biomed Anal. 2010 Oct 10;53(2):165-71. doi:10.1016/j.jpba.2010.04.013. Epub 2010 Apr 24. PMID: 20457504

Denison MR, Graham RL, Donaldson EF, Eckerle LD, Baric RS. Coronaviruses: an RNA proofreading machine regulates replication fidelity and diversity. RNA Biol. 2011 Mar-Apr;8(2):270-9. doi: 10.4161/rna.8.2.15013. Epub 2011 Mar 1. PMID: 21593585; PMCID: PMC3127101

Desmarets L, Millot M, Chollet-Krugler M, Boustie J, Camuzet C, François N, Rouillé Y, Belouzard S, Tomasi S, Mambu L, Séron K. Lichen or Associated Micro-Organism Compounds Are Active against Human Coronaviruses. Viruses. 2023 Aug 31;15(9):1859. doi: 10.3390/v15091859. PMID: 37766264; PMCID: PMC10536056

Ding L, Zhang XX, Wei P, Fan K, Lai L. The interaction between severe acute respiratory syndrome coronavirus 3C-like proteinase and a dimeric inhibitor by capillary electrophoresis. Anal Biochem. 2005 Aug 1;343(1):159-65. doi:10.1016/j.ab.2005.04.027. PMID: 15935325; PMCID: PMC7094366

Dong E, Du H, Gardner L. An interactive web-based dashboard to track COVID-19 in real time. Lancet Infect Dis. 2020 May;20(5):533-534. DOI: 10.1016/S1473-3099(20)30120-1. Epub 2020 Feb 19. Erratum in: Lancet Infect Dis. 2020 Sep;20(9):e215. PMID: 32087114; PMCID: PMC7159018

Du S, Huang X, Cai Y, Hao Y, Qiu S, Liu L, Cui M, Luo L. Differential Antioxidant Compounds and Activities in Seedlings of Two Rice Cultivars Under Chilling Treatment. Front Plant Sci. 2021 Feb 26;12:631421. doi:10.3389/fpls.2021.631421. PMID: 33719304; PMCID: PMC7952967

Dubanevics I, McLeish TCB. Computational analysis of dynamic allostery and control in the SARS-CoV-2 main protease. J R Soc Interface. 2021 Jan;18(174):20200591. doi: 10.1098/rsif.2020.0591. Epub 2021 Jan 6. PMID: 33402024; PMCID: PMC7879766

Dudas G, Carvalho LM, Rambaut A, Bedford T. MERS-CoV spillover at the camel-human interface. Elife. 2018 Jan 16;7:e31257.doi:10.7554/eLife.31257. Erratum in: Elife. 2018 Apr 19;7: PMID: 29336306; PMCID: PMC5777824

Eberle RJ, Olivier DS, Amaral MS, Gering I, Willbold D, Arni RK, Coronado MA. The Repurposed Drugs Suramin and Quinacrine Cooperatively Inhibit SARS-CoV-2 3CLpro In Vitro. Viruses. 2021 May 10;13(5):873. doi: 10.3390/v13050873. PMID: 34068686; PMCID: PMC8170883

El Houari I, Boerjan W, Vanholme B. Behind the Scenes: The Impact of Bioactive Phenylpropanoids on the Growth Phenotypes of Arabidopsis Lignin Mutants. Front Plant Sci. 2021 Sep 9;12:734070. doi:10.3389/fpls.2021.734070. PMID: 34567045; PMCID: PMC8458929

Elebeedy D, Elkhatib WF, Kandeil A, Ghanem A, Kutkat O, Alnajjar R, Saleh MA, Abd El Maksoud AI, Badawy I, Al-Karmalawy AA. Anti-SARS-CoV-2 activities of tanshinone IIA, carnosic acid, rosmarinic acid, salvianolic acid, baicalein, and glycyrrhetinic acid between computational and in vitro insights. RSC Adv. 2021 Sep 1;11(47):29267-29286. doi:10.1039/d1ra05268c. PMID: 35492070; PMCID: PMC9040650

Elsbaey M, Ibrahim MAA, Bar FA, Elgazar AA. Chemical constituents from coconut waste and their in silico evaluation as potential antiviral agents against SARS-CoV-2. S Afr J Bot. 2021 Sep;141:278-289. doi: 10.1016/j.sajb.2021.05.018. Epub 2021 May 28. PMID: 34092840; PMCID: PMC8162769

European Center for Disease Control (ECDC). Severe acute respiratory syndrome (SARS). https://www.ecdc.europa.eu/en/severeacute-respiratory-syndrome

Fan K, Wei P, Feng Q, Chen S, Huang C, Ma L, Lai B, Pei J, Liu Y, Chen J, Lai L. Biosynthesis, purification, and substrate specificity of severe acute respiratory syndrome coronavirus 3C-like proteinase. J Biol Chem. 2004 Jan 16;279(3):1637-42. doi: 10.1074/jbc.M310875200. Epub 2003 Oct 15. PMID: 14561748; PMCID: PMC7980035

Fazio AT, Adler MT, Bertoni MD, Sepúlveda CS, Damonte EB, Maier MS. Lichen secondary metabolites from the cultured lichen mycobionts of Teloschistes chrysophthalmus and Ramalina celastri and their antiviral activities. Z Naturforsch C J Biosci. 2007 Jul-Aug;62(7-8):543-9. doi: 10.1515/znc-2007-7-813. PMID: 17913069

Fehr AR, Perlman S. Coronaviruses: an overview of their replication and pathogenesis. Methods Mol Biol. 2015;1282:1-23. doi:10.1007/978-1-4939-2438-7_1. PMID: 25720466; PMCID: PMC4369385

Ferrari, G., Ghione, and M., Ghirardi, P., 1988, Antiplaque anticaries dentifrices containing usnic acid, S. African ZA 8704549, pp. 24

Ferreira JC, Fadl S, Rabeh WM. Key dimer interface residues impact the catalytic activity of 3CLpro, the main protease of SARS-CoV-2. J Biol Chem. 2022 Jun;298(6):102023. doi: 10.1016/j.jbc.2022.102023. Epub 2022 May 11. PMID: 35568197; PMCID: PMC9091064

Fishbane S, Hirsch JS, Nair V. Special Considerations for Paxlovid Treatment Among Transplant Recipients With SARS-CoV-2 Infection. Am J Kidney Dis. 2022 Apr;79(4):480-482. doi: 10.1053/j.ajkd.2022.01.001. Epub 2022 Jan 12. PMID: 35032591; PMCID: PMC8754454

Forni D, Cagliani R, Clerici M, Sironi M. Molecular Evolution of Human Coronavirus Genomes. Trends Microbiol. 2017 Jan;25(1):35-48. DOI: 10.1016/j.tim.2016.09.001. Epub 2016 Oct 19. PMID: 27743750; PMCID: PMC7111218

Fu L, Ye F, Feng Y, Yu F, Wang Q, Wu Y, Zhao C, Sun H, Huang B, Niu P, Song H, Shi Y, Li X, Tan W, Qi J, Gao GF. Both Boceprevir and GC376 efficaciously inhibit SARS-CoV-2 by targeting its main protease. Nat Commun. 2020 Sep 4;11(1):4417. doi:10.1038/s41467-020-18233-x. PMID: 32887884; PMCID: PMC7474075

Fu YZ, Wang SY, Zheng ZQ, Yi Huang, Li WW, Xu ZS, Wang YY. SARS-CoV-2 membrane glycoprotein M antagonizes the MAVS-mediated innate antiviral response. Cell Mol Immunol. 2021 Mar;18(3):613-620. doi:10.1038/s41423-020-00571-x. Epub 2020 Oct 27. PMID: 33110251; PMCID: PMC7588591

Fung TS, Liu DX. Human Coronavirus: Host-Pathogen Interaction. Annu Rev Microbiol. 2019 Sep 8;73:529-557. doi:10.1146/annurev-micro-020518-115759. Epub 2019 Jun 21. PMID: 31226023

Gallage NJ, Møller BL. Vanillin-bioconversion and bioengineering of the most popular plant flavor and its de novo biosynthesis in the vanilla orchid. Mol Plant. 2015 Jan;8(1):40-57. doi: 10.1016/j.molp.2014.11.008. Epub 2014 Dec 11. PMID: 25578271

Gamaro GD, Suyenaga E, Borsoi M, Lermen J, Pereira P, Ardenghi P. Effect of rosmarinic and caffeic acids on inflammatory and nociception process in rats. ISRN Pharmacol. 2011;2011:451682. doi: 10.5402/2011/451682. Epub 2011 Mar 30. PMID: 22084714; PMCID: PMC3197075

Gan C, Jia X, Fan S, Wang S, Jing W, and Wei X. Virtual screening and molecular dynamics simulation to identify potential SARS-CoV-2 3CLpro inhibitors from a natural product compounds library. Acta Virol., 15 December 2023. doi: https://doi.org/10.3389/av.2023.12464

Gao X, Zhu K, Qin B, Olieric V, Wang M, Cui S. Crystal structure of SARS-CoV-2 Orf9b in complex with human TOM70 suggests unusual virus-host interactions. Nat Commun. 2021 May 14;12(1):2843. doi: 10.1038/s41467-021-23118-8. PMID: 33990585; PMCID: PMC8121815

García-Niño WR, Pedraza-Chaverrí J. Protective effect of curcumin against heavy metals-induced liver damage. Food Chem Toxicol. 2014 Jul;69:182-201. doi: 10.1016/j.fct.2014.04.016. Epub 2014 Apr 18. PMID: 24751969

Gardner, Charles R., and Dale M. J. Mueller. Factors Affecting the Toxicity of Several Lichen Acids: Effect of pH and Lichen Acid Concentration. American Journal of Botany, vol. 68, no. 1, 1981, pp. 87–95. JSTOR, https://doi.org/10.2307/2442995

Gautam R, Saklani A, Jachak SM. Indian medicinal plants as a source of antimycobacterial agents. J Ethnopharmacol. 2007 Mar 21;110(2):200-34. doi: 10.1016/j.jep.2006.12.031. Epub 2007 Jan 4. PMID: 17276637

Gebru AA, Birhanu T, Wendimu E, Ayalew AF, Mulat S, Abasimel HZ, et al. Global burden of COVID-19: Situational analysis and review. Hum Antibodies. 2021;29(2):139-148. DOI: 10.3233/HAB-200420. PMID: 32804122

Ghosh AK, Raghavaiah J, Shahabi D, Yadav M, Anson BJ, Lendy EK, et al. Indole Chloropyridinyl Ester-Derived SARS-CoV-2 3CLpro Inhibitors: Enzyme Inhibition, Antiviral Efficacy, Structure-Activity Relationship, and X-ray Structural Studies. J Med Chem. 2021 Oct 14;64(19):14702-14714. doi: 10.1021/acs.jmedchem.1c01214. Epub 2021 Sep 16. PMID: 34528437; PMCID: PMC8457330

Gibbons S, Udo EE. The effect of reserpine, a modulator of multidrug efflux pumps, on the in vitro activity of tetracycline against clinical isolates of methicillin resistant Staphylococcus aureus (MRSA) possessing the tet(K) determinant. Phytother Res. 2000 Mar;14(2):139-40. doi: 10.1002/(sici)1099-1573(200003)14:2<139::aid-ptr608>3.0.co;2-8. PMID: 10685116

Giovanetti M, Branda F, Cella E, Scarpa F, Bazzani L, Ciccozzi A, et al. Epidemic history and evolution of an emerging threat of international concern, the severe acute respiratory syndrome coronavirus 2. J Med Virol. 2023 Aug;95(8):e29012. doi: 10.1002/jmv.29012. PMID: 37548148.

Girawale SD, Meena SN, Nandre VS, Waghmode SB, Kodam KM. Biosynthesis of vanillic acid by Ochrobactrum anthropi and its applications. Bioorg Med Chem. 2022 Oct 15;72:117000. doi: 10.1016/j.bmc.2022.117000. Epub 2022 Sep 7. PMID: 36095944

Goel A, Kunnumakkara AB, Aggarwal BB. Curcumin as "Curecumin": from kitchen to clinic. Biochem Pharmacol. 2008 Feb 15;75(4):787-809. doi: 10.1016/j.bcp.2007.08.016. Epub 2007 Aug 19. PMID: 17900536

Goh VSL, Mok CK, Chu JJH. Antiviral Natural Products for Arbovirus Infections. Molecules. 2020 Jun 17;25(12):2796. doi: 10.3390/molecules25122796. PMID: 32560438; PMCID: PMC7356825

Gorbalenya, A. E. et al. The species Severe acute respiratory syndrome-related coronavirus: classifying 2019-nCoV and naming it SARS-CoV-2. Nat. Microbiol. 5, 536–544 (2020)

Goyal B. and Goyal D., Targeting the Dimerization of the Main Protease of Coronaviruses: A Potential Broad-Spectrum Therapeutic Strategy. ACS Combinatorial Science 2020 22 (6), 297-305. DOI: 10.1021/acscombsci.0c00058

Graziano V, McGrath WJ, Yang L, Mangel WF. SARS CoV main proteinase: The monomer-dimer equilibrium dissociation constant. Biochemistry. 2006 Dec 12;45(49):14632-41. doi: 10.1021/bi061746y. PMID: 17144656

Greco WR, Bravo G, Parsons JC. The search for synergy: a critical review from a response surface perspective. Pharmacol Rev. 1995 Jun;47(2):331-85. PMID: 7568331

Grosdidier A, Zoete V, Michielin O. Fast docking using the CHARMM force field with EADock DSS. J Comput Chem. 2011b Jul 30;32(10):2149-59. doi: 10.1002/jcc.21797. Epub 2011 May 3. PMID: 21541955

Grosdidier A, Zoete V, Michielin O. SwissDock, a protein-small molecule docking web service based on EADock DSS. Nucleic Acids Res. 2011a Jul;39(Web Server issue):W270-7. doi: 10.1093/nar/gkr366. Epub 2011 May 29. PMID: 21624888; PMCID: PMC3125772

Grynkiewicz G, Ślifirski P. Curcumin and curcuminoids in quest for medicinal status. Acta Biochim Pol. 2012;59(2):201-12. Epub 2012 May 14. PMID: 22590694

Guijarro-Real C, Plazas M, Rodríguez-Burruezo A, Prohens J, Fita A. Potential In Vitro Inhibition of Selected Plant Extracts against SARS-CoV-2 Chymotripsin-Like Protease (3CLPro) Activity. Foods. 2021 Jun 29;10(7):1503. doi: 10.3390/foods10071503. PMID: 34209659; PMCID: PMC8304378.

Gupta M, Azumaya CM, Moritz M, Pourmal S, Diallo A, Merz GE, et al. CryoEM and AI reveal a structure of SARS-CoV-2 Nsp2, a multifunctional protein involved in key host processes. bioRxiv [Preprint]. 2021 May 11:2021.05.10.443524. doi: 10.1101/2021.05.10.443524. PMID: 34013269; PMCID: PMC8132225

Hansen EH, Møller BL, Kock GR, Bünner CM, Kristensen C, Jensen OR, Okkels FT, Olsen CE, Motawia MS, Hansen J. De novo biosynthesis of vanillin in fission yeast (Schizosaccharomyces pombe) and baker's yeast (Saccharomyces cerevisiae). Appl Environ Microbiol. 2009 May;75(9):2765-74. doi: 10.1128/AEM.02681-08. Epub 2009 Mar 13. PMID: 19286778; PMCID: PMC2681717

Hao YM, Yan YC, Zhang Q, Liu BQ, Wu CS, Wang LN. Phytochemical composition, antimicrobial activities, and cholinesterase inhibitory properties of the lichen Usnea diffracta Vain. Front Chem. 2023 Jan 6;10:1063645. doi: 10.3389/fchem.2022.1063645. PMID: 36688056; PMCID: PMC9853987

Harrison AG, Lin T, Wang P. Mechanisms of SARS-CoV-2 Transmission and Pathogenesis. Trends Immunol. 2020 Dec;41(12):1100-1115. doi: 10.1016/j.it.2020.10.004. Epub 2020 Oct 14. PMID: 33132005; PMCID: PMC7556779

Harvey AL, Edrada-Ebel R, Quinn RJ. The re-emergence of natural products for drug discovery in the genomics era. Nat Rev Drug Discov. 2015 Feb;14(2):111-29. doi: 10.1038/nrd4510. Epub 2015 Jan 23. PMID: 25614221

Harvey AL. Natural products in drug discovery. Drug Discov Today. 2008 Oct;13(19-20):894-901. doi: 10.1016/j.drudis.2008.07.004. Epub 2008 Aug 22. PMID: 18691670

He G, Chen G, Liu W, Ye D, Liu X, Liang X, Song J. Salvianolic Acid B: A Review of Pharmacological Effects, Safety, Combination Therapy, New Dosage Forms, and Novel Drug Delivery Routes. Pharmaceutics. 2023 Aug 29;15(9):2235. doi: 10.3390/pharmaceutics15092235. PMID: 37765204; PMCID: PMC10538146

Hemaiswarya S, Kruthiventi AK, Doble M. Synergism between natural products and antibiotics against infectious diseases. Phytomedicine. 2008 Aug;15(8):639-52. doi: 10.1016/j.phymed.2008.06.008. PMID: 18599280

Hewlings SJ, Kalman DS. Curcumin: A Review of Its Effects on Human Health. Foods. 2017 Oct 22;6(10):92. doi: 10.3390/foods6100092. PMID: 29065496; PMCID: PMC5664031

Hicks EG, Kandel SE, Lampe JN. Identification of Aloe-derived natural products as prospective lead scaffolds for SARS-CoV-2 main protease (Mpro) inhibitors. Bioorg Med Chem Lett. 2022 Jun

15;66:128732. doi: 10.1016/j.bmcl.2022.128732. Epub 2022 Apr 12. PMID: 35427739; PMCID: PMC9004148

Hidalgo ME, Fernández E, Quilhot W, Lissi E. Antioxidant activity of depsides and depsidones. Phytochemistry. 1994 Dec;37(6):1585-7. doi: 10.1016/s0031-9422(00)89571-0. PMID: 7765999

Higuchi, M., Miura, Y., Kinoshita, Y., Yamamoto, Y., and Mayama, S., 1993, Acne-controlling antibacterial agents containing usnic acids or lichesterinic acids, Jpn. Kokai Tokkyo Koho, pp. 3

Ho BL, Cheng SC, Shi L, Wang TY, Ho KI, Chou CY. Critical Assessment of the Important Residues Involved in the Dimerization and Catalysis of MERS Coronavirus Main Protease. PLoS One. 2015 Dec 14;10(12):e0144865. doi: 10.1371/journal.pone.0144865. PMID: 26658006; PMCID: PMC4682845

Ho J.HC. and Hong CY. Salvianolic acids: small compounds with multiple mechanisms for cardiovascular protection. J Biomed Sci 18, 30 (2011). https://doi.org/10.1186/1423-0127-18-30

Hoehle SI, Pfeiffer E, Metzler M. Glucuronidation of curcuminoids by human microsomal and recombinant UDP-glucuronosyltransferases. Mol Nutr Food Res. 2007 Aug;51(8):932-8. doi: 10.1002/mnfr.200600283. PMID: 17628876)

Hoffmann M, Kleine-Weber H, Schroeder S, Krüger N, Herrler T, Erichsen S, Schiergens TS, Herrler G, Wu NH, Nitsche A, Müller MA, Drosten C, Pöhlmann S. SARS-CoV-2 Cell Entry Depends on ACE2 and TMPRSS2 and Is Blocked by a Clinically Proven Protease Inhibitor. Cell. 2020 Apr 16;181(2):271-280.e8. doi: 10.1016/j.cell.2020.02.052. Epub 2020 Mar 5. PMID: 32142651; PMCID: PMC7102627

Hollósy F, Mészáros G, Bökönyi G, Idei M, Seprödi A, Szende B, Kéri G. Cytostatic, cytotoxic and protein tyrosine kinase inhibitory activity of ursolic acid in A431 human tumor cells. Anticancer Res. 2000 Nov-Dec;20(6B):4563-70. PMID: 11205305

Holmes EC, Goldstein SA, Rasmussen AL, Robertson DL, Crits-Christoph A, Wertheim JO, et al. The origins of SARS-CoV-2: A critical review. Cell. 2021 Sep 16;184(19):4848-4856. doi: 10.1016/j.cell.2021.08.017. Epub 2021 Aug 19. PMID: 34480864; PMCID: PMC8373617

Holshue ML, DeBolt C, Lindquist S, Lofy KH, Wiesman J, Bruce H, et al. Washington State 2019-nCoV Case Investigation Team. First Case of 2019 Novel Coronavirus in the United States. N Engl J Med. 2020 Mar 5;382(10):929-936. doi: 10.1056/NEJMoa2001191. Epub 2020 Jan 31. PMID: 32004427; PMCID: PMC7092802

Hsu WC, Chang HC, Chou CY, Tsai PJ, Lin PI, Chang GG. Critical assessment of important regions in the subunit association and catalytic action of the severe acute respiratory syndrome coronavirus main protease. J Biol Chem. 2005 Jun 17;280(24):22741-8. doi: 10.1074/jbc.M502556200. Epub 2005 Apr 14. PMID: 15831489; PMCID: PMC8060872

Huang Y, Yang C, Xu XF, Xu W, Liu SW. Structural and functional properties of SARS-CoV-2 spike protein: potential antivirus drug development for COVID-19. Acta Pharmacol Sin. 2020 Sep;41(9):1141-1149. doi: 10.1038/s41401-020-0485-4. Epub 2020 Aug 3. PMID: 32747721; PMCID: PMC7396720

Huneck S. The significance of lichens and their metabolites. Naturwissenschaften. 1999 Dec;86(12):559-70. doi: 10.1007/s001140050676. PMID: 10643590

Huneck, S. and Yoshimura, I. 1996. Identification of lichen substances (Berlin, Heidelberg; Springer-Verlag)

Ianni A, Ruggeri P, Bellio P, Martino F, Celenza G, Martino G, Franceschini N. Salvianolic Acid B Strikes Back: New Evidence in the Modulation of Expression and Activity of Matrix Metalloproteinase 9 in MDA-MB-231 Human Breast Cancer Cells. Molecules. 2022 Dec 3;27(23):8514. doi: 10.3390/molecules27238514. PMID: 36500603; PMCID: PMC9740829

Ichinose T, Miller M, Shibamoto T. Inhibition of malondialdehyde formation from liver microsomes by a lichen constituent. Food Chem Toxicol. 1994 Dec;32(12):1167-8. doi: 10.1016/0278-6915(94)90133-3. PMID: 7813989

Ingelfinger R, Henke M, Roser L, Ulshöfer T, Calchera A, Singh G, Parnham MJ, Geisslinger G, Fürst R, Schmitt I, Schiffmann S. Unraveling the Pharmacological Potential of Lichen Extracts in the Context of Cancer and Inflammation With a Broad Screening Approach. Front Pharmacol. 2020 Sep 4;11:1322. doi: 10.3389/fphar.2020.01322. PMID: 33013369; PMCID: PMC7509413

Ingólfsdóttir K, Bloomfield SF, Hylands PJ. In vitro evaluation of the antimicrobial activity of lichen metabolites as potential preservatives. Antimicrob Agents Chemother. 1985 Aug;28(2):289-92. doi: 10.1128/AAC.28.2.289. PMID: 3834834; PMCID: PMC180233

Ingólfsdóttir K, Gudmundsdóttir GF, Ogmundsdóttir HM, Paulus K, Haraldsdóttir S, Kristinsson H, Bauer R. Effects of tenuiorin and methyl orsellinate from the lichen Peltigera leucophlebia on 5-/15-lipoxygenases and proliferation of malignant cell lines in vitro. Phytomedicine. 2002 Oct;9(7):654-8. doi: 10.1078/094471102321616481. PMID: 12487331

Ingólfsdóttir K. Usnic acid. Phytochemistry. 2002 Dec;61(7):729-36. doi: 10.1016/s0031-9422(02)00383-7. PMID: 12453567

Insarova ID, Blagoveshchenskaya EY. Lichen Symbiosis: Search and Recognition of Partners. Izv Akad Nauk Ser Biol. 2016 Sep;(5):479-490. English, Russian. PMID: 30226935

Ireson CR, Jones DJ, Orr S, Coughtrie MW, Boocock DJ, Williams ML, Farmer PB, Steward WP, Gescher AJ. Metabolism of the cancer chemopreventive agent curcumin in human and rat intestine. Cancer Epidemiol Biomarkers Prev. 2002 Jan;11(1):105-11. PMID: 11815407

Jennings MR, Parks RJ. Curcumin as an Antiviral Agent. Viruses. 2020 Oct 31;12(11):1242. doi: 10.3390/v12111242. PMID: 33142686; PMCID: PMC7693600.

Jiang W., Chen X., Feng Y., Sun J., Jiang Y., Zhang W., Xin F., and Jiang M. Current Status, Challenges, and Prospects for the Biological Production of Vanillin. Fermentation, 2023. doi.org/10.3390/fermentation9040389

Jiang Y, Yin W, Xu HE. RNA-dependent RNA polymerase: Structure, mechanism, and drug discovery for COVID-19. Biochem Biophys Res Commun. 2021 Jan 29;538:47-53. doi: 10.1016/j.bbrc.2020.08.116. Epub 2020 Sep 4. PMID: 32943188; PMCID: PMC7473028

Jones D. 1988 Lichens and pedogenesis. In: Galun M (ed) CRC handbook of lichenology, vol III. CRC, Boca Raton, p 109

Kamath AK, Nasim I, Muralidharan NP, Kothuri RN. Anti-microbial efficacy of Vanilla planifolia leaf extract against common oral micro-biomes: A comparative study of two different antibiotic sensitivity tests. J Oral Maxillofac Pathol. 2022 Jul-Sep;26(3):330-334. doi: 10.4103/jomfp.jomfp_293_21. Epub 2022 Oct 17. PMID: 36588845; PMCID: PMC9802507

Kang S, Yang M, Hong Z, Zhang L, Huang Z, Chen X, He S, Zhou Z, Zhou Z, Chen Q, Yan Y, Zhang C, Shan H, Chen S. Crystal structure of SARS-CoV-2 nucleocapsid protein RNA binding domain reveals potential unique drug targeting sites. Acta Pharm Sin B. 2020 Jul;10(7):1228-1238. doi: 10.1016/j.apsb.2020.04.009. Epub 2020 Apr 20. PMID: 32363136; PMCID: PMC7194921

Kern DM, Sorum B, Mali SS, Hoel CM, Sridharan S, Remis JP, Toso DB, Kotecha A, Bautista DM, Brohawn SG. Cryo-EM structure of the SARS-CoV-2 3a ion channel in lipid nanodiscs. bioRxiv [Preprint]. 2021 Jan 26:2020.06.17.156554. doi: 10.1101/2020.06.17.156554. Update in: Nat Struct Mol Biol. 2021 Jul;28(7):573-582. PMID: 32587976; PMCID: PMC7310636

Khan F, Bamunuarachchi NI, Tabassum N, Kim YM. Caffeic Acid and Its Derivatives: Antimicrobial Drugs toward Microbial Pathogens. J Agric Food Chem. 2021 Mar 17;69(10):2979-3004. doi: 10.1021/acs.jafc.0c07579. Epub 2021 Mar 3. PMID: 33656341

Kim Y, Jedrzejczak R, Maltseva NI, Wilamowski M, Endres M, Godzik A, Michalska K, Joachimiak A. Crystal structure of Nsp15 endoribonuclease NendoU from SARS-CoV-2. Protein Sci. 2020 Jul;29(7):1596-1605. doi: 10.1002/pro.3873. Epub 2020 May 2. PMID: 32304108; PMCID: PMC7264519

Kim Y, Lovell S, Tiew KC, Mandadapu SR, Alliston KR, Battaile KP, Groutas WC, Chang KO. Broad-spectrum antivirals against 3C or 3C-like proteases of picornaviruses, noroviruses, and coronaviruses. J Virol. 2012 Nov;86(21):11754-62. doi: 10.1128/JVI.01348-12. Epub 2012 Aug 22. PMID: 22915796; PMCID: PMC3486288

Kotha RR, Luthria DL. Curcumin: Biological, Pharmaceutical, Nutraceutical, and Analytical Aspects. Molecules. 2019 Aug 13;24(16):2930. doi: 10.3390/molecules24162930. PMID: 31412624; PMCID: PMC6720683

Kranner I, Cram WJ, Zorn M, Wornik S, Yoshimura I, Stabentheiner E, Pfeifhofer HW. Antioxidants and photoprotection in a lichen as compared with its isolated symbiotic partners. Proc Natl Acad Sci U S A. 2005 Feb 22;102(8):3141-6. doi: 10.1073/pnas.0407716102. Epub 2005 Feb 14. PMID: 15710882; PMCID: PMC549463

Kumar KC S, Müller K. Depsides as non-redox inhibitors of leukotriene B(4) biosynthesis and HaCaT cell growth, 2. Novel analogues of obtusatic acid. Eur J Med Chem. 2000 Apr;35(4):405-11. doi: 10.1016/s0223-5234(00)00132-x. PMID: 10858601

Kunnumakkara AB, Anand P, Aggarwal BB. Curcumin inhibits proliferation, invasion, angiogenesis and metastasis of different cancers through interaction with multiple cell signaling proteins. Cancer Lett. 2008 Oct 8;269(2):199-225. doi: 10.1016/j.canlet.2008.03.009. Epub 2008 May 13. PMID: 18479807

Kurt Yilmaz N, Swanstrom R, Schiffer CA. Improving Viral Protease Inhibitors to Counter Drug Resistance. Trends Microbiol. 2016 Jul;24(7):547-557. doi: 10.1016/j.tim.2016.03.010. Epub 2016 Apr 15. PMID: 27090931; PMCID: PMC4912444

Kuzmic P. Program DYNAFIT for the analysis of enzyme kinetic data: application to HIV proteinase. Anal Biochem. 1996 Jun 1;237(2):260-73. doi: 10.1006/abio.1996.0238. PMID: 8660575

Kuzmič P. DynaFit--a software package for enzymology. Methods Enzymol. 2009;467:247-280. doi: 10.1016/S0076-6879(09)67010-5. PMID: 19897096

Lam TT, Jia N, Zhang YW, Shum MH, Jiang JF, Zhu HC, et al. Identifying SARS-CoV-2-related coronaviruses in Malayan pangolins. Nature. 2020 Jul;583(7815):282-285. doi: 10.1038/s41586-020-2169-0. Epub 2020 Mar 26. PMID: 32218527

Law WY, Asaruddin MR, Bhawani SA, Mohamad S. Pharmacophore modelling of vanillin derivatives, favipiravir, chloroquine, hydroxychloroquine, monolaurin and tetrodotoxin as MPro inhibitors of severe acute respiratory syndrome coronavirus-2 (SARS-CoV-2). BMC Res Notes. 2020 Nov 11;13(1):527. doi: 10.1186/s13104-020-05379-6. PMID: 33176880; PMCID: PMC7656897

Lawrey JD. The chemical ecology of lichen mycoparasites. 1995. Can J Bot 73:603–608. https://doi.org/10.1139/b95-301

Lawrey, JD. “Biological Role of Lichen Substances.” The Bryologist, vol. 89, no. 2, 1986, pp. 111–22. JSTOR, https://doi.org/10.2307/3242751. Accessed 23 Feb. 2024

Lee J, Scagel CF. Chicoric acid: chemistry, distribution, and production. Front Chem. 2013 Dec 31;1:40. doi: 10.3389/fchem.2013.00040. PMID: 24790967; PMCID: PMC3982519

Lei J, Kusov Y, Hilgenfeld R. Nsp3 of coronaviruses: Structures and functions of a large multi-domain protein. Antiviral Res. 2018 Jan;149:58-74. doi: 10.1016/j.antiviral.2017.11.001. Epub 2017 Nov 8. PMID: 29128390; PMCID: PMC7113668

Leyon PV, Kuttan G. Studies on the role of some synthetic curcuminoid derivatives in the inhibition of tumour specific angiogenesis. J Exp Clin Cancer Res. 2003 Mar;22(1):77-83. PMID: 12725326

Li D, Rui YX, Guo SD, Luan F, Liu R, Zeng N. Ferulic acid: A review of its pharmacology, pharmacokinetics and derivatives. Life Sci. 2021 Nov 1;284:119921. doi: 10.1016/j.lfs.2021.119921. Epub 2021 Sep 3. PMID: 34481866

Li F. Structure, Function, and Evolution of Coronavirus Spike Proteins. Annu Rev Virol. 2016 Sep 29;3(1):237-261. doi: 10.1146/annurev-virology-110615-042301. Epub 2016 Aug 25. PMID: 27578435; PMCID: PMC5457962

Li Q, Guan X, et al. Early transmission dynamics in Wuhan, China, of novel coronavirus-infected pneumonia. N Engl J Med 2020;DOI:10.1056/NEJMoa2001316

Li Q, Guan X, Wu P, Wang X, Zhou L, Tong Y, et al. Early Transmission Dynamics in Wuhan, China, of Novel Coronavirus-Infected Pneumonia. N Engl J Med. 2020 Mar 26;382(13):1199-1207. doi: 10.1056/NEJMoa2001316. Epub 2020 Jan 29. PMID: 31995857; PMCID: PMC7121484

Lim YX, Ng YL, Tam JP, Liu DX. Human Coronaviruses: A Review of Virus-Host Interactions. Diseases. 2016 Jul 25;4(3):26. DOI: 10.3390/diseases4030026. PMID: 28933406; PMCID: PMC5456285

Lin CY, Eudes A. Strategies for the production of biochemicals in bioenergy crops. Biotechnol Biofuels. 2020 Apr 15;13:71. doi: 10.1186/s13068-020-01707-x. PMID: 32318116; PMCID: PMC7158082

Lin PY, Chou CY, Chang HC, Hsu WC, Chang GG. Correlation between dissociation and catalysis of SARS-CoV main protease. Arch Biochem Biophys. 2008 Apr 1;472(1):34-42. doi: 10.1016/j.abb.2008.01.023. Epub 2008 Feb 5. PMID: 18275836; PMCID: PMC7094404

Lin S, Chen H, Chen Z, Yang F, Ye F, Zheng Y, Yang J, Lin X, Sun H, Wang L, Wen A, Dong H, Xiao Q, Deng D, Cao Y, Lu G. Crystal structure of SARS-CoV-2 nsp10 bound to nsp14-ExoN domain reveals an exoribonuclease with both structural and functional integrity. Nucleic Acids Res. 2021 May 21;49(9):5382-5392. doi: 10.1093/nar/gkab320. PMID: 33956156; PMCID: PMC8136770

Lipinski CA, Lombardo F, Dominy BW, Feeney PJ. Experimental and computational approaches to estimate solubility and permeability in drug discovery and development settings. Adv Drug Deliv Rev. 2001 Mar 1;46(1-3):3-26. doi: 10.1016/s0169-409x(00)00129-0. PMID: 11259830

Liu DX, Fung TS, Chong KK, Shukla A, Hilgenfeld R. Accessory proteins of SARS-CoV and other coronaviruses. Antiviral Res. 2014 Sep;109:97-109. DOI: 10.1016/j.antiviral.2014.06.013. Epub 2014 Jul 1. PMID: 24995382; PMCID: PMC7113789

Liu N, Yang Z, Liu Y, Dang X, Zhang Q, Wang J, Liu X, Zhang J, Pan X. Identification of a Putative SARS-CoV-2 Main Protease Inhibitor through In Silico Screening of Self-Designed Molecular Library. Int J Mol Sci. 2023 Jul 13;24(14):11390. doi: 10.3390/ijms241411390. PMID: 37511149; PMCID: PMC10379331

Liu Y, Cruz-Morales P, Zargar A, Belcher MS, Pang B, Englund E, Dan Q, Yin K, Keasling JD. Biofuels for a sustainable future. Cell. 2021 Mar 18;184(6):1636-1647. doi: 10.1016/j.cell.2021.01.052. Epub 2021 Feb 26. PMID: 33639085

Lockbaum GJ, Reyes AC, Lee JM, Tilvawala R, Nalivaika EA, Ali A, Kurt Yilmaz N, Thompson PR, Schiffer CA. Crystal Structure of SARS-CoV-2 Main Protease in Complex with the Non-Covalent Inhibitor ML188. Viruses. 2021 Jan 25;13(2):174. doi: 10.3390/v13020174. PMID: 33503819; PMCID: PMC7911568

Lohézic-Le Dévéhat F, Tomasi S, Elix JA, Bernard A, Rouaud I, Uriac P, Boustie J. Stictic acid derivatives from the lichen Usnea articulata and their antioxidant activities. J Nat Prod. 2007 Jul;70(7):1218-20. doi: 10.1021/np070145k. Epub 2007 Jul 13. PMID: 17629329

Lopes TIB, Coelho RG, Yoshida NC et al (2008) Radical scavenging activity of Orsellinates. Chem Pharm Bull 56:1551–1554) (Paudel B, Bhattarai HD, Lee JS et al (2008) Antioxidant activity of polar lichens from King George Island (Antarctica). Polar Biol 31:605–608

Lu R, Zhao X, Li J, Niu P, Yang B, Wu H, et al. Genomic characterisation and epidemiology of 2019 novel coronavirus: implications for virus origins and receptor binding. Lancet. 2020 Feb 22;395(10224):565-574. doi: 10.1016/S0140-6736(20)30251-8. Epub 2020 Jan 30. PMID: 32007145; PMCID: PMC7159086

Luk HKH, Li X, Fung J, Lau SKP, Woo PCY. Molecular epidemiology, evolution and phylogeny of SARS coronavirus. Infect Genet Evol. 2019 Jul;71:21-30. doi: 10.1016/j.meegid.2019.03.001. Epub 2019 Mar 4. PMID: 30844511; PMCID: PMC7106202

Ma C, Sacco MD, Hurst B, Townsend JA, Hu Y, Szeto T, Zhang X, Tarbet B, Marty MT, Chen Y, Wang J. Boceprevir, GC-376, and calpain inhibitors II, XII inhibit SARS-CoV-2 viral replication by targeting the viral main protease. Cell Res. 2020 Aug;30(8):678-692. doi: 10.1038/s41422-020-0356-z. Epub 2020 Jun 15. PMID: 32541865; PMCID: PMC7294525

Malcolm BA, Liu R, Lahser F, Agrawal S, Belanger B, Butkiewicz N, et al. SCH 503034, a mechanism-based inhibitor of hepatitis C virus NS3 protease, suppresses polyprotein maturation and enhances the antiviral activity of alpha interferon in replicon cells. Antimicrob Agents Chemother. 2006 Mar;50(3):1013-20. doi: 10.1128/AAC.50.3.1013-1020.2006. PMID: 16495264; PMCID: PMC1426438

Mandal A, Jha AK, Hazra B. Plant Products as Inhibitors of Coronavirus 3CL Protease. Front Pharmacol. 2021 Mar 9;12:583387. doi: 10.3389/fphar.2021.583387. PMID: 33767619; PMCID: PMC7985176.

Manju M, Sherin TG, Rajasekharan KN, Oommen OV. Curcumin analogue inhibits lipid peroxidation in a freshwater teleost, Anabas testudineus (Bloch)--an in vitro and in vivo study. Fish Physiol Biochem. 2009 Aug;35(3):413-20. doi: 10.1007/s10695-008-9266-6. Epub 2008 Oct 25. PMID: 18953661

Manojlovic NT, Vasiljevic PJ, Maskovic PZ, Juskovic M, Bogdanovic-Dusanovic G. Chemical Composition, Antioxidant, and Antimicrobial Activities of Lichen Umbilicaria cylindrica (L.) Delise (Umbilicariaceae). Evid Based Complement Alternat Med. 2012;2012:452431. doi: 10.1155/2012/452431. Epub 2011 Sep 7. PMID: 21915186; PMCID: PMC3170701

Marx J. Cancer research. Anti-inflammatories inhibit cancer growth--but how? Science. 2001 Jan 26;291(5504):581-2. doi: 10.1126/science.291.5504.581. PMID: 11233414

McBride R, Fielding BC. The role of severe acute respiratory syndrome (SARS)-coronavirus accessory proteins in virus pathogenesis. Viruses. 2012 Nov 7;4(11):2902-23. doi: 10.3390/v4112902. PMID: 23202509; PMCID: PMC3509677

Méndez-Vilas. Antimicrobial activity of secondary metabolites and lectins from plants. Current Research, Technology and Education Topics in Applied Microbiology and Microbial Biotechnology. 396-406. Formatex Research Center, 2010

Mirzaei H, Shakeri A, Rashidi B, Jalili A, Banikazemi Z, Sahebkar A. Phytosomal curcumin: A review of pharmacokinetic, experimental and clinical studies. Biomed Pharmacother. 2017 Jan;85:102-112. doi: 10.1016/j.biopha.2016.11.098. Epub 2016 Dec 5. PMID: 27930973

Mitrović T, Stamenković S, Cvetković V, Tošić S, Stanković M, Radojević I, Stefanović O, Comić L, Dačić D, Curčić M, Marković S. Antioxidant, antimicrobial and antiproliferative activities of five lichen species. Int J Mol Sci. 2011;12(8):5428-48. doi: 10.3390/ijms12085428. Epub 2011 Aug 23. PMID: 21954369; PMCID: PMC3179176

Mody V, Ho J, Wills S, Mawri A, Lawson L, Ebert MCCJC, Fortin GM, Rayalam S, Taval S. Identification of 3-chymotrypsin like protease (3CLPro) inhibitors as potential anti-SARS-CoV-2 agents. Commun Biol. 2021 Jan 20;4(1):93. doi: 10.1038/s42003-020-01577-x. PMID: 33473151; PMCID: PMC7817688.

Moghadamtousi SZ, Kadir HA, Hassandarvish P, Tajik H, Abubakar S, Zandi K. A review on antibacterial, antiviral, and antifungal activity of curcumin. Biomed Res Int. 2014;2014:186864. doi: 10.1155/2014/186864. Epub 2014 Apr 29. PMID: 24877064; PMCID: PMC4022204

Moldovan M, Lahmar A, Bogdan C, Părăuan S, Tomuţă I, Crişan M: Formulation and evaluation of a water-in-oil cream containing herbal active ingredients and ferulic acid. Clujul Med 2017; 90: 212–219

Monton C, Charoenchai L, Suksaeree J, Sueree L. Quantitation of curcuminoid contents, dissolution profile, and volatile oil content of turmeric capsules produced at some secondary government hospitals. J Food Drug Anal. 2016 Jul;24(3):493-499. doi: 10.1016/j.jfda.2016.01.007. Epub 2016 Feb 23. PMID: 28911554; PMCID: PMC9336658)

Moreira RA, Guzman HV, Boopathi S, Baker JL, Poma AB. Characterization of Structural and Energetic Differences between Conformations of the SARS-CoV-2 Spike Protein. Materials (Basel). 2020 Nov 26;13(23):5362. doi: 10.3390/ma13235362. PMID: 33255977; PMCID: PMC7730245

Morrison JF, Walsh CT. The behavior and significance of slow-binding enzyme inhibitors. Adv Enzymol Relat Areas Mol Biol. 1988;61:201-301. doi: 10.1002/9780470123072.ch5. PMID: 3281418

Moskalenko SA. Preliminary screening of far-eastern ethnomedicinal plants for antibacterial activity. J Ethnopharmacol. 1986 Mar;15(3):231-59. doi: 10.1016/0378-8741(86)90163-7. PMID: 3724205

Mounce BC, Cesaro T, Carrau L, Vallet T, Vignuzzi M. Curcumin inhibits Zika and chikungunya virus infection by inhibiting cell binding. Antiviral Res. 2017 Jun;142:148-157. doi: 10.1016/j.antiviral.2017.03.014. Epub 2017 Mar 24. PMID: 28343845.

Muramatsu T, Takemoto C, Kim YT, Wang H, Nishii W, Terada T, Shirouzu M, Yokoyama S. SARS-CoV 3CL protease cleaves its C-terminal autoprocessing site by novel subsite cooperativity. Proc Natl Acad Sci U S A. 2016 Nov 15;113(46):12997-13002. doi: 10.1073/pnas.1601327113. Epub 2016 Oct 31. PMID: 27799534; PMCID: PMC5135343

Neamati, N., Hong, H., Mazumder, A., Wang, S., Sunder, S., Nicklaus, M.C., Milne, G.W.A., Proksa, B., and Pommier, Y., 1997, Depsides and depsidones as inhibitors of HIV -1 integrase : Discovery of novel inhibitors through 3D database searching,J. Med. Chem. 40: 942-95

Needle D, Lountos GT, Waugh DS. Structures of the Middle East respiratory syndrome coronavirus 3C-like protease reveal insights into substrate specificity. Acta Crystallogr D Biol Crystallogr. 2015 May;71(Pt 5):1102-11. doi: 10.1107/S1399004715003521. Epub 2015 Apr 24. PMID: 25945576; PMCID: PMC4427198

Nelson KM, Dahlin JL, Bisson J, Graham J, Pauli GF, Walters MA. The Essential Medicinal Chemistry of Curcumin. J Med Chem. 2017 Mar 9;60(5):1620-1637. doi: 10.1021/acs.jmedchem.6b00975. Epub 2017 Jan 11. PMID: 28074653; PMCID: PMC5346970

Ngo YL, Lau CH, Chua LS. Review on rosmarinic acid extraction, fractionation and its anti-diabetic potential. Food Chem Toxicol. 2018 Nov;121:687-700. doi: 10.1016/j.fct.2018.09.064. Epub 2018 Sep 28. PMID: 30273632

Nieto-Torres JL, DeDiego ML, Verdiá-Báguena C, Jimenez-Guardeño JM, Regla-Nava JA, Fernandez-Delgado R, Castaño-Rodriguez C, Alcaraz A, Torres J, Aguilella VM, Enjuanes L. Severe acute respiratory syndrome coronavirus envelope protein ion channel activity promotes virus fitness and pathogenesis. PLoS Pathog. 2014 May 1;10(5):e1004077. doi: 10.1371/journal.ppat.1004077. PMID: 24788150; PMCID: PMC4006877

Nioi M, Napoli PE, Lobina J, Fossarello M, d'Aloja E. COVID-19 and Italian Healthcare Workers From the Initial Sacrifice to the mRNA Vaccine: Pandemic Chrono-History, Epidemiological Data,

Ethical Dilemmas, and Future Challenges. Front Public Health. 2021 Jan 21;8:591900. DOI: 10.3389/fpubh.2020.591900. PMID: 33553091; PMCID: PMC7859528

Nishitoba Y., Nishimura I., Nishiyama T., Mizutani J. (1987). Lichen acids, plant growth inhibitors from Usnea longissima . Phytochemistry 6 (12), 3181–3185. 10.1016/S0031-9422(00)82466-8

Novaretti R, Lemordant D. Plants in the traditional medicine of the Ubaye Valley. J Ethnopharmacol. 1990 Aug;30(1):1-34. doi: 10.1016/0378-8741(90)90014-k. PMID: 2214819

Odabasoglu F, Cakir A, Suleyman H, Aslan A, Bayir Y, Halici M, Kazaz C. Gastroprotective and antioxidant effects of usnic acid on indomethacin-induced gastric ulcer in rats. J Ethnopharmacol. 2006 Jan 3;103(1):59-65. doi: 10.1016/j.jep.2005.06.043. Epub 2005 Oct 5. PMID: 16169175

Ogmundsdóttir HM, Zoëga GM, Gissurarson SR, Ingólfsdóttir K. Anti-proliferative effects of lichen-derived inhibitors of 5-lipoxygenase on malignant cell-lines and mitogen-stimulated lymphocytes. J Pharm Pharmacol. 1998 Jan;50(1):107-15. doi: 10.1111/j.2042-7158.1998.tb03312.x. PMID: 9504441

Okuyama E, Umeyama K, Yamazaki M, Kinoshita Y, Yamamoto Y. Usnic acid and diffractaic acid as analgesic and antipyretic components of Usnea diffracta. Planta Med. 1995 Apr;61(2):113-5. doi: 10.1055/s-2006-958027. PMID: 7753915

Oostra M, Hagemeijer MC, van Gent M, Bekker CP, te Lintelo EG, Rottier PJ, de Haan CA. Topology and membrane anchoring of the coronavirus replication complex: not all hydrophobic domains of nsp3 and nsp6 are membrane spanning. J Virol. 2008 Dec;82(24):12392-405. doi: 10.1128/JVI.01219-08. Epub 2008 Oct 8. PMID: 18842706; PMCID: PMC2593338

Ortiz A, Sansinenea E. Phenylpropanoid Derivatives and Their Role in Plants' Health and as antimicrobials. Curr Microbiol. 2023 Oct 20;80(12):380. doi: 10.1007/s00284-023-03502-x. PMID: 37864088

Otsuka H, Komiya T, Tsukumi M et al (1972) Studies on anti-inflammatory drug) (Okuyama E, Umeyama K, Yamazaki M et al (1995) Usnic acid and diffractaic acid as analgesic and antipyretic components of Usnea diffracta. Planta Med 61:113–115

Owen DR, Allerton CMN, Anderson AS, Aschenbrenner L, Avery M, Berritt S, et al. An oral SARS-CoV-2 Mpro inhibitor clinical candidate for the treatment of COVID-19. Science. 2021 Dec 24;374(6575):1586-1593. doi: 10.1126/science.abl4784. Epub 2021 Nov 2. PMID: 34726479

Panagiotopoulos AA, Karakasiliotis I, Kotzampasi DM, Dimitriou M, Sourvinos G, Kampa M, Pirintsos S, Castanas E, Daskalakis V. Natural Polyphenols Inhibit the Dimerization of the SARS-CoV-2 Main Protease: The Case of Fortunellin and Its Structural Analogs. Molecules. 2021 Oct 7;26(19):6068. doi: 10.3390/molecules26196068. PMID: 34641612; PMCID: PMC8512273

Pancer K, Milewska A, Owczarek K, Dabrowska A, Kowalski M, Łabaj PP, Branicki W, Sanak M, Pyrc K. The SARS-CoV-2 ORF10 is not essential in vitro or in vivo in humans. PLoS Pathog. 2020 Dec 10;16(12):e1008959. doi: 10.1371/journal.ppat.1008959. PMID: 33301543; PMCID: PMC7755277

Park JY, Kim JH, Kim YM, Jeong HJ, Kim DW, Park KH, Kwon HJ, Park SJ, Lee WS, Ryu YB. Tanshinones as selective and slow-binding inhibitors for SARS-CoV cysteine proteases. Bioorg Med Chem. 2012 Oct 1;20(19):5928-35. doi: 10.1016/j.bmc.2012.07.038. Epub 2012 Aug 2. PMID: 22884354; PMCID: PMC7127169

Paudel B, Bhattarai HD, Lee JS et al (2008) Antioxidant activity of polar lichens from King George Island (Antarctica). Polar Biol 31:605–608

Paules CI, Marston HD, Fauci AS. Coronavirus Infections-More Than Just the Common Cold. JAMA. 2020 Feb 25;323(8):707-708. doi: 10.1001/jama.2020.0757. PMID: 31971553

Pavlíková N. Caffeic Acid and Diseases-Mechanisms of Action. Int J Mol Sci. 2022 Dec 29;24(1):588. doi: 10.3390/ijms24010588. PMID: 36614030; PMCID: PMC9820408

Pedersen NC, Kim Y, Liu H, Galasiti Kankanamalage AC, Eckstrand C, Groutas WC, Bannasch M, Meadows JM, Chang KO. Efficacy of a 3C-like protease inhibitor in treating various forms of acquired feline infectious peritonitis. J Feline Med Surg. 2018 Apr;20(4):378-392. doi: 10.1177/1098612X17729626. Epub 2017 Sep 13. PMID: 28901812; PMCID: PMC5871025

Peng, Y., Sun, Q., Gao, R., and Park, Y. (2019). AAK-2 and SKN-1 Are Involved in Chicoric-Acid-Induced Lifespan Extension in caenorhabditis Elegans. J. Agric. Food Chem. 67, 9178–9186. doi:10.1021/acs.jafc.9b00705

Pennisi R, Gentile D, Rescifina A, Napoli E, Trischitta P, Piperno A, Sciortino MT. An Integrated In Silico and In Vitro Approach for the Identification of Natural Products Active against SARS-CoV-2. Biomolecules. 2023 Dec 28;14(1):43. doi: 10.3390/biom14010043. PMID: 38254643; PMCID: PMC10813393

Petersen M, Simmonds MS. Rosmarinic acid. Phytochemistry. 2003 Jan;62(2):121-5. doi: 10.1016/s0031-9422(02)00513-7. PMID: 12482446

Petricca, S.; Flati, V.; Celenza, G.; Di Gregorio, J.; Lizzi, A.R.; Luzi, C.; Cristiano, L.; Cinque, B.; Rossi, G.; Festuccia, C.; et al. Tebuconazole and econazole act synergistically in mediating mitochondrial stress, energy imbalance, and sequential activation of autophagy and apoptosis in mouse Sertoli TM4 cells: Possible role of AMPK/ULK1 axis. Toxicol. Sci. 2019, 169, 209–223

Petrzik, K., Vondrák, J., Barták, M. et al. Lichens—a new source or yet unknown host of herbaceous plant viruses? Eur J Plant Pathol 138, 549–559 (2014). https://doi.org/10.1007/s10658-013-0246-z

Phan LT, Nguyen TV, Luong QC, Nguyen TV, Nguyen HT, Le HQ, Nguyen TT, Cao TM, Pham QD. Importation and Human-to-Human Transmission of a Novel Coronavirus in Vietnam. N Engl J Med. 2020 Feb 27;382(9):872-874. doi: 10.1056/NEJMc2001272. Epub 2020 Jan 28. PMID: 31991079; PMCID: PMC7121428

Pietrucci F, Vargiu AV, Kranjc A. HIV-1 Protease Dimerization Dynamics Reveals a Transient Druggable Binding Pocket at the Interface. Sci Rep. 2015 Dec 22;5:18555. doi: 10.1038/srep18555. PMID: 26692118; PMCID: PMC4686983

Pillaiyar T, Manickam M, Namasivayam V, Hayashi Y, Jung SH. An Overview of Severe Acute Respiratory Syndrome-Coronavirus (SARS-CoV) 3CL Protease Inhibitors: Peptidomimetics and Small Molecule Chemotherapy. J Med Chem. 2016 Jul 28;59(14):6595-628. doi: 10.1021/acs.jmedchem.5b01461. Epub 2016 Feb 29. PMID: 26878082; PMCID: PMC7075650

Prasad S, Gupta SC, Tyagi AK, Aggarwal BB. Curcumin, a component of golden spice: from bedside to bench and back. Biotechnol Adv. 2014 Nov 1;32(6):1053-64. doi: 10.1016/j.biotechadv.2014.04.004. Epub 2014 Apr 30. PMID: 24793420

Priefert H., Rabenhorst J. and Steinbüchel A. Biotechnological production of vanillin. Appl Microbiol Biotechnol 56, 296–314 (2001). https://doi.org/10.1007/s002530100687

Priyadarsini KI. The chemistry of curcumin: from extraction to therapeutic agent. Molecules. 2014 Dec 1;19(12):20091-112. doi: 10.3390/molecules191220091. PMID: 25470276; PMCID: PMC6270789

Purvis OW, Elix JA, Broomhead JA, Jones GC. 1987 The occurrence of copper-norstictic acid in lichens from cupriferous substrata. Lichenologist 19 :193

Reis MM, Moreira AC, Sousa M, Mathur PP, Oliveira PF, Alves MG. Sertoli cell as a model in male reproductive toxicology: Advantages and disadvantages. J Appl Toxicol. 2015 Aug;35(8):870-83. doi: 10.1002/jat.3122. Epub 2015 Feb 18. PMID: 25693974

Ren LL, Wang YM, Wu ZQ, Xiang ZC, Guo L, Xu T, Jiang YZ, et al. Identification of a novel coronavirus causing severe pneumonia in human: a descriptive study. Chin Med J (Engl). 2020 May 5;133(9):1015-1024. doi: 10.1097/CM9.0000000000000722. PMID: 32004165; PMCID: PMC7147275

Rosado MJ, Rencoret J, Marques G, Gutiérrez A, Del Río JC. Structural Characteristics of the Guaiacyl-Rich Lignins From Rice (Oryza sativa L.) Husks and Straw. Front Plant Sci. 2021 Feb 19;12:640475. doi: 10.3389/fpls.2021.640475. PMID: 33679856; PMCID: PMC7932998

Rosas-Lemus M, Minasov G, Shuvalova L, Inniss NL, Kiryukhina O, Brunzelle J, Satchell KJF. High-resolution structures of the SARS-CoV-2 2'-O-methyltransferase reveal strategies for structure-based inhibitor design. Sci Signal. 2020 Sep 29;13(651):eabe1202. doi: 10.1126/scisignal.abe1202. PMID: 32994211; PMCID: PMC8028745

Rosén J, Gottfries J, Muresan S, Backlund A, Oprea TI. Novel chemical space exploration via natural products. J Med Chem. 2009 Apr 9;52(7):1953-62. doi: 10.1021/jm801514w. PMID: 19265440; PMCID: PMC2696019

Rundel PW., The ecological role of secondary lichen substances. Biochemical Systematics and Ecology, Volume 6, Issue 3, 1978, Pages 157-170. https://doi.org/10.1016/0305-1978(78)90002-9

Rupasinghe HP., Vasantha & Jiang, Yuanyuan & Zhang L. The anticancer properties of phytochemical extracts from Salvia plants. Botanics: Targets and Therapy. 2016. 25. 10.2147/BTAT.S98610

Russo A, Piovano M, Lombardo L, Vanella L, Cardile V, Garbarino J. Pannarin inhibits cell growth and induces cell death in human prostate carcinoma DU-145 cells. Anticancer Drugs. 2006 Nov;17(10):1163-9. doi: 10.1097/01.cad.0000236310.66080.ed. PMID: 17075315

Ryu YB, Park SJ, Kim YM, Lee JY, Seo WD, Chang JS, Park KH, Rho MC, Lee WS. SARS-CoV 3CLpro inhibitory effects of quinone-methide triterpenes from Tripterygium regelii. Bioorg Med Chem Lett. 2010 Mar 15;20(6):1873-6. doi: 10.1016/j.bmcl.2010.01.152. Epub 2010 Feb 4. PMID: 20167482; PMCID: PMC7127101.

Safiabadi Tali SH, LeBlanc JJ, Sadiq Z, Oyewunmi OD, Camargo C, Nikpour B, Armanfard N, Sagan SM, Jahanshahi-Anbuhi S. Tools and Techniques for Severe Acute Respiratory Syndrome Coronavirus 2 (SARS-CoV-2)/COVID-19 Detection. Clin Microbiol Rev. 2021 May 12;34(3):e00228-20. doi: 10.1128/CMR.00228-20. PMID: 33980687; PMCID: PMC8142517

Sahebkar A. Are curcuminoids effective C-reactive protein-lowering agents in clinical practice? Evidence from a meta-analysis. Phytother Res. 2014 May;28(5):633-42. doi: 10.1002/ptr.5045. Epub 2013 Aug 7. PMID: 23922235

Saklani A, Upreti DK. Folk uses of some lichens in Sikkim. J Ethnopharmacol. 1992 Oct;37(3):229-33. doi: 10.1016/0378-8741(92)90038-s. PMID: 1453712

Santosh K. Sandur, Manoj K. Pandey, Bokyung Sung, Kwang Seok Ahn, Akira Murakami, Gautam Sethi, Pornngarm Limtrakul, Vladimir Badmaev, Bharat B. Aggarwal, Curcumin, demethoxycurcumin, bisdemethoxycurcumin, tetrahydrocurcumin and turmerones differentially regulate anti-inflammatory and anti-proliferative responses through a ROS-independent mechanism, Carcinogenesis, Volume 28, Issue 8, August 2007, Pages 1765–1773, https://doi.org/10.1093/carcin/bgm123

Santos-López G, Cortés-Hernández P, Vallejo-Ruiz V, Reyes-Leyva J. SARS-CoV-2: basic concepts, origin and treatment advances. Gac Med Mex. 2021;157(1):84-89. English. doi: 10.24875/GMM.M21000524. PMID: 34125824

Sargsyan R, Gasparyan A, Tadevosyan G, Panosyan H. Antimicrobial and antioxidant potentials of non-cytotoxic extracts of corticolous lichens sampled in Armenia. AMB Express. 2021 Jul 29;11(1):110. doi: 10.1186/s13568-021-01271-z. PMID: 34324070; PMCID: PMC8322222

Schatz A. 1962 Pedogenic (soil-forming) activity of lichen acids. Naturwissenschaften 49 :518

Schinazi RF, Chu CK, Babu JR, Oswald BJ, Saalmann V, Cannon DL, Eriksson BF, Nasr M. Anthraquinones as a new class of antiviral agents against human immunodeficiency virus. Antiviral Res. 1990 May;13(5):265-72. doi: 10.1016/0166-3542(90)90071-e. PMID: 1697740

Schmeda-Hirschmann G, Tapia A, Lima B, Pertino M, Sortino M, Zacchino S, Arias AR, Feresin GE. A new antifungal and antiprotozoal depside from the Andean lichen Protousnea poeppigii. Phytother Res. 2008 Mar;22(3):349-55. doi: 10.1002/ptr.2321. PMID: 18058986

Schneider C, Gordon ON, Edwards RL, Luis PB. Degradation of Curcumin: From Mechanism to Biological Implications. J Agric Food Chem. 2015 Sep 9;63(35):7606-14. doi: 10.1021/acs.jafc.5b00244. Epub 2015 Apr 2. PMID: 25817068; PMCID: PMC4752206

Schoeman D, Fielding BC. Coronavirus envelope protein: current knowledge. Virol J. 2019 May 27;16(1):69. doi: 10.1186/s12985-019-1182-0. PMID: 31133031; PMCID: PMC6537279

Schramm HJ, Nakashima H, Schramm W, Wakayama H, Yamamoto N. HIV-1 reproduction is inhibited by peptides derived frm the N- and C-termini of HIV-1 protease. Biochem Biophys Res Commun. 1991 Sep 16;179(2):847-51. doi: 10.1016/0006-291x(91)91895-j. PMID: 1680323

Schulz, H., and Albroscheit, G., 1989, Characterization of oakmoss products used in perfumery by high-performance liquid chromatography, J. Chromatogr. 466: 301-306

Segatore B, Bellio P, Setacci D, Brisdelli F, Piovano M, Garbarino JA, Nicoletti M, Amicosante G, Perilli M, Celenza G. In vitro interaction of usnic acid in combination with antimicrobial agents against methicillin-resistant Staphylococcus aureus clinical isolates determined by FICI and ΔE model methods. Phytomedicine. 2012 Feb 15;19(3-4):341-7. doi: 10.1016/j.phymed.2011.10.012. Epub 2011 Nov 25. PMID: 22119041

Shahhamzehei N, Abdelfatah S, Efferth T. In Silico and In Vitro Identification of Pan-Coronaviral Main Protease Inhibitors from a Large Natural Product Library. Pharmaceuticals (Basel). 2022 Mar 3;15(3):308. doi: 10.3390/ph15030308. PMID: 35337106; PMCID: PMC8952009

Shahrajabian MH, Sun W. The Golden Spice for Life: Turmeric with the Pharmacological Benefits of Curcuminoids Components, including Curcumin, Bisdemethoxycurcumin, and Demethoxycurcumin. Curr Org Synth. 2023 Jun 7. doi: 10.2174/1570179420666230607124949. Epub ahead of print. PMID: 37287298

Sharma A, Goyal S, Yadav AK, Kumar P, Gupta L. In-silico screening of plant-derived antivirals against main protease, 3CLpro and endoribonuclease, NSP15 proteins of SARS-CoV-2. J Biomol Struct Dyn. 2022 Jan;40(1):86-100. doi: 10.1080/07391102.2020.1808077. Epub 2020 Sep 8. PMID: 32896226; PMCID: PMC7544953

Sharma RA, Gescher AJ, Steward WP. Curcumin: the story so far. Eur J Cancer. 2005 Sep;41(13):1955-68. doi: 10.1016/j.ejca.2005.05.009. PMID: 16081279

Sheikh A, Al-Taher A, Al-Nazawi M, Al-Mubarak AI, Kandeel M. Analysis of preferred codon usage in the coronavirus N genes and their implications for genome evolution and vaccine design. J Virol Methods. 2020 Mar;277:113806. doi: 10.1016/j.jviromet.2019.113806. Epub 2020 Jan 5. PMID: 31911390; PMCID: PMC7119019

Shi J, Sivaraman J, Song J. Mechanism for controlling the dimer-monomer switch and coupling dimerization to catalysis of the severe acute respiratory syndrome coronavirus 3C-like protease. J Virol. 2008 May;82(9):4620-9. doi: 10.1128/JVI.02680-07. Epub 2008 Feb 27. PMID: 18305031; PMCID: PMC2293028

Shi J, Song J. The catalysis of the SARS 3C-like protease is under extensive regulation by its extra domain. FEBS J. 2006 Mar;273(5):1035-45. doi: 10.1111/j.1742-4658.2006.05130.x. PMID: 16478476; PMCID: PMC7164011

Shibata, S. Especial compounds of lichens. 1958. Handbuch der Pflanzenphysiologie 10:560-623

Shibata, S. Great discoveries in bryology and lichenology - Yasuhiko Asahina (1880-1975) and his studies on lichenology and chemistry of lichen metabolites. 2000. Bryologist 103:710-719

Shibata, S., Nishikawa, Y., Tanaka, M. et al. Antitumour activities of lichen polysaccharides. Z Krebsforsch 71, 102–104 (1968). https://doi.org/10.1007/BF00524509

Silva JA, Bomfim RR, Estevam Cdos S, Antoniolli AR, Araújo AA, Thomazzi SM. Pharmacological properties of lichen Cladonia clathrata. Pharm Biol. 2010 Jul;48(7):745-52. doi: 10.3109/13880200903273914. PMID: 20645771

Simpson JP, Olson J, Dilkes B, Chapple C. Identification of the Tyrosine- and Phenylalanine-Derived Soluble Metabolomes of Sorghum. Front Plant Sci. 2021 Sep 14;12:714164. doi: 10.3389/fpls.2021.714164. PMID: 34594350; PMCID: PMC8476951

Singh D, Yi SV. On the origin and evolution of SARS-CoV-2. Exp Mol Med. 2021 Apr;53(4):537-547. DOI: 10.1038/s12276-021-00604-z. Epub 2021 Apr 16. PMID: 33864026; PMCID: PMC8050477

Siu YL, Teoh KT, Lo J, Chan CM, Kien F, Escriou N, Tsao SW, Nicholls JM, Altmeyer R, Peiris JS, Bruzzone R, Nal B. The M, E, and N structural proteins of the severe acute respiratory syndrome coronavirus are required for efficient assembly, trafficking, and release of virus-like particles. J Virol. 2008 Nov;82(22):11318-30. doi: 10.1128/JVI.01052-08. Epub 2008 Aug 27. PMID: 18753196; PMCID: PMC2573274

Sobhia ME, Kumar GS, Sivangula S, Ghosh K, Singh H, Haokip T, Gibson J. Rapid structure-based identification of potential SARS-CoV-2 main protease inhibitors. Future Med Chem. 2021 Sep;13(17):1435-1450. DOI: 10.4155/fmc-2020-0264. Epub 2021 Jun 25. PMID: 34169728; PMCID: PMC8240652

Song Z, Xu Y, Bao L, Zhang L, Yu P, Qu Y, Zhu H, Zhao W, Han Y, Qin C. From SARS to MERS, Thrusting Coronaviruses into the Spotlight. Viruses. 2019 Jan 14;11(1):59. doi: 10.3390/v11010059. PMID: 30646565; PMCID: PMC6357155

Souid I, Korchef A, Souid S. In silico evaluation of Vitis amurensis Rupr. Polyphenol compounds for their inhibition potency against COVID-19 main enzymes Mpro and RdRp. Saudi Pharm J. 2022 May;30(5):570-584. doi: 10.1016/j.jsps.2022.02.014. Epub 2022 Feb 25. PMID: 35250347; PMCID: PMC8883852

Stanton DE, Ormond A, Koch NM, Colesie C. Lichen ecophysiology in a changing climate. Am J Bot. 2023 Feb;110(2):e16131. doi: 10.1002/ajb2.16131. Epub 2023 Feb 16. PMID: 36795943

Stavri M, Piddock LJ, Gibbons S. Bacterial efflux pump inhibitors from natural sources. J Antimicrob Chemother. 2007 Jun;59(6):1247-60. doi: 10.1093/jac/dkl460. Epub 2006 Dec 4. PMID: 17145734

Stein, S.R., Ramelli, S.C., Grazioli, A. et al. SARS-CoV-2 infection and persistence in the human body and brain at autopsy. Nature 612, 758–763 (2022). https://doi.org/10.1038/s41586-022-05542-y

Stocker-Wörgötter, E.; Cordeiro, L.M.C.; Iacomini, M. Accumulation of Potential Pharmaceutically Relevant Lichen Metabolites in Lichens and Cultured Lichen Symbionts. Stud. Nat. Prod. Chem. 2013, 39, 337–380

Stuart D. Crawford. Lichens Used in Traditional Medicine. 2019. Springer. https://doi.org/10.1007/978-3-030-16814-8_2

Stubler D, Buchenauer H (1996) Antiviral activity of the glucan lichenan (poly-β{1!3, 1!4} D-anhydroglucose) 1. Biological activity in tobacco plants. J Phytopathol 144:37–43)

Su S, Wong G, Shi W, Liu J, Lai ACK, Zhou J, Liu W, Bi Y, Gao GF. Epidemiology, Genetic Recombination, and Pathogenesis of Coronaviruses. Trends Microbiol. 2016 Jun;24(6):490-502. DOI: 10.1016/j.tim.2016.03.003. Epub 2016 Mar 21. PMID: 27012512; PMCID: PMC7125511

Syers JK, Iskan.dar IK. 1973 Pedogenic significance of lichens. In: Ahmadjian V, Hale ME (eds) The lichens: 225. Academic, New York

Tam NM, Pham DH, Hiep DM, Tran PT, Quang DT, Ngo ST. Searching and designing potential inhibitors for SARS-CoV-2 Mpro from natural sources using atomistic and deep-learning calculations. RSC Adv. 2021 Nov 29;11(61):38495-38504. doi: 10.1039/d1ra06534c. PMID: 35493244; PMCID: PMC9044063

Tay T, Türk AO, Yilmaz M, Türk H, Kivanç M. Evaluation of the antimicrobial activity of the acetone extract of the lichen Ramalina farinacea and its (+)-usnic acid, norstictic acid, and protocetraric acid constituents. Z Naturforsch C J Biosci. 2004 May-Jun;59(5-6):384-8. doi: 10.1515/znc-2004-5-617. PMID: 18998406

Tee-ngam P, Nunant N, Rattanarat P, Siangproh W, Chailapakul O: Simple and rapid determination of ferulic acid levels in food and cosmetic samples using paper-based platforms. Sensors 2013; 13: 13039–13053

Tegos G, Stermitz FR, Lomovskaya O, Lewis K. Multidrug pump inhibitors uncover remarkable activity of plant antimicrobials. Antimicrob Agents Chemother. 2002 Oct;46(10):3133-41. doi: 10.1128/AAC.46.10.3133-3141.2002. PMID: 12234835; PMCID: PMC128777

Thomas S. Mapping the Nonstructural Transmembrane Proteins of Severe Acute Respiratory Syndrome Coronavirus 2. J Comput Biol. 2021 Sep;28(9):909-921. doi: 10.1089/cmb.2020.0627. Epub 2021 Jun 28. PMID: 34182794; PMCID: PMC8558077

Tseng CT, Sbrana E, Iwata-Yoshikawa N, Newman PC, Garron T, Atmar RL, Peters CJ, Couch RB. Immunization with SARS coronavirus vaccines leads to pulmonary immunopathology on challenge with the SARS virus. PLoS One. 2012;7(4):e35421. doi: 10.1371/journal.pone.0035421. Epub 2012 Apr 20. Erratum in: PLoS One. 2012;7(8). doi:10.1371/annotation/2965cfae-b77d-4014-8b7b-236e01a35492. PMID: 22536382; PMCID: PMC3335060

Tyrrell DA, Bynoe ML. Cultivation of viruses from a high proportion of patients with colds. Lancet. 1966 Jan 8;1(7428):76-7. DOI: 10.1016/s0140-6736(66)92364-6

Ureña-Vacas, I.; González-Burgos, E.; Divakar, K.; Pilar Gómez-Serranillos, M.; González Burgos, E. Lichen Depsidones with Biological Interest Reviews. Planta Med. 2021

V'kovski, P., Kratzel, A., Steiner, S. et al. Coronavirus biology and replication: implications for SARS-CoV-2. Nat Rev Microbiol 19, 155–170 (2021). https://doi.org/10.1038/s41579-020-00468-6

Vartia KO (1973) Antibiotics in lichens. In: Ahmadjiian V, Hale ME (eds) The lichens, 3rd edn. Academic, New York, pp 547–561

Verma, N., & Behera, B. C. (2014). Future Directions in the Study of Pharmaceutical Potential of Lichens. Lichen Secondary Metabolites, 179–202. doi:10.1007/978-3-319-13374-4_8

Vogt T. Phenylpropanoid biosynthesis. Mol Plant. 2010 Jan;3(1):2-20. doi: 10.1093/mp/ssp106. Epub 2009 Dec 24. PMID: 20035037

von Rhein C, Weidner T, Henß L, Martin J, Weber C, Sliva K, Schnierle BS. Curcumin and Boswellia serrata gum resin extract inhibit chikungunya and vesicular stomatitis virus infections in vitro. Antiviral Res. 2016 Jan;125:51-7. doi: 10.1016/j.antiviral.2015.11.007. Epub 2015 Dec 2. PMID: 26611396.

Waley SG. The kinetics of slow-binding and slow, tight-binding inhibition: the effects of substrate depletion. Biochem J. 1993 Aug 15;294 (Pt 1):195-200. doi: 10.1042/bj2940195. PMID: 8363573; PMCID: PMC1134584

Wang G, Venegas FA, Rueda AM, Weerasinghe NW, Uggowitzer KA, Thibodeaux CJ, Moitessier N, Mittermaier AK. A naturally occurring G11S mutation in the 3C-like protease from the SARS-

CoV-2 virus dramatically weakens the dimer interface. Protein Sci. 2024 Jan;33(1):e4857. doi: 10.1002/pro.4857. PMID: 38058248; PMCID: PMC10731504

Wang J, Wang K, Lyu S, Huang J, Huang C, Xing Y, Wang Y, Xu Y, Li P, Hong J, Xi J, Si X, Ye H, Li Y. Genome-Wide Identification of Tannase Genes and Their Function of Wound Response and Astringent Substances Accumulation in Juglandaceae. Front Plant Sci. 2021 May 17;12:664470. doi: 10.3389/fpls.2021.664470. PMID: 34079571; PMCID: PMC8165273

Wang Z, Yang L. In the age of Omicron variant: Paxlovid raises new hopes of COVID-19 recovery. J Med Virol. 2022 May;94(5):1766-1767. doi: 10.1002/jmv.27540. Epub 2021 Dec 29. PMID: 34936106

Wang, BQ. Salvia miltiorrhiza: Chemical and pharmacological review of a medicinal plant. J. Med. Plants Res. 2010, 4, 2813–2820

Wei P, Fan K, Chen H, Ma L, Huang C, Tan L, Xi D, Li C, Liu Y, Cao A, Lai L. The N-terminal octapeptide acts as a dimerization inhibitor of SARS coronavirus 3C-like proteinase. Biochem Biophys Res Commun. 2006 Jan 20;339(3):865-72. doi: 10.1016/j.bbrc.2005.11.102. Epub 2005 Nov 28. PMID: 16329994; PMCID: PMC7092940

Wertheim JO, Chu DK, Peiris JS, Kosakovsky Pond SL, Poon LL (2013) A case for the ancient origin of coronaviruses. J Virol 87:7039–7045

White PA, Oliveira RC, Oliveira AP, Serafini MR, Araújo AA, Gelain DP, Moreira JC, Almeida JR, Quintans JS, Quintans-Junior LJ, Santos MR. Antioxidant activity and mechanisms of action of natural compounds isolated from lichens: a systematic review. Molecules. 2014 Sep 12;19(9):14496-527. doi: 10.3390/molecules190914496. PMID: 25221871; PMCID: PMC6271897

World Health Organization. https://www.who.int/ (accessed on 30 January 2022)

World Health Organization. 2015. https://www.who.int/publications/m/item/summary-of-probable-sars-cases-with-onset-of-illness-from-1-november-2002-to-31-july-2003

WHO Director General's opening remarks at the media briefing on COVID-19-11 March 2020. 2021. https://www.who.int/director general/speeches/detail/who-director-general-s-openingremarks-at-the-media-briefing-on-covid-19---11-march-2020

World Health Organization. COVID-19 weekly epidemiological update, edition 44. (2021)

World Health Organization (2019) MERS situation update, December 2019. Epidemic and pandemic-prone diseases. http://www.emro. who.int/pandemic-epidemic-diseases/mers-cov/merssituation-update-december-2019.html

World Health Organization. Middle East respiratory syndrome coronavirus (MERS-CoV). https://www.who.int/emergencies/mers-cov/en/

World Health Organization. Severe Acute Respiratory Syndrome (SARS). https://www.who.int/csr/sars/en/

Wrapp D, Wang N, Corbett KS, Goldsmith JA, Hsieh CL, Abiona O, Graham BS, McLellan JS. Cryo-EM structure of the 2019-nCoV spike in the prefusion conformation. Science. 2020 Mar 13;367(6483):1260-1263. doi: 10.1126/science.abb2507. Epub 2020 Feb 19. PMID: 32075877; PMCID: PMC7164637

Wu CR, Yin WC, Jiang Y, Xu HE. Structure genomics of SARS-CoV-2 and its Omicron variant: drug design templates for COVID-19. Acta Pharmacol Sin. 2022 Dec;43(12):3021-3033. doi: 10.1038/s41401-021-00851-w. Epub 2022 Jan 20. PMID: 35058587; PMCID: PMC8771608

Wu JX, Xu JY, Yuan YZ. Effect of emodin and sandostatin on metabolism of eicosanoids in acute necrotizing pancreatitis. World J Gastroenterol. 2000 Apr;6(2):293-294. doi: 10.3748/wjg.v6.i2.293. PMID: 11819581; PMCID: PMC4723509

Xia B, Kang X. Activation and maturation of SARS-CoV main protease. Protein Cell. 2011 Apr;2(4):282-90. doi: 10.1007/s13238-011-1034-1. Epub 2011 Apr 28. PMID: 21533772; PMCID: PMC4875205

Yamamoto Y, Miura Y, Kinoshita Y, Higuchi M, Yamada Y, Murakami A, Ohigashi H, Koshimizu K. Screening of tissue cultures and thalli of lichens and some of their active constituents for inhibition of tumor promoter-induced Epstein-Barr virus activation. Chem Pharm Bull (Tokyo). 1995 Aug;43(8):1388-90. doi: 10.1248/cpb.43.1388. PMID: 7553984

Yan L, Ge J, Zheng L, Zhang Y, Gao Y, Wang T, Huang Y, Yang Y, Gao S, Li M, Liu Z, Wang H, Li Y, Chen Y, Guddat LW, Wang Q, Rao Z, Lou Z. Cryo-EM Structure of an Extended SARS-CoV-2 Replication and Transcription Complex Reveals an Intermediate State in Cap Synthesis. Cell. 2021 Jan 7;184(1):184-193.e10. doi: 10.1016/j.cell.2020.11.016. Epub 2020 Nov 14. PMID: 33232691; PMCID: PMC7666536

Yang H, Bartlam M, Rao Z. Drug design targeting the main protease, the Achilles' heel of coronaviruses. Curr Pharm Des. 2006;12(35):4573-90. doi: 10.2174/138161206779010369. PMID: 17168763

Yang H, Xie W, Xue X, Yang K, Ma J, Liang W, Zhao Q, Zhou Z, Pei D, Ziebuhr J, Hilgenfeld R, Yuen KY, Wong L, Gao G, Chen S, Chen Z, Ma D, Bartlam M, Rao Z. Design of wide-spectrum inhibitors targeting coronavirus main proteases. PLoS Biol. 2005 Oct;3(10):e324. doi: 10.1371/journal.pbio.0030324. Epub 2005 Sep 6. Erratum in: PLoS Biol. 2005 Nov;3(11):e428. PMID: 16128623; PMCID: PMC1197287

Yang H, Yang M, Ding Y, Liu Y, Lou Z, Zhou Z, Sun L, Mo L, Ye S, Pang H, Gao GF, Anand K, Bartlam M, Hilgenfeld R, Rao Z. The crystal structures of severe acute respiratory syndrome virus main protease and its complex with an inhibitor. Proc Natl Acad Sci U S A. 2003 Nov 11;100(23):13190-5. doi: 10.1073/pnas.1835675100. Epub 2003 Oct 29. PMID: 14585926; PMCID: PMC263746

Yang J, Zheng Y, Gou X, Pu K, Chen Z, Guo Q, Ji R, Wang H, Wang Y, Zhou Y. Prevalence of comorbidities and its effects in patients infected with SARS-CoV-2: a systematic review and meta-analysis. Int J Infect Dis. 2020 May;94:91-95. DOI: 10.1016/j.ijid.2020.03.017. Epub 2020 Mar 12. PMID: 32173574; PMCID: PMC7194638

Yang M, Wu C, Zhang T, Shi L, Li J, Liang H, Lv X, Jing F, Qin L, Zhao T, Wang C, Liu G, Feng S, Li F. Chicoric Acid: Natural Occurrence, Chemical Synthesis, Biosynthesis, and Their Bioactive Effects. Front Chem. 2022 Jun 23;10:888673. doi: 10.3389/fchem.2022.888673. PMID: 35815211; PMCID: PMC9262330

Yao T, Feng K, Xie M, Barros J, Tschaplinski TJ, Tuskan GA, Muchero W, Chen JG. Phylogenetic Occurrence of the Phenylpropanoid Pathway and Lignin Biosynthesis in Plants. Front Plant Sci. 2021 Aug 17;12:704697. doi: 10.3389/fpls.2021.704697. PMID: 34484267; PMCID: PMC8416159

Ye C, Bian P, Zhang J, Xiao H, Zhang L, Ye W, Dong Y, Zhou Y, Jia Z, Lei Y. Structure-based discovery of antiviral inhibitors targeting the E dimer interface of Japanese encephalitis virus. Biochem Biophys Res Commun. 2019 Jul 23;515(2):366-371. doi: 10.1016/j.bbrc.2019.05.148. Epub 2019 May 30. PMID: 31155294

Ye ZW, Yuan S, Yuen KS, Fung SY, Chan CP, Jin DY. Zoonotic origins of human coronaviruses. Int J Biol Sci. 2020 Mar 15;16(10):1686-1697. DOI: 10.7150/ijbs.45472. PMID: 32226286; PMCID: PMC7098031

Yin W, Luan X, Li Z, Zhou Z, Wang Q, Gao M, Wang X, Zhou F, Shi J, You E, Liu M, Wang Q, Jiang Y, Jiang H, Xiao G, Zhang L, Yu X, Zhang S, Eric Xu H. Structural basis for inhibition of the SARS-CoV-2 RNA polymerase by suramin. Nat Struct Mol Biol. 2021 Mar;28(3):319-325. doi: 10.1038/s41594-021-00570-0. Epub 2021 Mar 5. PMID: 33674802

Zaki AM, van Boheemen S, Bestebroer TM, Osterhaus AD, Fouchier RA. Isolation of a novel coronavirus from a man with pneumonia in Saudi Arabia. N Engl J Med. 2012 Nov 8;367(19):1814-20. doi: 10.1056/NEJMoa1211721. Epub 2012 Oct 17. Erratum in: N Engl J Med. 2013 Jul 25;369(4):394. PMID: 23075143

Zeng W, Liu G, Ma H, Zhao D, Yang Y, Liu M, Mohammed A, Zhao C, Yang Y, Xie J, Ding C, Ma X, Weng J, Gao Y, He H, Jin T. Biochemical characterization of SARS-CoV-2 nucleocapsid protein. Biochem Biophys Res Commun. 2020 Jun 30;527(3):618-623. doi: 10.1016/j.bbrc.2020.04.136. Epub 2020 Apr 30. Erratum in: Biochem Biophys Res Commun. 2022 Jul 23;614:225. PMID: 32416961; PMCID: PMC7190499

Zhang L, Lin D, Sun X, Curth U, Drosten C, Sauerhering L, Becker S, Rox K, Hilgenfeld R. Crystal structure of SARS-CoV-2 main protease provides a basis for design of improved α-ketoamide inhibitors. Science. 2020 Apr 24;368(6489):409-412. doi: 10.1126/science.abb3405. Epub 2020 Mar 20. PMID: 32198291; PMCID: PMC7164518

Zhang SF, Tuo JL, Huang XB, Zhu X, Zhang DM, Zhou K, Yuan L, Luo HJ, Zheng BJ, Yuen KY, Li MF, Cao KY, Xu L (2018) Epidemiology characteristics of human coronaviruses in patients with respiratory infection symptoms and phylogenetic analysis of HCoV-OC43 during 2010-2015 in Guangzhou. PLoS One 13: e019178

Zhang W, Du RH, Li B, Zheng XS, Yang XL, Hu B, Wang YY, Xiao GF, Yan B, Shi ZL, Zhou P. Molecular and serological investigation of 2019-nCoV infected patients: implication of multiple shedding routes. Emerg Microbes Infect. 2020 Feb 17;9(1):386-389. doi: 10.1080/22221751.2020.1729071. PMID: 32065057; PMCID: PMC7048229

Zhang Y, Chen Y, Li Y, Huang F, Luo B, Yuan Y, et al. The ORF8 protein of SARS-CoV-2 mediates immune evasion through down-regulating MHC-I. Proc Natl Acad Sci U S A. 2021 Jun 8;118(23):e2024202118. doi: 10.1073/pnas.2024202118. PMID: 34021074; PMCID: PMC8201919

Zhang YN, Zhu GH, Liu W, Xiong Y, Hu Q, Zhuang XY, Jia GH, Zhang WD, Ge GB. Discovery and characterization of the covalent SARS-CoV-2 3CLpro inhibitors from Ginkgo biloba extract via integrating chemoproteomic and biochemical approaches. Phytomedicine. 2023 Jun;114:154796. doi: 10.1016/j.phymed.2023.154796. Epub 2023 Mar 29. PMID: 37037086; PMCID: PMC10052880

Zhao GR, Zhang HM, Ye TX, Xiang ZJ, Yuan YJ, Guo ZX, Zhao LB. Characterization of the radical scavenging and antioxidant activities of danshensu and salvianolic acid B. Food Chem Toxicol. 2008 Jan;46(1):73-81. doi: 10.1016/j.fct.2007.06.034. Epub 2007 Jul 4. PMID: 17719161

Zhao Y, Fang C, Zhang Q, Zhang R, Zhao X, Duan Y, Wang H, Zhu Y, Feng L, Zhao J, Shao M, Yang X, Zhang L, Peng C, Yang K, Ma D, Rao Z, Yang H. Crystal structure of SARS-CoV-2 main protease in complex with protease inhibitor PF-07321332. Protein Cell. 2022 Sep;13(9):689-693. doi: 10.1007/s13238-021-00883-2. Epub 2021 Oct 22. PMID: 34687004; PMCID: PMC8533666

Zheng K, Ma G, Zhou J, Zen M, Zhao W, Jiang Y, Yu Q, Feng J. Insight into the activity of SARS main protease: Molecular dynamics study of dimeric and monomeric form of enzyme. Proteins. 2007 Feb 1;66(2):467-79. doi: 10.1002/prot.21160. PMID: 17083088; PMCID: PMC7167853

Zhou P, Yang XL, Wang XG, Hu B, Zhang L, Zhang W, et al. A pneumonia outbreak associated with a new coronavirus of probable bat origin. Nature. 2020 Mar;579(7798):270-273. doi: 10.1038/s41586-020-2012-7. Epub 2020 Feb 3. Erratum in: Nature. 2020 Dec;588(7836):E6. PMID: 32015507; PMCID: PMC7095418

Zumla A, Chan JF, Azhar EI, Hui DS, Yuen KY. Coronaviruses - drug discovery and therapeutic options. Nat Rev Drug Discov. 2016 May;15(5):327-47. doi: 10.1038/nrd.2015.37. Epub 2016 Feb 12. PMID: 26868298; PMCID: PMC7097181